國　立　交　通　大　學

電信工程學系碩士班

碩士論文

應用於時變與非時變 OFDM 系統之新通道估測法

New Channel Estimation Methods for Time Invariant/Variant OFDM Systems

研 究 生：楊植纓

指導教授：吳 文 榕　博士

中華民國九十八年七月

應用於時變與非時變 OFDM 系統之新通道估測法

New Channel Estimation Methods for Time Invariant/Variant OFDM Systems

研 究 生：楊植纓　　Student：Chih-Ying Young

指導教授：吳文榕 博士　　Advisor：Dr. Wen-Rong Wu

國 立 交 通 大 學

電信工程學系碩士班

碩 士 論 文

A Thesis
Submitted to Department of Communication Engineering
College of Electrical and Computer Engineering
National Chiao-Tung University
in Partial Fulfillment of the Requirements
for the Degree of
Master of Science
In
Communication Engineering
July 2009
Hsinchu, Taiwan, Republic of China

中華民國九十八年七月

應用於時變與非時變 OFDM 系統之新通道估測法

New Channel Estimation Methods for Time Invariant/Variant OFDM Systems

研究生：楊植纓　　指導教授：吳文榕 教授

國立交通大學電信工程學系碩士班

摘要

通道估測(channel estimation)通常是依靠系統中的領航訊號(pilot)來完成。當通道的時間延遲較長時，估測效能可能會因為受限於有限的領航訊號而下降。最近有研究者在 DVB-T 系統下提出的聯合時域和頻域通道估測法，比舊有頻域通道估測法的效能好很多。然而，因為這個估測方法需要四個 OFDM 訊號的資訊來完成，所以對於記憶體的使用量大，在時變通道中也不適用。在本篇論文中，我們提出了一個新的通道估測法來解決此問題。在本篇論文的第一部分，我們提出適用於非時變通道的新通道估測法，而在本篇論文的第二部分，我們延伸此新通道估測法，使它適用於時變通道的估測。我們所提出的通道估測法，最主要的特色是即使在領航訊號(pilot)密度很低時，也只需要一個 OFDM 訊號就可以完成。而從模擬結果也可以看出，我們所提出的通道估測法有很好的效能。

New Channel Estimation Methods for Time Invariant/Variant OFDM Systems

Student: Chih-Ying Young Advisor: Dr. Wen-Rong Wu

Department of Communication Engineering
National Chiao-Tung University

Abstract

In pilots-aided OFDM systems, the channel estimation relies on the pilots inserted in the systems. Since the number of pilots is usually limited, the performance of the channel estimate may not be satisfactory when the delay spreard of the channel is large. Recently, a joint time and frequency domain estimator, which can grealty outperform the conventional frequency domain channel estimator, has been proposed for DVB-T systems. However, this method need to collect four OFDM symbols in order to conduct the estimation. This will significantly increase the memory size and cause problems in time-variant channels. In this thesis, we propose new joint time and frequency domain methods to solve the problem. In the first part of this thesis, we propose new methods for the time-invariant channel estimation. In the second part of this thesis, we extend the proposed methods to accommodate time-variant channels. The distinct feature of the proposed methods is that only one OFDM symbol is required even when the pilot density is very low. Simulations show that the performance of the proposed methods can approach the optimum.

誌謝

本篇論文得以順利完成，首先要特別感謝我的指導教授 吳文榕博士。當我在課業和研究上有不能理解和困難時，老師總是適時的給予協助和引導，並耐心的教導和提出指正。在老師身上，讓我學習到很多通訊專業的知識和做研究有效的方法和嚴謹認真的態度，也謝謝老師對生活和未來規劃中給予的意見和鼓勵。

此外，也要感謝實驗室的學長們、同學們在課業和論文研究上的討論和幫助，當然還有感謝我大學和高中的好朋友們，在課業、研究和生活上都幫忙了我許多，也因為你們，讓我的碩士生活可以過的開心又有趣，還要謝謝我的室友和男朋友，不管是在課業和研究上實質的幫助和討論，還是精神上的鼓勵和支持，都讓我的碩士生涯過的更好，謝謝你們。

最後，誠摯感謝始終在我背後支持我的雙親和哥哥。謹以此文獻給你們。

Catalog

List of Tables

List of Figures

Chapter 1

Introduction

Orthogonal Frequency Division Multiplexing (OFDM) has been an important modulation technique in wireless communication. The distinct advantage of OFDM is that it can significantly increase the spectrum efficiency. Also, it can effectively combat the multipath channel fading, and allow multiple users to access the channel at the same time. The OFDM technique has been successfully used in many commercial systems such as wireless local area network (LAN), digital video broadcasting (DVB), WiMAX etc.

Due to multipath propagation, the channel is often fading in wireless systems. In order to recover the transmitted signals in the receiver, accurate channel estimation is essential. For OFDM systems, pilot subcarriers are frequently inserted in the OFDM symbols to aid the channel estimation. Since the inserted pilots will reduce the transmission bandwidth, the number of pilots is usually kept to a minimum. As a result, the channel estimation becomes challenging in some scenarios. In this thesis, we consider the channel estimation problem in the DVB-terrestrial (DVB-T) system. This is a standardized system for digital terrestrial television broadcasting and has been adopted in Taiwan and many other countries. The DVB-T system transmits and receives compressed digital audio, video and other data in an MPEG transport stream and use OFDM as its modulation technique.

Channel estimation has been considered in the literature [2]-[4]. To obtain satisfactory performance, the implementation complexity is generally high. This is because the pilot density in DVB-T system is 1/12 which is not enough to conduct the channel estimation

accurately. As a result, we have to cluster four OFDM symbols to make the density up to 1/3, and this significantly increase the memory size and subsequently the implementation complexity. Also, in high-mobility environments, the channel responses of four consecutive OFDM symbols will not be the same, the clustering approach will not work. We propose new algorithms to use the limited pilots to conduct the channel estimation effectively. Conventional approaches conduct the channel estimation in the frequency domain and perform poorly when the pilot density is low. In this thesis, we propose a new joint time/frequency domain channel estimation method to overcome the problem. Using the proposed method, we needs only one OFDM symbol to achieve precise channel estimation.

In the high-mobility wireless communication environments, the channel may become time variant even in one OFDM symbol. This will cause the intercarrier interference (ICI) degrading the receiver performance. Many ICI mitigation methods have been proposed [7], [9]-[14]. However, all algorithms require the knowledge of the channel state information. Although some estimation methods for time-variant channel have been proposed [3], [6], [8], [14] there is still much room for performance improvement. We extend the joint time and frequency domain channel estimator proposed for the time-invariant channel to the time-variant channel scenario. It is shown that the estimation performance can be greatly enhanced.

This thesis is organized as follows. First, we will briefly describe the OFDM technique and the wireless communication system of DVB-T in Chapter 2. Then, we will describe the existing channel estimation method in Chapter 3. In Chapter 4, we propose new joint time and frequency domain channel estimators for systems with uniform distributed pilot-subcarriers such as the DVB-T system. In Chapter 5, we propose new joint time and frequency domain channel estimator for time-variant channel in the DVB-T system. Then we evaluate the performance of the proposed algorithms using the simulations and the results are reported in Chapter 6. Finally, the conclusion and future work is summarized in Chapter 7.

Chapter 2

Introduction to OFDM and DVB-T Systems

2.1 OFDM system

As the data rate of a communication system becomes higher and higher, the symbol duration becomes smaller and smaller. The system then becomes more susceptible to loss of information due to impulse noise, signal reflections and other impairments. A remedy for this problem is to split a higher data-rate stream into lower data-rate sub-streams, and this is equivalently to divide the available wideband channel into narrowband subchannels. Each data stream is transmitted with a subcarrier in a subchannel. This approach is called Frequency division multiplexing (FDM). In FDM, the data to be transmitted do not have to be divided equally nor do they have to originate from the same information source.

FDM offers an advantage over single-carrier modulation in terms of the immunity to the narrowband frequency interference. Since the bandwidth of each subchannel is narrow, each transmitted signal in the subchannel experiences flat channel fading. Thus, channel equalization is simplified to a one-tap frequency domain equalizer. And the narrowband interference will only affect one of the frequency subbands. Since the data rate for each subcarrier is lower, the symbol period will be longer, adding some additional immunity to impulse noise and other impairments.

In OFDM systems, these subcarriers are designed orthogonal to allow spectrum overlapping, achieving a high spectral efficiency. As long as the orthogonality is maintained, we can recover each individual subcarrier's signal despite the overlapped spectrum. Figure 2-1 shows the overlapped spectrums of OFDM modulated signals. With the sinc-shaped spectrums, we can guarantee the spectrum of one subcarrier is nulled at other subcarriers'

frequencies. The subcarrier spacing between two neighbor subcarrier can be calculated as $\Delta f = \frac{W}{N} = \frac{1}{T}$. Where W is the bandwidth, N is the number of subcarriers, and T is the symbol period.

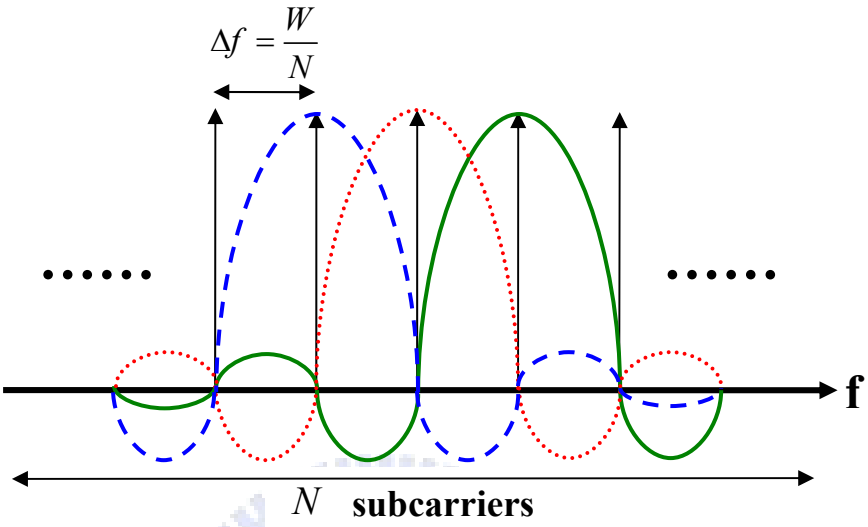

Figure 2-1 Overlapped and orthogonal transmission spectrums

A major problem in most wireless systems are the presence of the multipath channel causing the intersymbol interference (ISI) effect. To combat the problem, a cyclic prefix (CP) whose size is larger than the maximum channel delay spread, is added in front of each OFDM symbol. Due to the CP, the ISI is avoided and the transmitted signal becomes partially periodic, and the effect of the linear convolution with a multipath channel can be translated to a circular convolution at the receiver. Thanks to circular convolution, in the frequency domain the channel effect is simplified to a point-to-point multiplication of the data symbol and channel frequency response. Thus, only a one-tap frequency domain equalizer is required. The generation of the CP is shown in Figure 2-2.

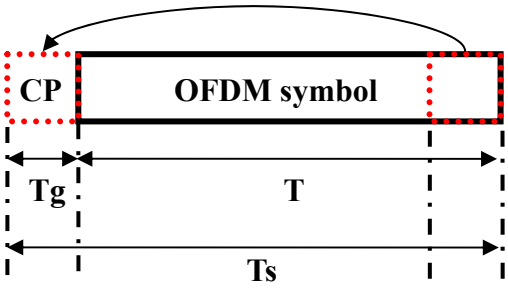

Figure 2-2 Cyclic prefix

2.1.1 Continuous-time OFDM signal model

A typical continuous-time OFDM baseband modulator is shown in Figure 2-3. The input data steam is first split into parallel streams which modulate different subcarriers, and then transmitted simultaneously.

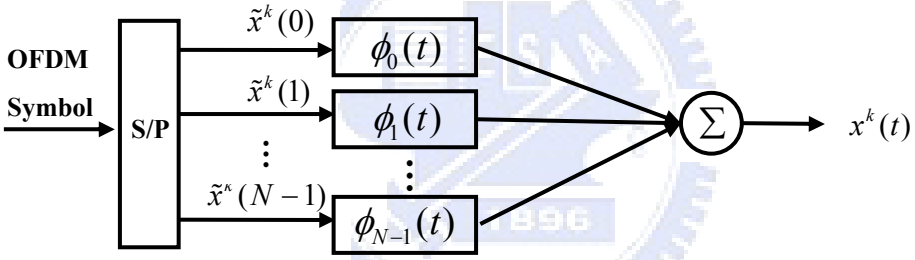

Figure 2-3 Continuous-time OFDM baseband modulator

The i-th modulating subcarrier $\phi_i(t)$ can be represented as

$$\phi_i(t) = \begin{cases} e^{\frac{j2\pi i(t-T_g)}{T}}, 0 \le t \le T_s \\ 0, otherwise \end{cases} \quad , \; T_s = T + T_g \qquad (2.1)$$

where T is the symbol duration excluding CP, T_g is the length of CP and T_s is the total symbol duration. $x^k(i)$ is the transmitted signal, which is a complex number from a set of signal constellation points, at the i-th subcarrier for the k-th OFDM symbol. The modulated baseband signal for the k-th OFDM symbol can be expressed as

$$x^k(t) = \sum_{i=0}^{N-1} \tilde{x}^k(i)\phi_i(t - kT_s) \qquad (2.2)$$

where N is the number of subcarriers. When an infinite sequence of OFDM symbols is

considered, the transmit signal can be represented as

$$x(t) = \sum_{k=-\infty}^{\infty} x^k(t) = \sum_{k=-\infty}^{\infty} \sum_{i=0}^{N-1} \tilde{x}^k(i)\phi_i(t - kT_s) \tag{2.3}$$

And, the received signal $y(t)$ can be expressed as

$$y(t) = \int_{-\infty}^{\infty} h(t,\tau)x(t-\tau)d\tau + w(t) \tag{2.4}$$

where $h(t,\tau)$ denotes the time-variant channel impulse response at time t, and $w(t)$ is the additive white complex Gaussian noise.

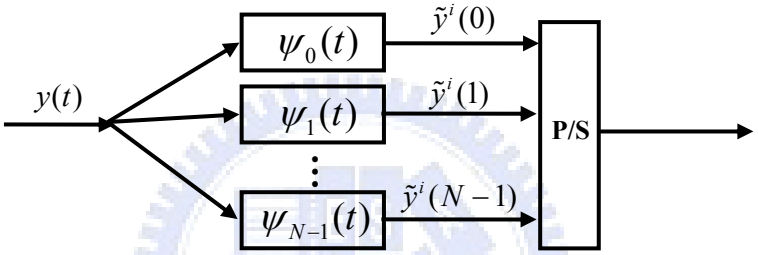

Figure 2-4 Continuous-time OFDM baseband demodulator

A typical continuous-time OFDM baseband demodulator is shown in Figure 2-4, in which $\psi_i(t)$ denotes the matched filter for the i-th subcarrier.

$$\psi_i(t) = \begin{cases} \frac{1}{\sqrt{T}} e^{j2\pi it}, 0 \le t \le T_s \\ 0, otherwise \end{cases} \quad , \; T_s = T + T_g \tag{2.5}$$

where T is the symbol duration excluding CP, T_g is the length of CP and T_s is the total symbol duration. $\tilde{y}^k(i)$ is the demodulated signal at i-th subcarrier for the k-th symbol.

2.1.2 Discrete-time OFDM system model

Consider a particular OFDM symbol, the modulated baseband signal is given by

$$x(t) = \frac{1}{\sqrt{T}} \sum_{i=0}^{N-1} \tilde{x}_i e^{\frac{j2\pi it}{T}}, 0 \le t \le T \tag{2.6}$$

where X_k is the transmitted data symbol. Now, consider a sampled discrete-time system.

Let $t = nT_d$, in which $T_d = \frac{T}{N}$ is the sampling period. Equation (2.6) can be rewritten as

$$x[n] = x(t)\,|_{t=nT_d} = \frac{1}{\sqrt{N}} \sum_{i=0}^{N-1} \tilde{x}_i e^{\frac{j2\pi in}{T}}, 0 \le n \le N-1 \qquad (2.7)$$

For a noise-free system, we can recover the transmit symbols from (2.7) as $\tilde{y}_i$

$$\tilde{y}_i = \frac{1}{\sqrt{N}} \sum_{n=0}^{N-1} x[n] e^{\frac{-j2\pi in}{N}} \qquad (2.8)$$

From (2.7) and (2.8), it is simple to see that modulation/demodulation in OFDM systems can be conducted by inverse discrete Fourier transform (IDFT) and discrete Fourier transform (DFT). In practice, IDFT/DFT is implemented with inverse fast Fourier transform (FFT)/fast Fourier Transform (IFFT). Figure 2-5 shows the OFDM modulator/demodulator.

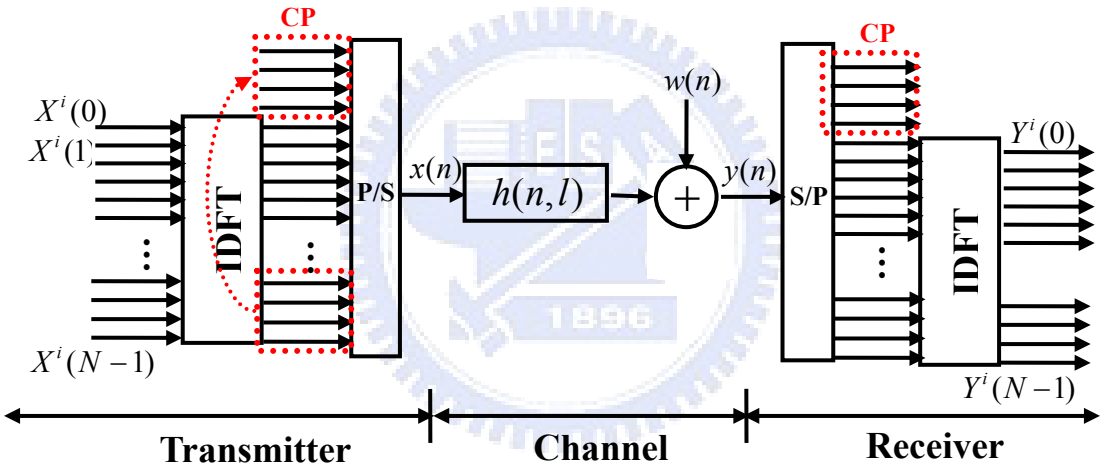

Figure 2-5 Equivalent discrete-time model

The modulation operation can then be described as follows. In the transmitter, the data stream is grouped in blocks of data symbols, called OFDM symbols. Then an IDFT is performed for each data symbol block, and a CP of length T_g is added. Passing the resultant signal through a time-variant multipath channel, we have the received signal as

$$y(n) = \sum_{l=0}^{L-1} h(n,l) x(n-l)_N + w(n) \qquad (2.9)$$

where $h(n,l)$ is the l-th channel path at time instant n, L is the number of channel taps, $(\,.\,)_N$ represents a cyclic shift in the base of N, and $w(n)$ is sampled additive white

complex Gaussion noise with variance σ^2. In the receiver, the received sequence is first split into blocks, and the CP associated with each block is removed. Then, a DFT is performed for each symbol to recover the original data symbols.

As mentioned, carriers in subbands experience flat fading, which reduces equalization to a single complex multiplication per carrier. A matrix equivalent model can be used to obtain a more compact expression. For a single OFDM symbol, the received signal can be represented as

$$\begin{bmatrix} \tilde{y}_0 \\ \tilde{y}_1 \\ \tilde{y}_2 \\ \vdots \\ \tilde{y}_{N_C-1} \end{bmatrix} = \begin{bmatrix} \tilde{h}_{00} & 0 & 0 & \cdots & 0 \\ 0 & \tilde{h}_{11} & 0 & \cdots & 0 \\ 0 & 0 & \tilde{h}_{22} & \cdots & 0 \\ \vdots & \vdots & \vdots & \ddots & \vdots \\ 0 & 0 & 0 & \cdots & \tilde{h}_{(N_C-1)(N_C-1)} \end{bmatrix} \begin{bmatrix} \tilde{x}_0 \\ \tilde{x}_1 \\ \tilde{x}_2 \\ \vdots \\ \tilde{x}_{N_C-1} \end{bmatrix} + \tilde{\mathbf{w}} \tag{2.10}$$

where $[\tilde{x}_0, \tilde{x}_1, \cdots \tilde{x}_{N_c-1}]^T$ is the frequency domain transmitted data vector, $[\tilde{y}_0, \tilde{y}_1, \cdots \tilde{y}_{N_c-1}]^T$ is the frequency domain received data vector, $\mathbf{W}$ is the AWGN noise vector, and $diag\{[\tilde{h}_{00}, \tilde{h}_{11}, \cdots \tilde{h}_{(N_c-1)(N_c-1)}]\}$ are the channel frequency response.

2.1.3 Complete OFDM system

Figure 2-6 shows the block diagram of a complete OFDM system, where the upper path is the transmitter chain, and the lower path is the receiver chain. First, input data are encoded by the channel encoder. The encoded bits are then interleaved and mapped onto QAM constellations. After that, each block of input QAM symbols is modulated onto subcarriers by the IFFT operation, and then a CP is added to form an OFDM symbol. Finally, the baseband OFDM signal is passed to the digital-to-analog (D/A) converter and the RF circuit for transmission. In the receiver, the received signal is first sampled by an analog-to-digital (A/D)

converter, and various receiver operations such as synchronization, channel estimation, demapping and decoding are conducted.

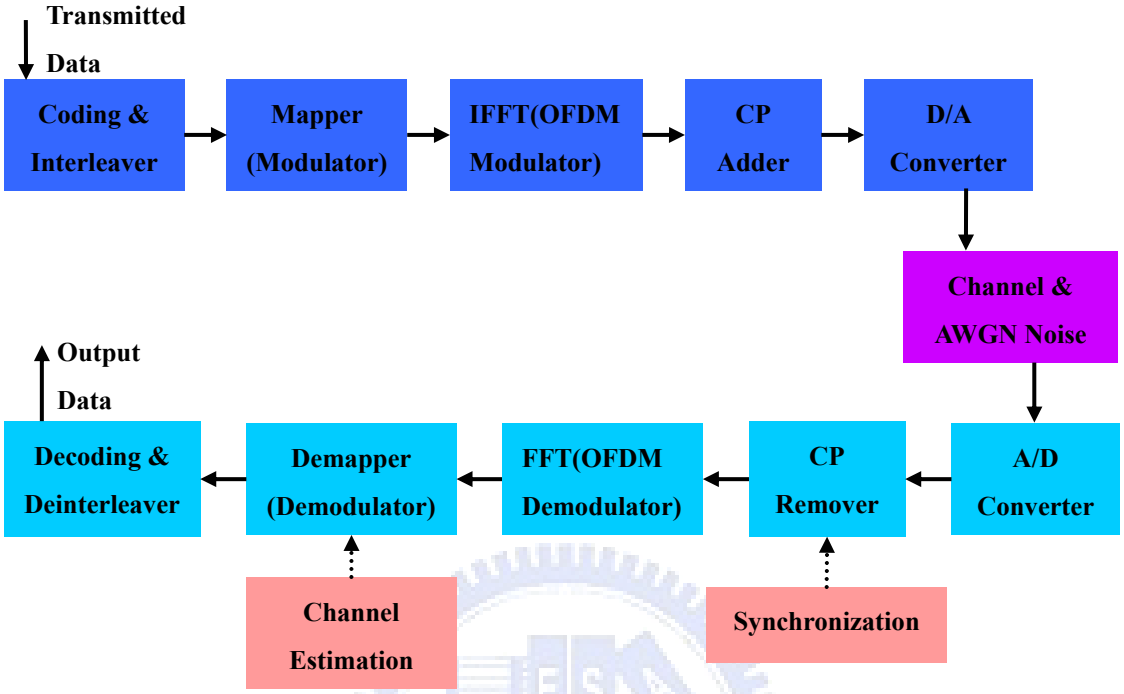

Figure 2-6 Block diagram of OFDM system

2.2 Introduction to DVB-T system

DVB-T uses the coded-OFDM transmission technique; it allows the receiver to cope with strong multipath situations. Within a geographical area, DVB-T also allows a single-frequency networks (SFN) operation, A single-frequency networks is a broadcast network where several transmitters simultaneously send the same signal over the same frequency channel.

2.2.1 System blocks of DVB-T

Figure 2-7 shows the block diagram of a DVB-T transmitter. The operations conducted in the transmitter include randomization, outer encoding, outer interleaving, inner encoding, inner interleaving, mapping, frame adaptation, OFDM modulation, and guard interval insertion.

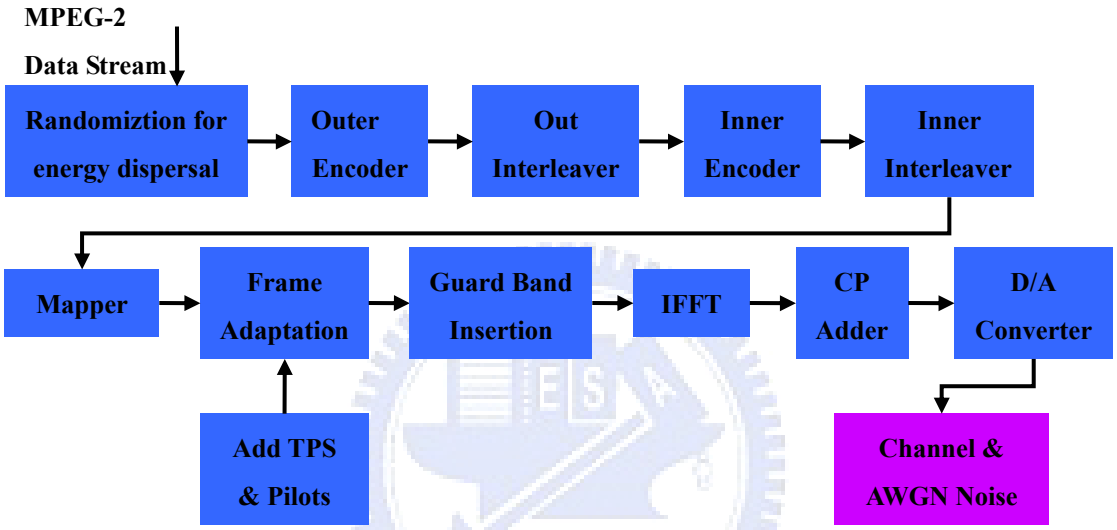

Figure 2-7 The Transmission system block of DVB-T

And the operations conducted in a DVB-T receiver should include time and frequency synchronization, CP removal, OFDM demodulation, frequency equalization, demapping , inner deinterleaving, inner decoding, outer deinterleaving, outer decoding, demultiplexing and source decoding.

2.2.2 The system parameters of DVB-T

A DVB-T channel have a bandwidth of 8,7 or 6MHz. The sampling period is $\frac{7}{48}\mu_s$, $\frac{1}{8}\mu_s$, or $\frac{7}{64}\mu_s$ .There are two different operating modes : 2k and 8k mode. The 2K mode is to split

the bandwidth into 2048 subchannels. It conducts 2048-point IFFT and FFT operations. The actual number of subchannels for data transmission is 1705. The 8K mode is to split the bandwidth into 8192 subchannels. It conducts 8192-point IFFT and FFT operations. The actual number of subchannels for data transmission is 6817. The 2K mode has greater subcarrier spacing which is about 4KHz. This is also indicates that the symbol period is shorter. The subcarrier spacing for the 8K mode is about 1KHz. The CP size can be chosen as $\frac{1}{4}$ or $\frac{1}{8}$ or $\frac{1}{16}$ or $\frac{1}{32}$ of the symbol length.

Parameter	8K mode	2K mode
Number of carriers K	6 817	1 705
Value of carrier number K_{min}	0	0
Value of carrier number K_{max}	6 816	1 704
Duration T_U (note 2)	896 µs	224 µs
Carrier spacing $1/T_U$ (note 1) (note 2)	*1 116 Hz*	*4 464 Hz*
Spacing between carriers K_{min} and K_{max} $(K-1)/T_U$ (note 2)	*7,61 MHz*	*7,61 MHz*
NOTE 1: Values in italics are approximate values. NOTE 2: Values for 8 MHz channels. Values for 6 MHz and 7 MHz channels are given in annex E, tables E.1 and E.2.		

Table 2-1 Parameters of the DVB-T system

DVB-T offers three different modulation schemes which are QPSK, 16QAM, and 64QAM, and it adopts gray mapping for modulation. System parameters for the DVB-T system are summarized in Table 2-1.

2.2.3 The frame structure of DVB-T

Under the 2K mode, a frame is constituted by 68 OFDM symbols. And a super OFDM frame can be constituted by 4 OFDM frames. An OFDM not only transmits information data, but also training data and system parameters which include scattered pilots, continual pilots, and transmission parameter signaling (TPS) data. The pilot signals are used for synchronization and channel estimation.

Figure 2-8 shows the subcarriers for the transmission of data, scattered pilots, continual

pilots, and TPC data.

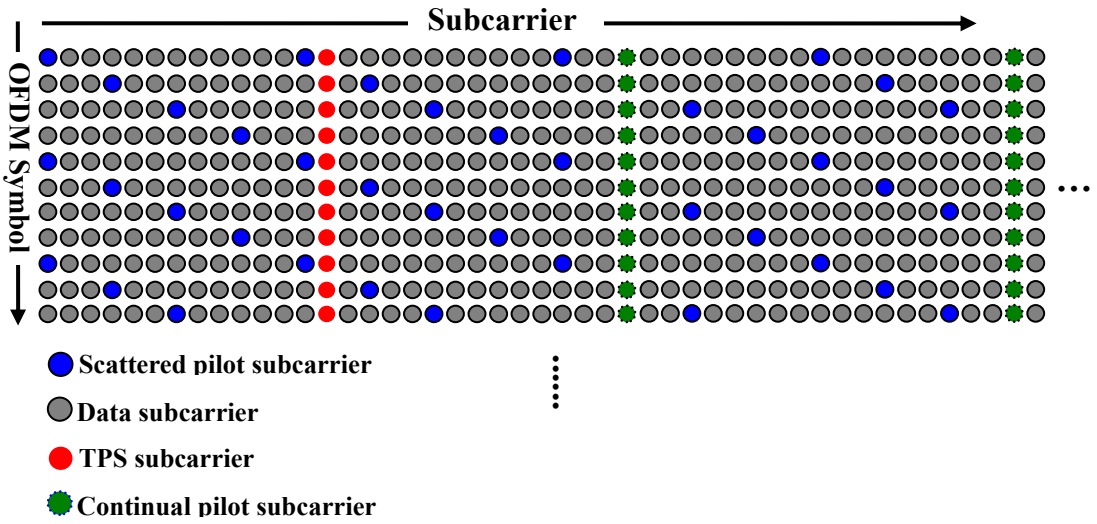

Figure 2-8 Subcarriers allocation

Within each symbol, a scattered pilot is inserted every 12 carriers. Each scattered pilot jumps forward by three carrier positions in the next symbol. So the scattered pilot will be on the same subcarrier positions every four OFDM symbols. The power level of a scattered pilot is boosted by $\frac{4}{3}$, and the BPSK data are sent as scattered pilots. The phase of a BPSK signal, either 0 or π, is decided by the Pseudo Random Binary Sequence (PRBS). The scattered pilots are mainly used to conduction channel estimation. Since the pilots are scattered, the complete channel response must be obtained using interpolation.

Unlike scattered pilots, the positions of the continual pilots are fixed. The power level of the continual pilot is also boosted by $\frac{4}{3}$, and the BPSK data are sent as continual pilots. The phase of a BPSK signal, either 0 or π, is also determined by the Pseudo Random Binary Sequence (PRBS). The continual pilots are mainly used for channel estimation and frequency synchronization. The frequency synchronization is also referred to as automatic frequency control (AFC), i.e. for locking the receive frequency to the transmit frequency. The subcarrier

positions for the continuous pilots are given in Table 2-2.

Continual pilot carrier positions (index number k)	
2K mode	8K mode
0 48 54 87 141 156 192 201 255 279 282 333 432 450 483 525 531 618 636 714 759 765 780 804 873 888 918 939 942 969 984 1050 1101 1107 1110 1137 1140 1146 1206 1269 1323 1377 1491 1683 1704	0 48 54 87 141 156 192 201 255 279 282 333 432 450 483 525 531 618 636 714 759 765 780 804 873 888 918 939 942 969 984 1050 1101 1107 1110 1137 1140 1146 1206 1269 1323 1377 1491 1683 1704 1752 1758 1791 1845 1860 1896 1905 1959 1983 1986 2037 2136 2154 2187 2229 2235 2322 2340 2418 2463 2469 2484 2508 2577 2592 2622 2643 2646 2673 2688 2754 2805 2811 2814 2841 2844 2850 2910 2973 3027 3081 3195 3387 3408 3456 3462 3495 3549 3564 3600 3609 3663 3687 3690 3741 3840 3858 3891 3933 3939 4026 4044 4122 4167 4173 4188 4212 4281 4296 4326 4347 4350 4377 4392 4458 4509 4515 4518 4545 4548 4554 4614 4677 4731 4785 4899 5091 5112 5160 5166 5199 5253 5268 5304 5313 5367 5391 5394 5445 5544 5562 5595 5637 5643 5730 5748 5826 5871 5877 5892 5916 5985 6000 6030 6051 6054 6081 6096 6162 6213 6219 6222 6249 6252 6258 6318 6381 6435 6489 6603 6795 6816

Table 2-2 Subcarrier index for continual pilots

TPS data give information about the current transmission status, including the frame number, QAM size, coding rate, CP size etc. The TPS data are sent through TPS pilots whose locations are given in Table 2-3. The complete TPS information is broadcasted over 68 symbols in one OFDM frame and carried in 68 bits. To lower the error rate, DBPSK is used for the modulation scheme.

2K mode	8K mode
34 50 209 346 413 569 595 688 790 901 1073 1219 1262 1286 1469 1594 1687	34 50 209 346 413 569 595 688 790 901 1073 1219 1262 1286 1469 1594 1687 1738 1754 1913 2050 2117 2273 2299 2392 2494 2605 2777 2923 2966 2990 3173 3298 3391 3442 3458 3617 3754 3821 3977 4003 4096 4198 4309 4481 4627 4670 4694 4877 5002 5095 5146 5162 5321 5458 5525 5681 5707 5800 5902 6013 6185 6331 6374 6398 6581 6706 6799

Table 2-3 Subcarrier index for TPS pilots

Table 2-4 shows the number of subcarriers allocated for data, scattered pilots, continual pilots, and TPS pilots.

Mode / Carriers	2K Mode	8K Mode
total carriers	2048	8192
active carriers	1705	6817
scattered carriers	142/131	568/524
continual carriers	45	177
TPS carriers	17	68

Table 2-4 The number of pilot carriers for 2K and 8K mode

Chapter 3

Joint Time and Frequency Domain Channel Estimation

Consider a specific subcarrier of subcarrier index i in an OFDM symbol. We have $\tilde{y}_i = \tilde{h}_i \tilde{x}_i + \tilde{w}_i$, where $\tilde{y}_i$ is the frequency-domain received signal, $\tilde{x}_i$ is the frequency-domain transmitted signal, $\tilde{h}_i$ is the channel frequency response, and $\tilde{w}_i$ is the corresponding AWGN noise. It is apparent that if both $\tilde{x}_i$ and $\tilde{y}_i$ are known, $\tilde{h}_i$ can then be estimated. Let $\tilde{y}_p = \tilde{h}_p \tilde{x}_p + \tilde{w}_p$ where the subscript denotes the subcarrier in a pilot position. We can estimate the channel response in the pilot position, denoted by $\hat{\tilde{h}}_p$, as:

$$\hat{\tilde{h}}_p = \frac{\tilde{y}_p}{\tilde{x}_p} \tag{3.1}$$

In the DVB-T system, there is a scattered pilot every 12 subcarriers, as shown in Figure 3-1.

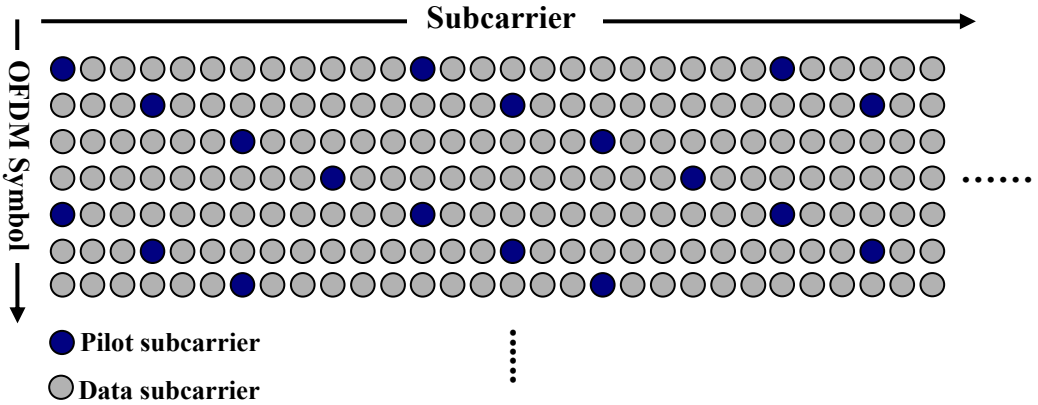

Figure 3-1 Scattered pilots in DVB-T

To obtain the channel responses in data subcarriers, we need to conduct interpolation. In the next two sections, we will describe two simple interpolation techniques, one-dimensional

and two-dimensional interpolation methods. If the number of pilot subcarriers is not sufficiently large, the interpolated result may not be satisfactory. In this case, the time-domain channel estimation requiring fewer pilots may be used. In the last section, we will describe a recently developed method, a joint time and frequency domain channel estimation method.

3.1 Interpolation methods

The classical approach for channel interpolation is to construct a polynomial interpolator fitting responses in known samples. The polynomial interpolator can be formulated in various ways, such as the power series, Lagrange interpolation and Newton interpolation. These various forms are mathematically equivalent and can be transformed from one to another. We will use the power series as our polynomial interpolator. Assume that there are some samples available, denoted as $\{\tilde{x}(f_o), \tilde{x}(f_1), \cdots, \tilde{x}(f_N)\}$, where $\tilde{x}(f_n)$ is the amplitude of the signal $\tilde{x}(f)$ at frequency f_n. The polynomial with order N, passing through the $N+1$ known samples, can be written in a power series form as

$$\tilde{x}(f) = P_N(f) = e_0 + e_1 f + e_2 f^2 + \cdots + e_N f^N \qquad (3.2)$$

where $P_N(f)$ is a polynomial of order N, and e_k's are the polynomial coefficients. An example of the polynomial interpolator is shown in Figure 3-2. As we can see from Figure 3-2 that the fitted polynomial is unique.

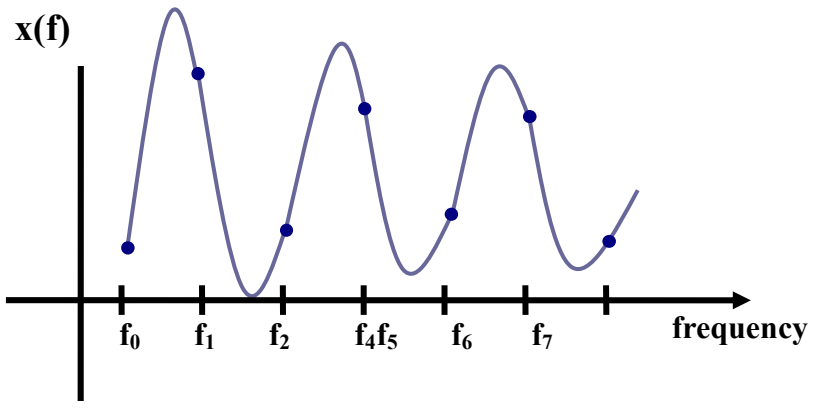

Figure 3-2 Polynomial interpolator

For all the signals in pilot subcarriers, we can write (3.2) into a matrix form.

$$\begin{bmatrix} \tilde{x}(f_{m_o}) \\ \tilde{x}(f_{m_1}) \\ \vdots \\ \tilde{x}(f_{m_{M-1}}) \end{bmatrix} = \begin{bmatrix} 1 & f_{m_o} & f_{m_o}^{\,2} & \cdots & f_{m_o}^{\,N-1} \\ 1 & f_{m_1} & f_{m_1}^{\,2} & \cdots & f_{m_1}^{\,N-1} \\ \vdots & \vdots & \vdots & \ddots & \vdots \\ 1 & f_{m_{M-1}} & f_{m_{M-1}}^{\,2} & \cdots & f_{m_{M-1}}^{\,N-1} \end{bmatrix} \begin{bmatrix} e_0 \\ e_1 \\ \vdots \\ e_{N-1} \end{bmatrix} \tag{3.3}$$

The matrix form can be expressed as:

$$\tilde{\mathbf{x}} = \mathbf{F}\mathbf{e} \tag{3.4}$$

where $\tilde{\mathbf{x}} = \left\{\tilde{x}(f_{m_0}), \tilde{x}(f_{m_1}), \cdots, \tilde{x}(f_{m_{M-1}})\right\}^T$, $m_i, 0 \le i \le M-1$ and M is the number of pilot signals, $\mathbf{F}$ is the matrix at the right hand side of (3.3), $\mathbf{e} = \left\{e_0, e_1, \cdots, e_{N-1}\right\}^T$ is the polynomial coefficients, and N is the order of polynomial interpolator. Note that N is usually small since the computational complexity of the interpolation is proportional to N. In practice, the linear (N=1) and quadratic (N=2) and cubic (N=3) interpolator is often used.

Since M is usually larger than N, the system in (3.4) is overdetermined. So, the polynomial coefficients can be solved by the least-squares (LS) algorithm. With the LS algorithm [5], we then have

$$\mathbf{e} = (\mathbf{F}^{\mathbf{H}}\mathbf{F})^{-1}\mathbf{F}^{\mathbf{H}}\tilde{\mathbf{x}} \tag{3.5}$$

The simplest polynomial interpolator is the first-order (i.e, the linear) polynomial interpolator. However, the performance is usually not satisfactory. The cubic interpolator being a third-order polynomial interpolator is widely used in real-world applications. It can have better performance while the computational complexity is acceptable.

The one dimensional linear interpolation method uses one OFDM symbol and simply conducts the interpolation for the channel responses in data subcarriers. In order to obtain better performance, we can change the linear interpolation to cubic interpolation in the one dimensional interpolation method. We will discuss the performance of the linear and cubic interpolation methods in the simulation chapter.

The main advantage of the one-dimensional interpolation approach is that it needs only one OFDM symbol and the requirement for the memory size is small. Also, the computational complexity of the one-dimensional linear interpolation is low. However, due to the low density of scattered pilots, this method cannot achieve satisfactory performance in general. To solve this problem, we will introduce the two-dimensional linear interpolation method below.

Since the positions of the scattered pilots are the same for every 4 OFDM symbols, we can conduct interpolation in the temporal domain. The two-dimensional interpolation method uses consecutive OFDM symbols to conduct interpolation both in the frequency and temporal domains. With this approach, the pilot density can be effectively increased. Figure 3-3 shows the linear interpolation in temporal domain. In the figure, the channel responses of the middle OFDM symbol are those we want to estimate (the dotted block). We first interpolate linearly the responses in the temporal domain. The interpolated responses can be seen as pseudo pilots which can be used in the interpolation in the frequency domain. As we can see, the pilot density is increased from $\frac{1}{12}$ to $\frac{1}{3}$.

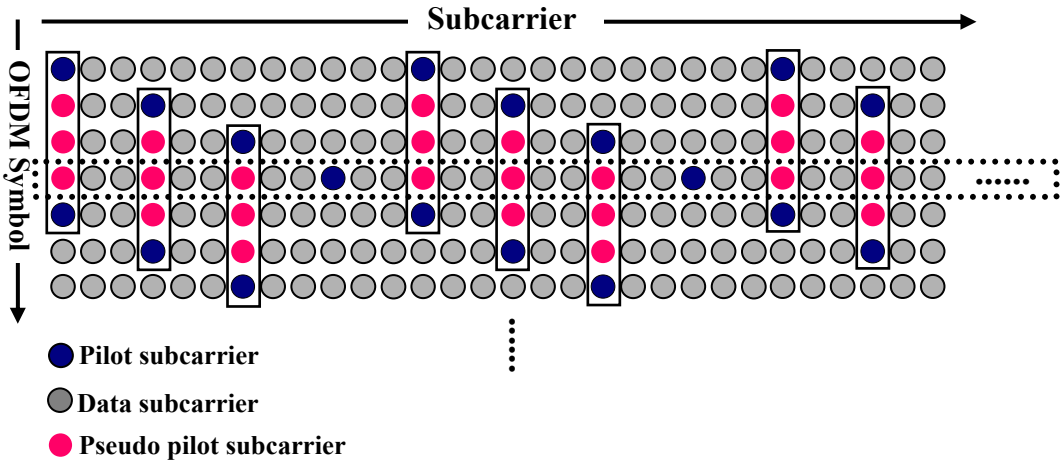

Figure 3-3 Interpolation in temporal domain

Since the scattered pilot density is raised to $\frac{1}{3}$, we can obtain the channel responses in frequency domain more accurately. The two-dimensional interpolation method is better than the one-dimensional interpolation method when the channel responses are highly variant. But the two-dimensional interpolation method needs 7 OFDM symbols to conduct interpolation in both frequency domain and temporal domain. The computational complexity is high and the required memory is large.

In order to obtain better performance, we can also use the cubic interpolation to replace the linear interpolation. The performance comparison of the one-dimensional interpolation methods and the two-dimensional interpolation methods will be shown in the simulation chapter. We will also discuss the performance comparison of the linear and cubic interpolation methods in the simulation chapter.

3.2 Joint time and frequency domain channel estimation

Due to limited pilot signals, channel estimation using the frequency domain interpolation will be degraded when the channel delay spread is large. In this case, the interpolation method may not be able to recover the frequency response, even with the two-dimensional

interpolation method.

In typical wireless channels, the delay spread may be large, but the number of non-zero taps is small. Since the taps of channel are usually fewer, the unknowns of channel responses in time domain are less than those we need to estimate in the frequency domain. As a result, it is possible for the time-domain approach to have better performance under the same number of pilots. In this subsection, we will describe a newly developed joint time/frequency domain channel estimation method [3], [4].

The first step of the method is to use a two-dimensional interpolation method, with the linear interpolation in the time domain and cubic interpolation in the frequency domain, to obtain the channel responses in the frequency domain. Then, we transform the channel response into the time-domain to obtain the time-domain channel response. One example of the time-domain channel responses is shown in Figure 3-4.

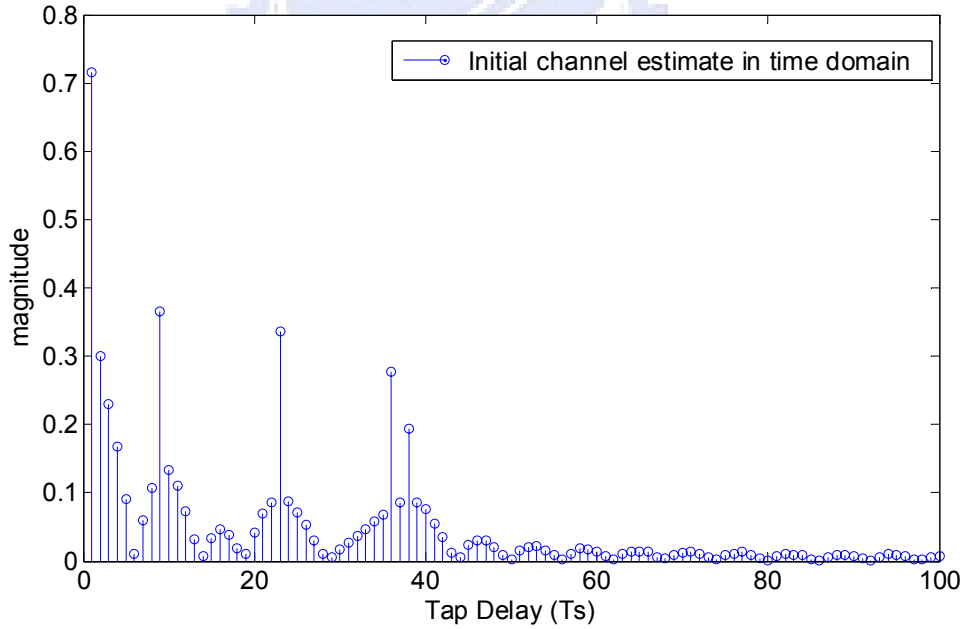

Figure 3-4 The initial time-domain channel estimate

As we can see, there are only a few significant channel taps. Then, the method locates those taps and estimates their values. The tap searching and the magnitude estimation

algorithms are described in following 3.2.1 and 3.2.2. A more efficient recursive procedure is finally described in 3.3.3.

3.2.1 Tap searching algorithm

As we can see from Figure 3-4, there is a low-pass signal embedded in the channel response. So some fake taps will occur near the significant taps. In this subsection, we outline an iterative method that can solve the problem.

If we take a first-order differentiation to the channel response, the low-pass signal will be removed. The differentiation operation is given by $d[k] = \hat{h}[k+1] - \hat{h}[k]$ ($\hat{h}[k+1]$, $\hat{h}[k]$ is the tap value of different taps). With a threshold, we can find the significant tap by this method. However, if there are consecutive significant taps, the operation can not find all the taps.

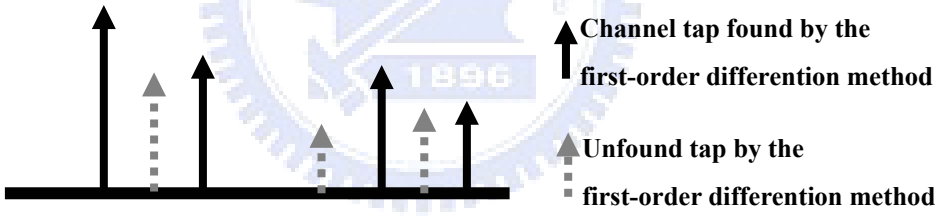

Figure 3-5 Channel tap searching method by the first-order differentiation method

Another method to find the taps is simply to compare the magnitude of a tap with a threshold. If it is larger than the threshold, the tap is deemed as a peak (significant tap). Apparently, some fake taps occurring near the significant taps will also be detected as significant taps.

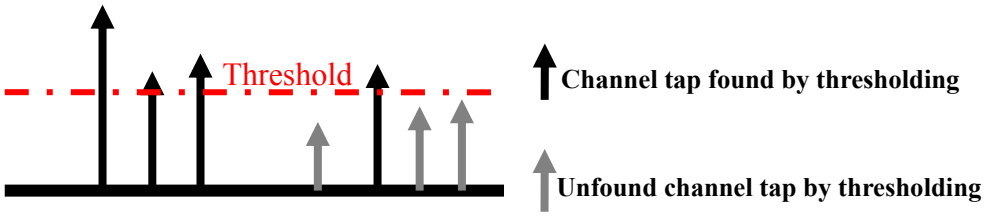

Figure 3-6 Channel tap searching by thresholding

We can combine the aforementioned two methods to obtain a more reliable method. The idea is to locate the taps in an iterative manner, rather than in one short. Figure 3-7 shows the iterative procedure. First, locate significant the channel taps by the first-order differentiation method (Figure 3-7-(a)) with a high threshold value (Figure 3-7-(b)). In this case, smaller or consecutive significant taps may not be detected. Using the estimation method described in the next subsection, we can estimate the magnitude of those located taps. Then, subtract the channel response formed by the located channel taps from the original channel response (Note that this operation is conducted in the frequency domain). We can then have a residual channel response. Thus, we can transform the response to the time-domain and conduct the tap searching algorithm again (the threshold can be made smaller). Repeat this process until no significant taps are detected.

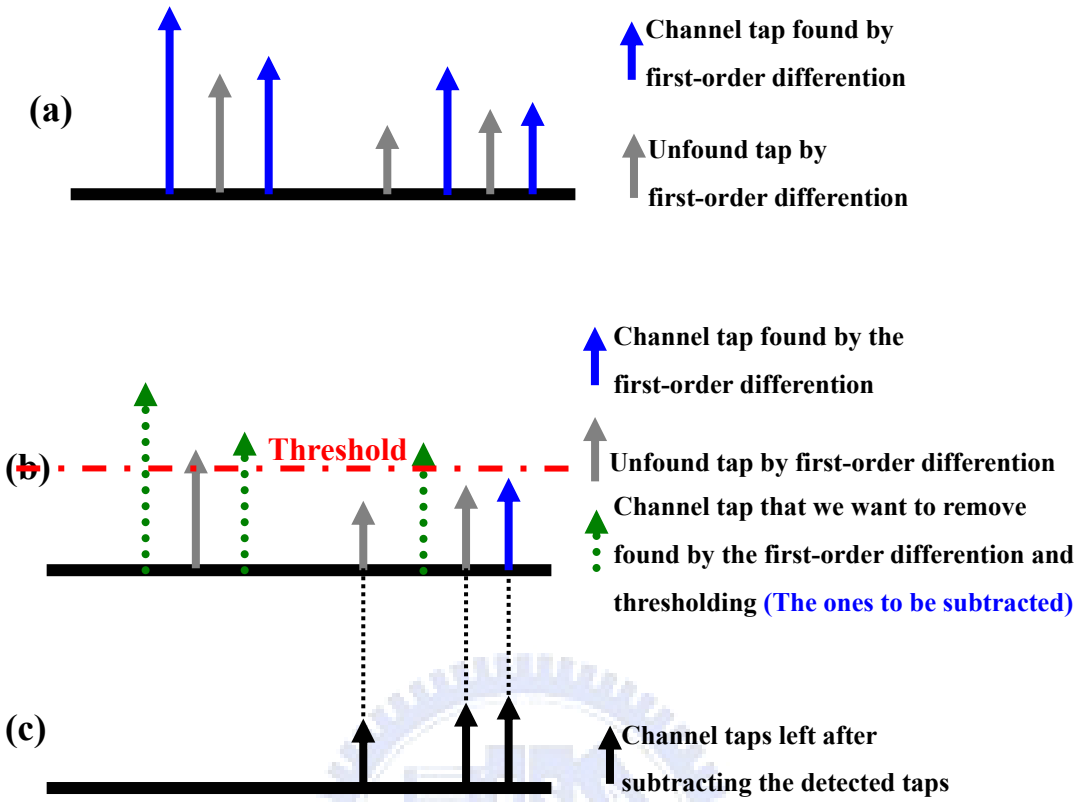

Figure 3-7 The procedure of the significant tap searching method

3.2.2 LS channel estimator

For a subcarrier of subcarrier index i in a particular OFDM symbol, the signal transmitted and passed through the channel can be expressed as $\tilde{y}_i = \tilde{h}_i \tilde{x}_i + \tilde{w}_i$. Let N be the FFT size. We can write the equation for all subcarriers. We have

$$\begin{bmatrix} \tilde{y}_0 \\ \tilde{y}_1 \\ \tilde{y}_2 \\ \vdots \\ \tilde{y}_{N_C-1} \end{bmatrix} = \begin{bmatrix} \tilde{h}_{00} & 0 & 0 & \cdots & 0 \\ 0 & \tilde{h}_{11} & 0 & \cdots & 0 \\ 0 & 0 & \tilde{h}_{22} & \cdots & 0 \\ \vdots & \vdots & \vdots & \ddots & \vdots \\ 0 & 0 & 0 & \cdots & \tilde{h}_{(N_C-1)(N_C-1)} \end{bmatrix} \begin{bmatrix} \tilde{x}_0 \\ \tilde{x}_1 \\ \tilde{x}_2 \\ \vdots \\ \tilde{x}_{N_C-1} \end{bmatrix} + \tilde{\mathbf{w}} \tag{2.10}$$

The LS channel estimator minimize the following squared errors:

$$\left\| \tilde{\mathbf{y}} - \hat{\mathbf{H}}_{LS} \tilde{\mathbf{x}} \right\|^2 \tag{3.6}$$

Where $\tilde{\mathbf{y}} = \left[\tilde{y}_0, \tilde{y}_1, ... \tilde{y}_{N-1} \right]^T$ is the frequency domain received signal vector, $\tilde{\mathbf{x}} = \left[\tilde{x}_0, \tilde{x}_1, ... \tilde{x}_{N-1} \right]^T$ is the frequency domain transmitted signal vector. Using pilot subcarriers, we can have the LS channel estimator minimize the following squared errors:

$$\left\| \tilde{y}_p - \hat{\mathbf{H}}_{p,LS} \, \tilde{x}_p \right\|^2 \tag{3.7}$$

where $\tilde{\mathbf{y}}_p = \left[\tilde{y}_{m_0}, \tilde{y}_{m_1}, ... \tilde{y}_{m_{M-1}} \right]^T$ is the frequency domain received vector on pilot locations, $\tilde{\mathbf{x}}_p = \left[\tilde{x}_{m_0}, \tilde{x}_{m_1}, ... \tilde{x}_{m_{M-1}} \right]^T$ is the frequency domain transmitted pilot signal vector ($m_i, 0 \le i \le M-1$ is pilot location and M is the number of pilots). With the LS algorithm, we then have

$$\hat{\mathbf{H}}_{p,LS} = \left(\tilde{\mathbf{x}}_p{}^H \tilde{\mathbf{x}}_p \right)^{-1} \tilde{\mathbf{x}}_p{}^H \tilde{\mathbf{y}}_p \tag{3.8}$$

The LS channel estimator also has a time-domain version. The signal transmitted and passed through the channel can be expressed as $\tilde{y}_i = \tilde{x}_i \mathbf{gh} + \tilde{w}_i$ where $\tilde{y}_i$ is the frequency domain received signal, $\tilde{x}_i$ is the frequency domain transmitted signal, $\mathbf{h}$ is the channel response in time domain, $\mathbf{g}$ is a row of the DFT matrix, $\tilde{w}_i$ is noise. Considering all pilot subcarriers, we can have

Let

$$\tilde{\mathbf{X}}_{D,p} = \begin{bmatrix} \tilde{x}_{m_0} & 0 & 0 & \cdots & 0 \\ 0 & \tilde{x}_{m_1} & 0 & \cdots & 0 \\ 0 & 0 & \tilde{x}_{m_2} & \cdots & 0 \\ \vdots & \vdots & \vdots & \ddots & \vdots \\ 0 & 0 & 0 & \cdots & \tilde{x}_{m_{M-1}} \end{bmatrix} \tag{3.9}$$

$$\begin{bmatrix} \tilde{y}_{m_0} \\ \tilde{y}_{m_1} \\ \tilde{y}_{m_2} \\ \vdots \\ \tilde{y}_{m_{M-1}} \end{bmatrix} = \tilde{\mathbf{X}}_{D,p} \begin{bmatrix} e^{-j2\pi\frac{m_0*0}{N}} & e^{-j2\pi\frac{m_0*1}{N}} & \cdots & e^{-j2\pi\frac{m_0*(L-1)}{N}} \\ e^{-j2\pi\frac{m_1*0}{N}} & e^{-j2\pi\frac{m_1*1}{N}} & \cdots & e^{-j2\pi\frac{m_1*(L-1)}{N}} \\ e^{-j2\pi\frac{m_2*0}{N}} & e^{-j2\pi\frac{m_2*1}{N}} & \cdots & e^{-j2\pi\frac{m_2*(L-1)}{N}} \\ \vdots & \vdots & \ddots & \vdots \\ e^{-j2\pi\frac{m_{M-1}*0}{N}} & e^{-j2\pi\frac{m_{M-1}*1}{N}} & \cdots & e^{-j2\pi\frac{m_{M-1}*(L-1)}{N}} \end{bmatrix} \begin{bmatrix} h_0 \\ h_1 \\ \vdots \\ h_{L-1} \end{bmatrix} + \tilde{\mathbf{w}} \tag{3.10}$$

Then, we can have a similar formulation as that in (3.7). The LS channel estimator in time domain minimizes the following squared errors:

$$\left\| \tilde{\mathbf{y}}_p - \tilde{\mathbf{X}}_{D,p} \mathbf{G} \hat{\mathbf{h}}_{LS} \right\|^2 \tag{3.11}$$

where **G** is the DFT matrix. And the LS solution to the time domain LS channel estimation is then:

$$\hat{\mathbf{h}}_{LS} = \left(\mathbf{G}^H \tilde{\mathbf{X}}_{D,p}{}^H \tilde{\mathbf{X}}_{D,p} \mathbf{G} \right)^{-1} \mathbf{G}^H \tilde{\mathbf{X}}_{D,p}{}^H \tilde{\mathbf{y}}_p \tag{3.12}$$

where $\tilde{\mathbf{X}}_{D,p}$ is a diagonal matrix containing pilot signals. The time-domain LS method requires $O(L^3)$ arithmetic operations where L is the maximum channel delay spread. If L is large, the required computational complexity is high. If we only consider $\tilde{L}$ significant taps in which $\tilde{L}$ is much less than L, the computational complexity can be reduced. For example, if we only consider h_0 and h_{L-1}, we only have to use the first and last column of $\mathbf{G}$ and the matrix to inverse in (3.11) becomes a 2×2 matrix.

We then have

$$\begin{bmatrix} \tilde{y}_{m_0} \\ \tilde{y}_{m_1} \\ \tilde{y}_{m_2} \\ \vdots \\ \tilde{y}_{m_{M-1}} \end{bmatrix} = \tilde{\mathbf{X}}_{D,p} \begin{bmatrix} e^{-j2\pi\frac{m_0*0}{N}} & e^{-j2\pi\frac{m_0*1}{N}} & \cdots & e^{-j2\pi\frac{m_0*(L-1)}{N}} \\ e^{-j2\pi\frac{m_1*0}{N}} & e^{-j2\pi\frac{m_1*1}{N}} & \cdots & e^{-j2\pi\frac{m_1*(L-1)}{N}} \\ e^{-j2\pi\frac{m_2*0}{N}} & e^{-j2\pi\frac{m_2*1}{N}} & \cdots & e^{-j2\pi\frac{m_2*(L-1)}{N}} \\ \vdots & \vdots & \ddots & \vdots \\ e^{-j2\pi\frac{m_{M-1}*0}{N}} & e^{-j2\pi\frac{m_{M-1}*1}{N}} & \cdots & e^{-j2\pi\frac{m_{M-1}*(L-1)}{N}} \end{bmatrix} \begin{bmatrix} h_0 \\ h_1 \\ \vdots \\ h_{L-1} \end{bmatrix} + \tilde{\mathbf{w}} \tag{3.13}$$

$$\tilde{\mathbf{y}}_p = \tilde{\mathbf{X}}_{D,p}\mathbf{G'h} + \tilde{\mathbf{w}} \tag{3.14}$$

where $\mathbf{G'}$ is a reduced DFT matrix contain the columns within the dotted block shown in (3.13). In an extreme case, we can only estimate a channel tap at one iteration. The computational complexity is further reduced since the DFT matrix is degenerated to a vector.

3.2.3 Iterative joint time and frequency domain channel estimation

In previous subsections, we have described a low-complexity yet high-performance channel estimator. We called this a joint time and frequency domain channel estimator. The estimation flowchart is shown in Figure 3-8, and the related procedure is summarized as follows: (Notice LSE represents LS error and R represents the LSE threshold)

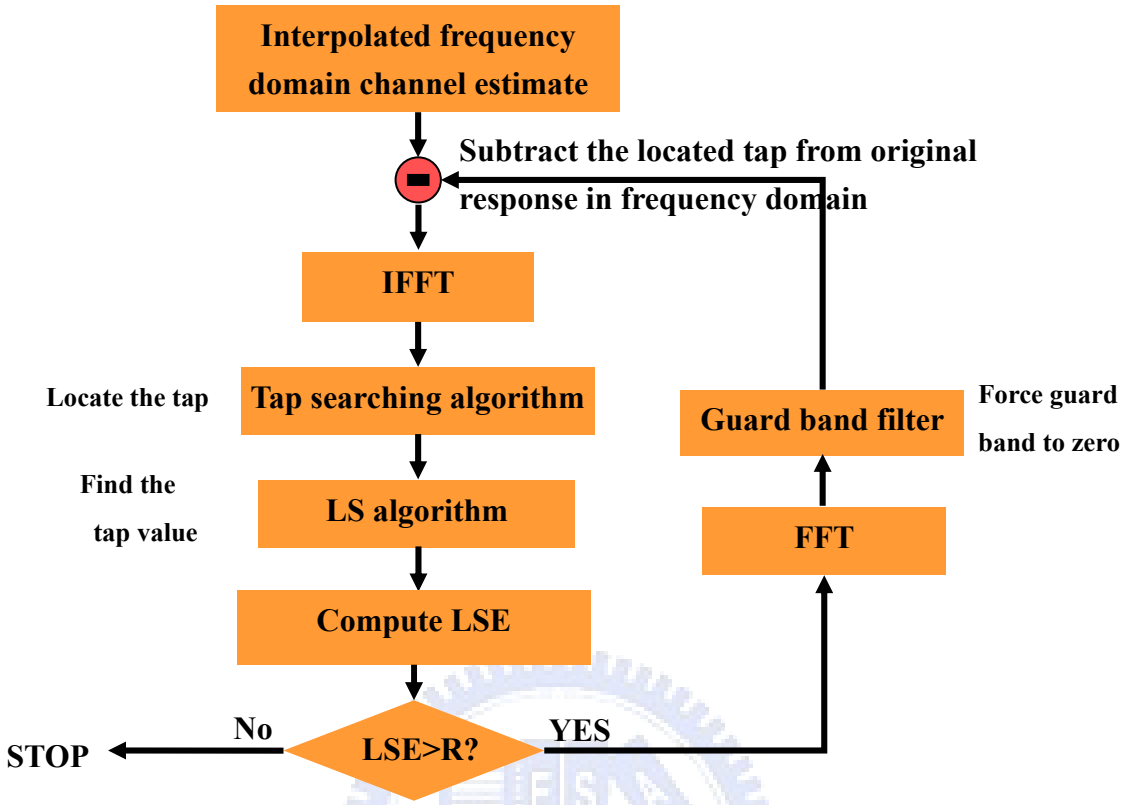

Figure 3-8 Iterative joint time and frequency domain channel estimation

STEP 1: Use the two-dimensional interpolation method to obtain the initial frequency-domain channel estimate.

STEP 2: Conduct the IFFT of the frequency domain channel estimate to obtain the time-domain channel estimate.

STEP 3: Find the tap with the maximum value (the threshold of tap search is iteration dependent) and use the LS algorithm to estimate the response of the maximum tap.

STEP 4: Compute the least-squares error (LSE) of all located and estimated taps with a threshold (LSE threshold). If the LSE is greater than the LSE threshold, Conduct the FFT of the channel response estimated in the time domain (with the located and estimated taps) and subtract the resultant response from the

channel response estimated in the previous iteration. Note that we have to null the responses in the guard band region. Then, go to **STEP 2**. If the LSE is smaller than the LSE threshold, stop the iteration.

Note that the LSE is a good indicator telling us when to stop the searching. In other words, it can avoid the redundant operations and reduce the computational complexity for the LS algorithm. In mobile environments, the channel tap positions may change with time suddenly. The LSE can also help us to check whether the channel taps' positions have changed or not. The iterative operation not only locates the channel taps more precisely, but also requires less computational complexity for the LS algorithm.

As seen, an FFT/IFFT operation is required for each iteration and this will increase the computational complexity significantly. This can be remedied with the following approach. The main idea is to transfer the response-subtraction operation in the frequency domain to the time domain. Note that the operation conducted in the frequency domain is windowing and subtraction, which can be transferred into convolution and subtraction in the time domain. The function to be convolved is the sinc filter. In practice, the sinc filter may be difficult to implement. So, we may replace it by some lowpass filter. Since the number of detected taps is expected to be small, the required computational complexity of the convolution operation will not be significant. The modified flowchart of the modified scheme is shown in Figure 3-9.

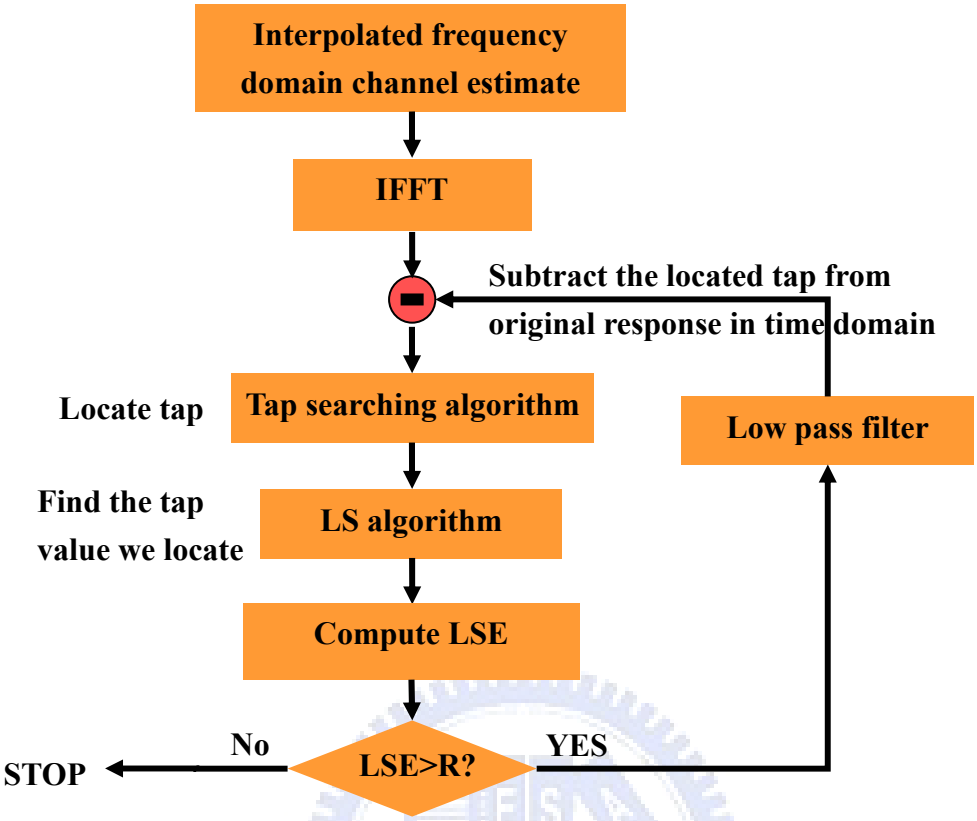

Figure 3-9 Joint time and frequency domain channel estimation with time domain filtering

3.2.4 Improved joint time and frequency domain channel estimation

One problem associated with method described above is that the estimation of a significant tap may be affected by the other significant taps. An improved method was then proposed in [4]. The main idea is to conduct a re-estimation for all significant taps. After all the taps has been estimated, we can conduct the re-estimation of one tap by subtracting the channel response contributed from the other taps and using the LS method shown above. Using the approach, the estimation accuracy can be improved. The procedure is summarized below. Figure 3-10 show the flowchart of the method. Note that the channel taps can be re-estimated more than one time until the satisfactory result is obtained.

STEP 1: With the channel estimation method described above, we get $\tilde{L}$ significant taps. We can order h_k 's and start from the maximum one.

STEP 2: With the FFT operation, we obtain the frequency response for a subcarrier of the other taps (the subcarrier index is i), denoted as $\tilde{h}_i$ ' .

STEP 3: For a specific pilot position, say *p*, we can subtract the response contributed by $\tilde{h}_p$ ' . Let the transmitted pilot signal be $\tilde{x}_p$ and the received pilot signal be $\tilde{y}_p$. We then have

$$\tilde{y}_p ' = \tilde{y}_p - \tilde{x}_p \tilde{h}_p ' \tag{3-14}$$

STEP 4: Using all $\tilde{y}_p$'s, we can conduct the LS channel estimator to re-estimate the designated tap.

STEP 5: Check if all taps are re-estimated. If no, then select the next largest tap and go to **STEP 2**.

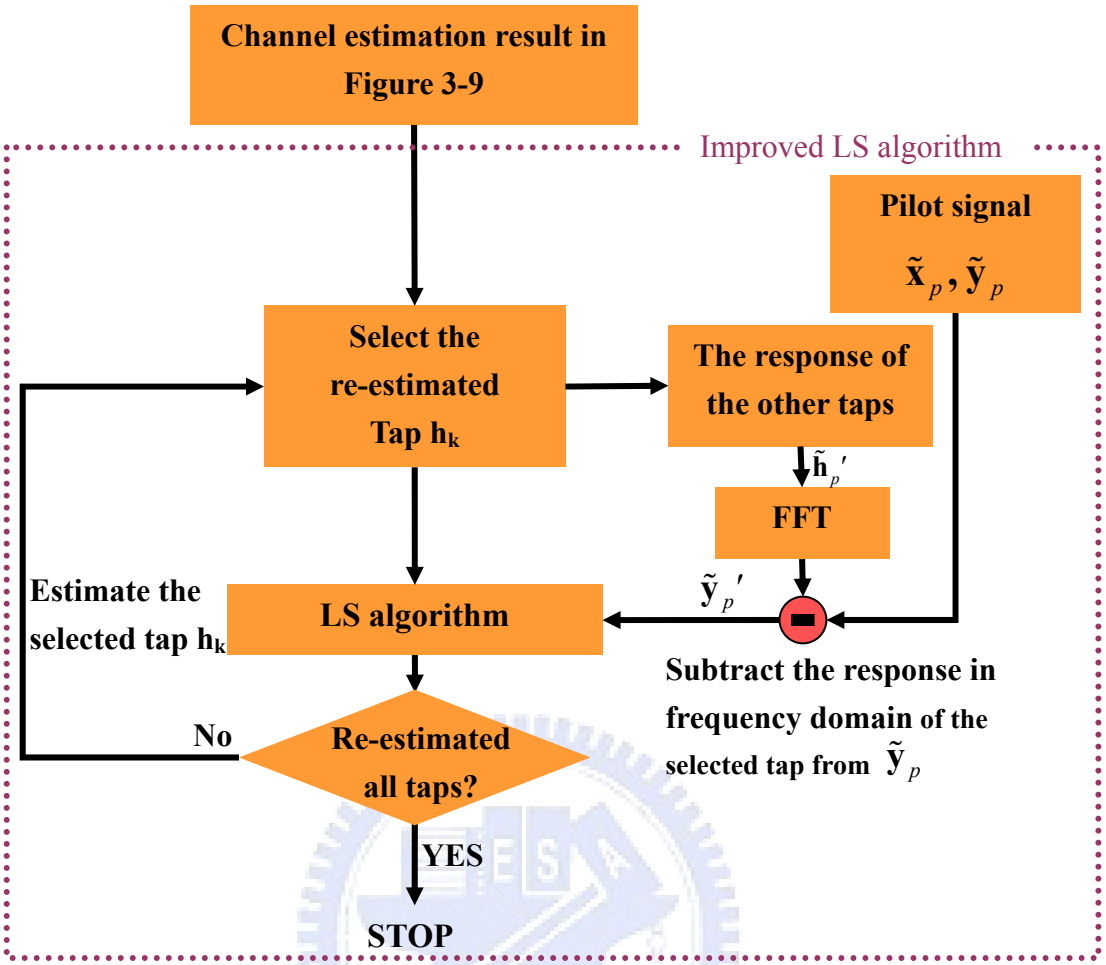

Figure 3-10 Improved joint time and frequency domain channel estimation

The dotted block is the improved LS algorithm which will be used in the next Chapter. It contains the iterative channel tap searching and improved LS operation.

Chapter 4

Proposed Joint Time and Frequency Channel Estimator for DVB-T Systems

As discussed in Chapter 3, the channel estimation with a two-dimensional interpolation requires 7 OFDM symbols. The computational complexity is high and the memory to store the OFDM symbols is large. For one symbol in the first three or the last three OFDM symbols (in a frame), we cannot collect 7 symbols (three before and three after) for channel estimation and the performance in these areas will degrade. Another problem is that the channel cannot have large variation in the selected 7 OFDM symbols. Thus, the methods described in Chapter 3 are only applicable in slow-fading environments. In this chapter, we will propose a new method to overcome this problem for DVB-T systems.

The proposed method uses only one OFDM symbol to conduct the channel estimation. As known, the pilot density is low in DVB-T systems. Direct estimation will result in poor performance. Our idea is to use decisions as pseudo pilots, which will be referred to as pseudo pilots in the sequel, such that the pilot density can be effectively enhanced. The proposed algorithm can be summarized as follows.

1. Obtain an initial channel estimate with one OFDM symbol.
2. Use the estimate with the LS algorithm to conduct data detection.
3. Use some detected data as pseudo pilots and conduct channel re-estimation.
4. Use the re-estimated channel with the LS algorithm to conduct data re-detection.

In the following subsection, we will describe each step in details.

4.1 Initial channel estimation with one OFDM symbol

As discussed in Chapter 3, we also conduct an initial frequency-domain channel estimate by pilot information and transfer it to time domain. However, we do not conduct interpolation. Since the pilot density is low, the initial estimate is not accurate. As known, the pilot subcarriers are uniformly spread in the frequency domain. If we only estimate the channel response with those in pilot subcarriers, it is equivalent to conduct a sampling on the frequency-domain channel response. As a result, the time-domain channel response will be periodic.

As known, sampling a frequency domain signal makes its time-domain signal periodic. If the sampling rate is not high enough, aliasing will occur. Figure 4-1 shows the aliasing problem of the channel estimation.

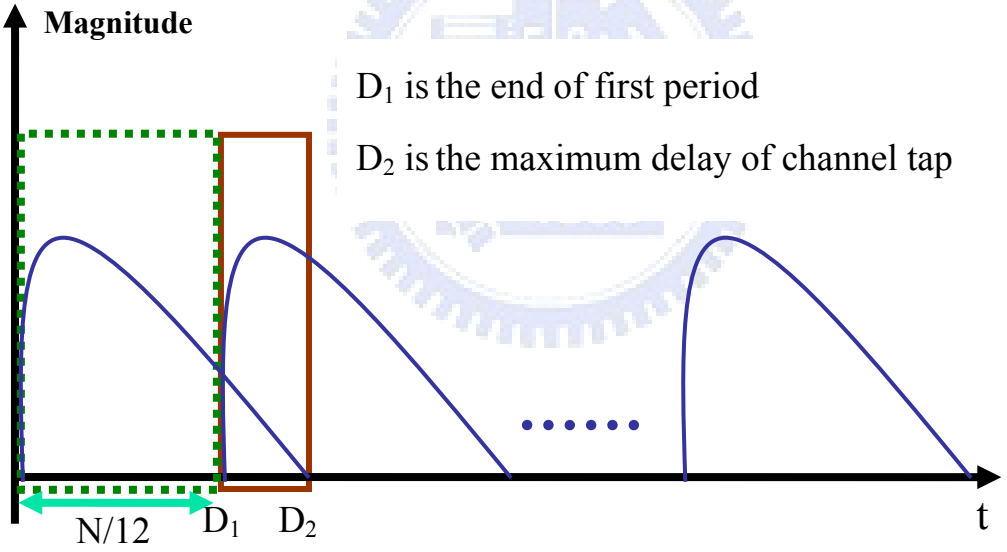

Figure 4-1 Aliasing in initial channel estimation

Let the sampling period be K. It is simple to see that the period of the time- domain channel estimate, denoted with D_1, will be N/K. In our case, K=12. Consider the 2K mode, we have N=2048. Thus, we know that the period of the time-domain channel estimate is about 171 ($\frac{2048}{12} \cong 170.67 \cong 171$). Let the maximum delay spread of the channel be D_2.

Thus, we can see that aliasing occurs when $D_2 \geq D_1$.

4.2 Tap search and estimation for initial channel estimate

As shown, there may be aliasing in the initial channel estimate. The channel response in the aliasing area cannot be recovered. Thus, we conduct tap searching only in the non-aliased area, and combine the LS methods described in Figure 3-10 and 3-8 to conduct the initial estimate. Given an initial frequency-domain channel estimate, Figure 4-2 shows the LS channel estimation method we use. Note that the method is essentially a successive interference cancellation (SIC) approach. For easy reference, we call the LS channel estimation method in Figure 4-2 as a SIC-LS method.

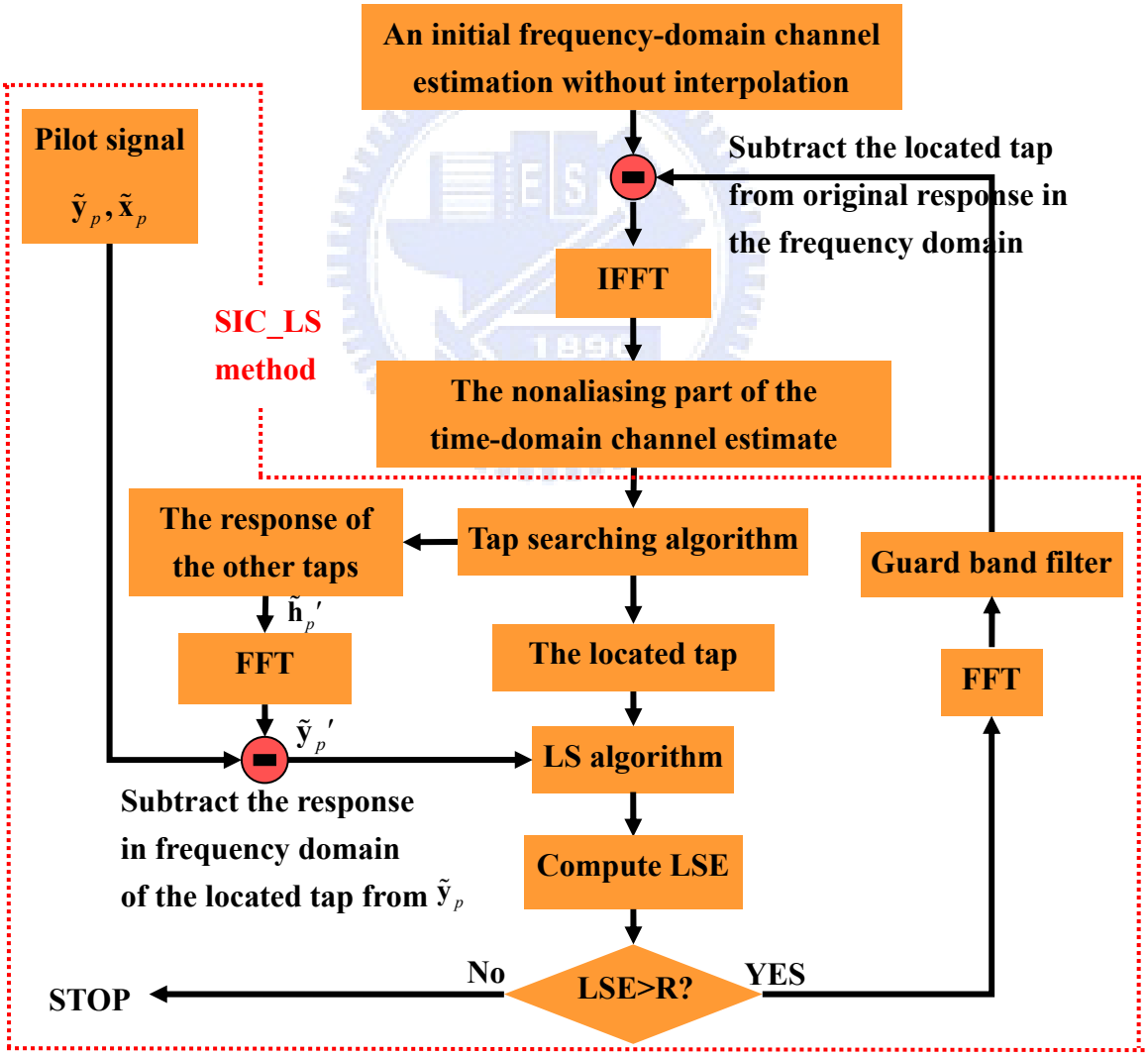

Figure 4-2 The SIC-LS channel estimation method

The LSE threshold here should be higher since the response in the initial channel estimate is not complete (some taps may be in the aliasing area). Figure 4-3 shows the complete block diagram of the proposed initial channel estimation method and the procedure is summarized in the following.

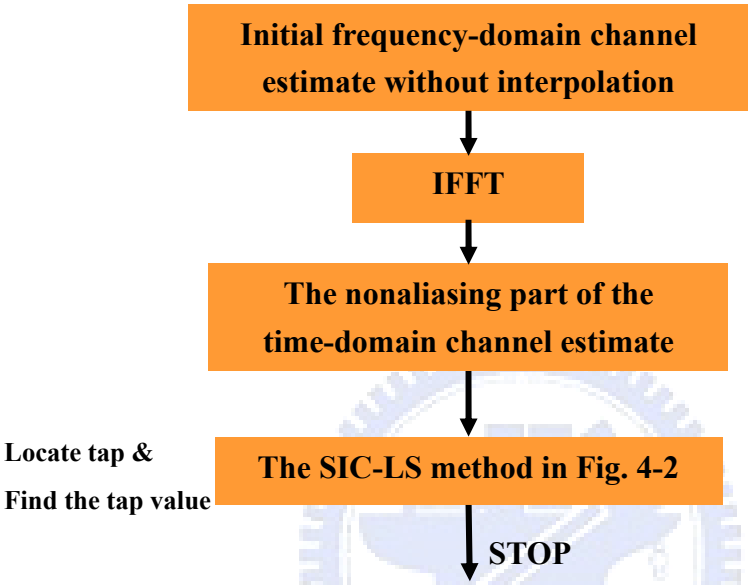

Figure 4-3 Proposed initial channel estimation method

STEP 1: Use pilot subcarriers to obtain an initial frequency-domain channel estimate.

STEP 2: Conduct the IFFT of the frequency-domain estimate to obtain the time-domain channel estimate.

STEP 3: Find the non-aliasing area of the initial time-domain channel estimate and use the SIC-LS method in Figure 4-2 to locate and identify the channel taps in the area.

Using the channel estimation method outlined above, we can obtain an initial time-domain channel estimate. Note that the channel response may be incomplete. However, since the aliasing area is not large and the power of the channel taps in the area may be small,

we can use the estimate to recovery data with an acceptable error probability. Let $\hat{\tilde{x}}_i$ ($\tilde{y}_i = \tilde{h}_i \tilde{x}_i + \tilde{w}_i$, $\frac{\tilde{y}_i}{\hat{\tilde{h}}_i} = \hat{\tilde{x}}_i$) be the estimated symbol for a subcarrier in subcarrier index i .We have $\tilde{y}_i = \tilde{h}_i \tilde{x}_i + \tilde{w}_i$, and then $\hat{\tilde{x}}_i = \frac{\tilde{y}_i}{\hat{\tilde{h}}_i}$ where $\tilde{y}_i$ is the received frequency domain signal at a subcarrier in subcarrier index i , $\hat{\tilde{h}}_i$ is the estimated channel response at that subcarrier, $\tilde{x}_i$ is the transmitted frequency domain signal, and $\hat{\tilde{x}}_i$ is the corresponding estimated signal. To recover the original transmit symbol, we can make decision based on $\hat{\tilde{x}}_i$. Let the detected data be $\hat{\tilde{x}}_{de}$. Figure 4-4 shows the procedure of data detection.

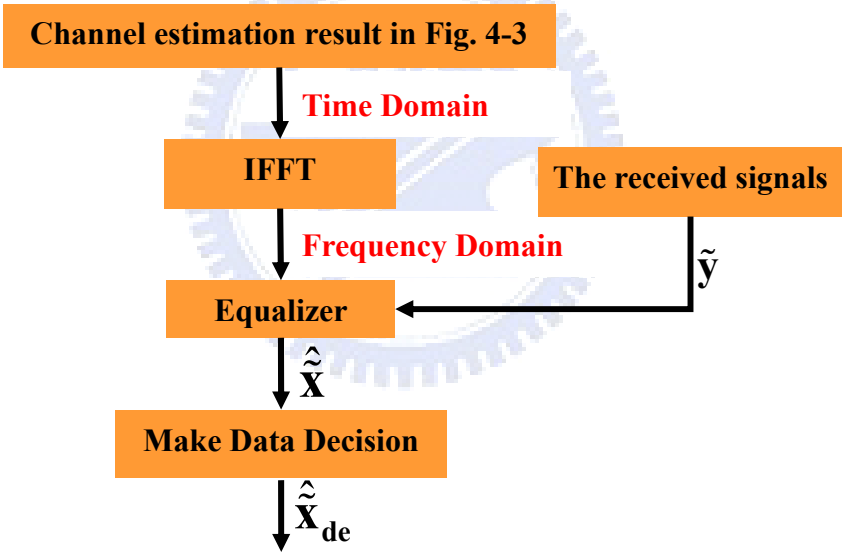

Figure 4-4 The block diagram of data detection

4.3 Proposed channel estimation with pilots and decisions

We now can use the detected data: $\hat{\tilde{x}}_{de}$'s as pseudo pilots and conduct the channel estimation of the whole channel. Note that as long as aliasing does not occur in the time-domain channel estimate, we can recovery the whole channel response. As a result, no all the decisions are needed to conduct the channel re-estimation. If we let the CP size be

1/8 of the FFT size (256 for the 2K mode), a pilot density of 1/6 will avoid the aliasing at the time-domain channel estimate. The performance comparison for different pilot densities will be shown in simulations. If we use all decisions (in all subcarriers) as pseudo pilots, we may have the best performance. However, the computational complexity is also highest. To compare the channel estimation result in Chapter 3, we may let the pilot density be 1/3. With the pseudo pilots, we can use the channel estimation method described above again. Note that if the pilot density is 1/3, the period in the time-domain channel estimate is $D_1 = \frac{Nc}{3} \cong 683$ which is actually much longer than the CP size. Thus, we can assume that all the channel taps will be in the non-aliasing region. Note that one can conduct the channel re-estimation more than once.

Since the guard band does not have any data, theoretically the channel response cannot be obtained. However, if we can conduct the time-domain channel estimate properly, we can obtain the frequency-domain channel response in the guard band. To obtain better result, when conducting channel re-estimation, we can insert the guard band response of the previous estimated channel. To have better performance, we do the guard band insertion only when the frequency domain channel estimation is accurate enough which means that all the channel taps of the time-domain channel estimate are in the nonaliasing area. Let the preset number of the channel re-estimation be N_{set} and the actual number of re-estimation be N_{re}. We let N_{re}=0 for the initial channel estimation. In this iteration, the guard band insertion will not be performed. When $N_{re} \neq 0$, all the channel taps are in the nonaliasing region and we can activate the guard band insertion scheme. The effect of the guard band insertion will also be discussed in the simulation chapter.

Figure 4-5 shows the block diagram of the proposed joint time and frequency domain channel estimation scheme.

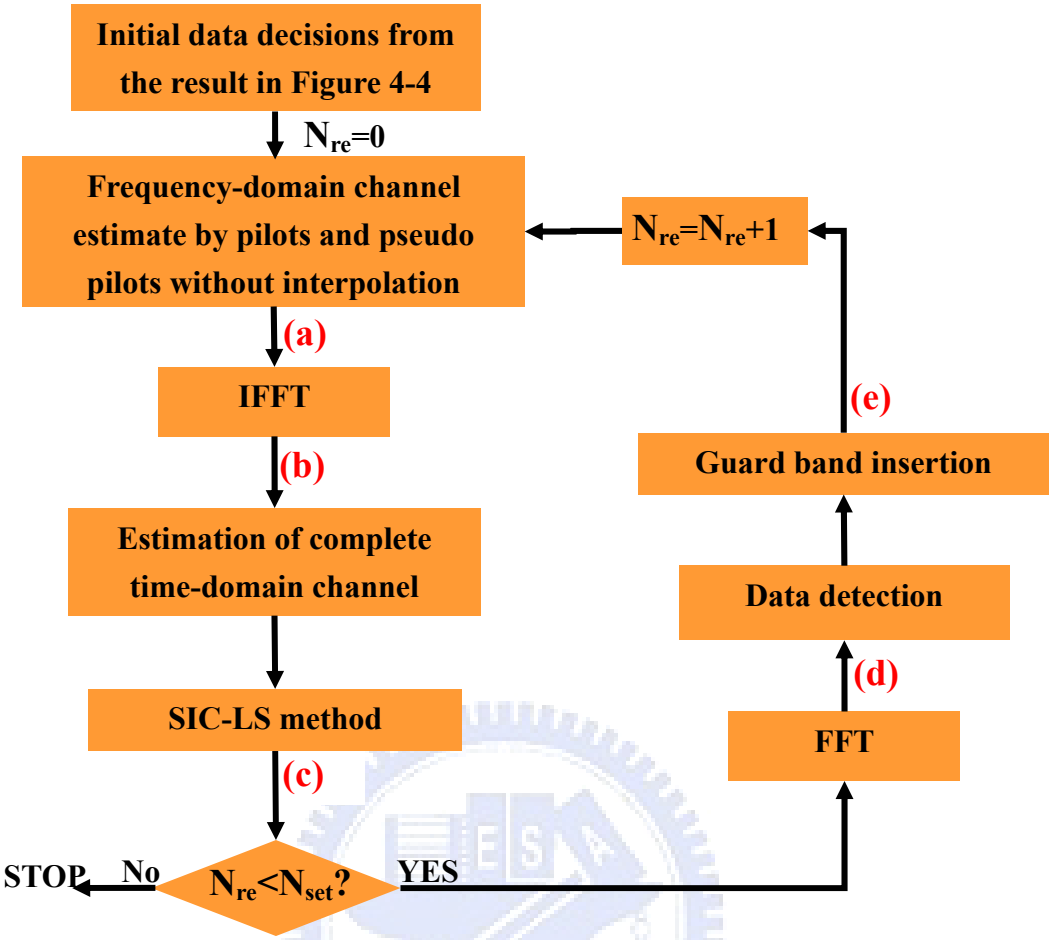

Figure 4-5 Proposed joint time and frequency domain channel estimation method

The operations can be summarized below:

STEP 0: Use the algorithm in Figure 4-4 to obtain initial data decisions.

STEP 1: Use pilot and pseudo pilot subcarriers (without interpolation) to obtain a frequency-domain channel estimate.

STEP 2: Conduct the IFFT of the frequency domain channel estimation to the time domain.

STEP 3: Find the nonaliasing region of the time-domain channel estimation.

STEP 4: Use the proposed SIC-LS method shown in Figure 4-2 to locate and identify significant taps.

STEP 5: If $N_{re}<N_{set}$, go to **STEP 6**. Otherwise, the iteration stops.

STEP 6: Conduct the FFT operation for the identified time-domain channel to obtain its

frequency domain response.

STEP 7: Estimate the transmitted QAM symbols at designated pilot subcarriers and make decisions.

STEP 8: Insert channel response in the guard band using the channel response estimated.

STEP 9: Let $N_{re}= N_{re} +1$ and go to **STEP 1** with a updated new channel estimate.

Notice that there are two differences between the SIC-LS block in Figure 4-5 and Figure 4-2. The block of "LSE>R?" in Figure 4-2 is changed to "Re-estimate all taps?" since all the channel taps have been initially detected here. As a result, we only have to check if all the taps have been re-estimated. Also, the block "Compute LSE" in Figure 4-2 is not necessary. Besides, the pseudo pilots can also be used in the SIC-LS method. Figure 4-6 shows a graphic example showing the channel response at each of the steps outlined above. Figure 4-6 (a) is the sketch of the channel estimate by the pilots and pseudo pilots. Figure 4-6 (b) is a sketch of the time-domain channel estimate. Figure 4-6 (c) is the channel taps after refined by the proposed LS algorithm. Figure 4-6 (d) is the frequency-domain channel estimate of Figure 4-6 (c). Figure 4-6 (e) is the sketch of the guard-band insertion (every 3 subcarriers).

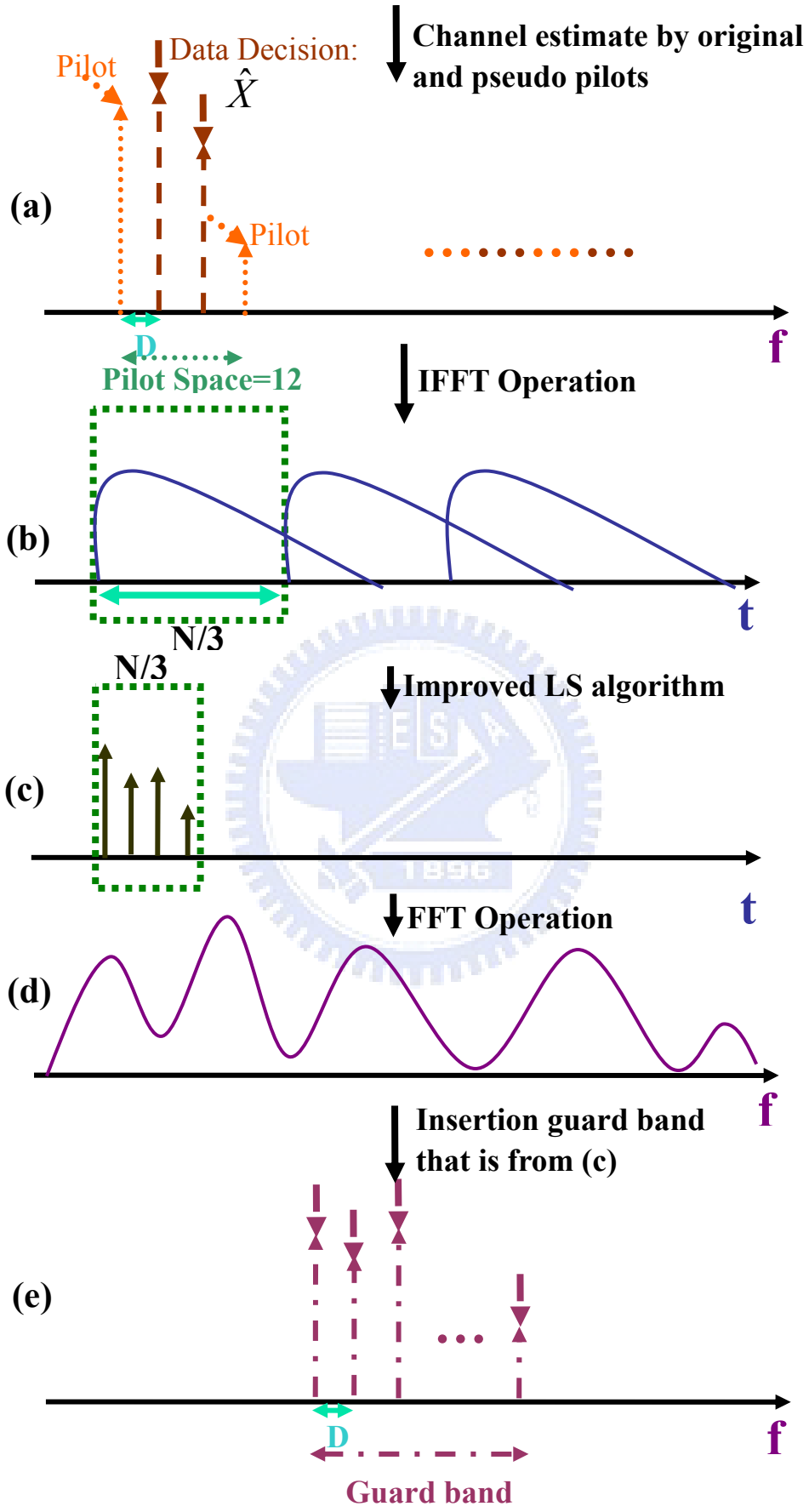

Figure 4-6 The channel response at each of the steps in Figure 4-5

When the number of pilots is not large enough, the proposed channel estimation scheme is still an effective way to obtain accurate channel estimate. We will have more discussions and simulation results in Section 4.4.

4.4 SIC-LS method with weighting

The method of channel estimation of joint pilot and decision data can be used not only in the DVB-T system but also in other OFDM systems. As long as the pilot assignment is periodic, the proposed method can be used. However, if the number of pilot subcarriers is not sufficient, the performance of the proposed method will be affected. For example, if the total number of subcarriers is 512, the CP is 64 (1/8 of 512) and the pilot density is still 1/12. The total number of the pilots used in this system is 39 which is much less that 142 used in the DVB-T system. As a result, the performance will be degraded in this system. In order to solve the problem of low pilot density, we use the pseudo pilots to conduct the SIC-LS method in Figure 4-5. However, the performance may be still not satisfactory. The problem comes from the decisions, i.e., erroneous decisions. Using erroneous decisions as pilots will degrade the performance of the SIC-LS channel estimation method. One way to alleviate the problem is to use the SIC-LS method with weighting (SIC-WLS), giving more weights to the decisions with higher correct probability. We first consider the LS problem without SIC. From (3.14), we have the received pilot signals as

$$\tilde{\mathbf{y}}_{p'} = \tilde{\mathbf{X}}_{D,p'}\mathbf{G}'\mathbf{h} + \tilde{\mathbf{w}} \tag{4.1}$$

where $p' = j_i, 0 \le j \le J-1$ is pilot location and J is the number of pilots

The weighted LS channel estimation can be formulated as

$$\left\| \mathbf{D}(\tilde{\mathbf{y}}_{p'} - \tilde{\mathbf{X}}_{D,p'}\mathbf{G}'\hat{\mathbf{h}}_{p',wls}) \right\|^2 \tag{4.2}$$

where $\tilde{\mathbf{y}}_{p'}$ and $\tilde{\mathbf{X}}_{D,p'}$ are the same as (4.1), $\hat{\mathbf{h}}_{p',wls}$ is the solution of the weighted LS channel estimate, and $\mathbf{D} = diag(d_0, d_1, \cdots, d_{J-1})$ is a diagonal weighing matrix. From (4.1),

we have

$$\mathbf{D}\tilde{\mathbf{y}}_{p'} = \mathbf{D}\tilde{\mathbf{X}}_{D,p'}\mathbf{G}'\mathbf{h} + \mathbf{D}\tilde{\mathbf{w}} \tag{4.3}$$

Thus, from (3.12), we can get the weighted LS solution as

$$\hat{\mathbf{h}}_{p',wls} = \left(\mathbf{G}^H \tilde{\mathbf{X}}_{D,p'}{}^H \mathbf{D}^H \mathbf{D}\tilde{\mathbf{X}}_{D,p'}\mathbf{G}\right)^{-1} \mathbf{G}^H \tilde{\mathbf{X}}_{D,p'}{}^H \mathbf{D}^H \mathbf{D}\tilde{\mathbf{y}}_{p'} \tag{4.4}$$

As mentioned, the weighted LS algorithm put more weights on the decisions having high probability of correctness. How to actually determine $\mathbf{D}$ will be the main concern. We proposed two methods to do the job as discussed in the following paragraphies.

The first method uses the estimated symbols to decide the values in $\mathbf{D}$. We use the BPSK scheme as our illustration example. Let $\hat{\tilde{x}}_i$ ($\tilde{y}_i = \tilde{h}_i \tilde{x}_i + \tilde{w}_i$, $\frac{\tilde{y}_i}{\hat{\tilde{h}}_i} = \hat{\tilde{x}}_i$) be the estimated symbol for a subcarrier in subcarrier index i. Since we know the decision of $\hat{\tilde{x}}_i$ is either 1 or –1. Thus, we can use the distance between the estimated transmitted signals $\hat{\tilde{\mathbf{x}}}$ and 1 or -1 to as a measure of the correct probability of the decision and then the corresponding weight. Figure 4-7 shows the proposed first method for the determination of the weight of a decision.

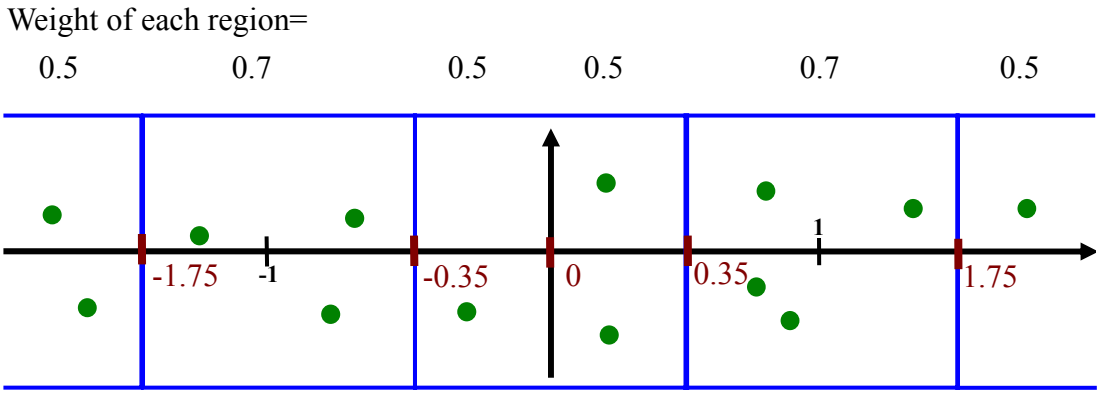

Figure 4-7 The proposed first weighting method

As shown in the figure, we partition the estimated signal value into various design regions and assign a weight for signal falling into the region. We assume that the distance

between the estimated transmitted signals $\hat{\tilde{\mathbf{x}}}$ and 1/ -1 is only affected by noise. So, when the distance between the estimated transmitted signal $\hat{\tilde{x}}_i$ and 1/ -1 is large, we can assume this estimated transmitted signal $\hat{\tilde{x}}_i$, the symbol transmitted in subcarrier index i, is affected by noise more seriously. The probability of making wrong decision for the symbol is high so we can put less weight on the decision. On the contrary, when the distance between the estimated transmitted signal $\hat{\tilde{x}}_i$ and 1/-1 is small, we can assume $\hat{\tilde{x}}_i$ is affected by noise lightly. Then we can give more weight for the decision. Notice that the weight of a pilot subcarrier is always 1 (the maximum value of the weights). Figure 4-7 shows one example of the weighting policy.

When the noise level is high, the received signal can cross the decision boundary. As a result, the decision is wrong/right even the distance is small/large. So the performance of this method may not be satisfactory even the averaged SNR is high. It is simple to see that for a subcarrier, the received signal-to-noise (SNR) ratio is the main factor determining the decision error rate. If the SNR is high/low, the error rate will be low/high. We then propose another method for the weight assignment. We assume that the SNR of each subcarrier is known or can be estimated. Similar to the previous approach, we separate the SNR value into various regions and assign a weight for signal falling into a specific region. Notice that we can let the SNR be represented in a dB scale. Also, the weight for the pilot subcarrier is always 1 (the maximum value of the weight). Figure 4-8 shows one example of the weighting policy of the proposed second weighting method. Notice that the weight mapping may be different for different modulation schemes.

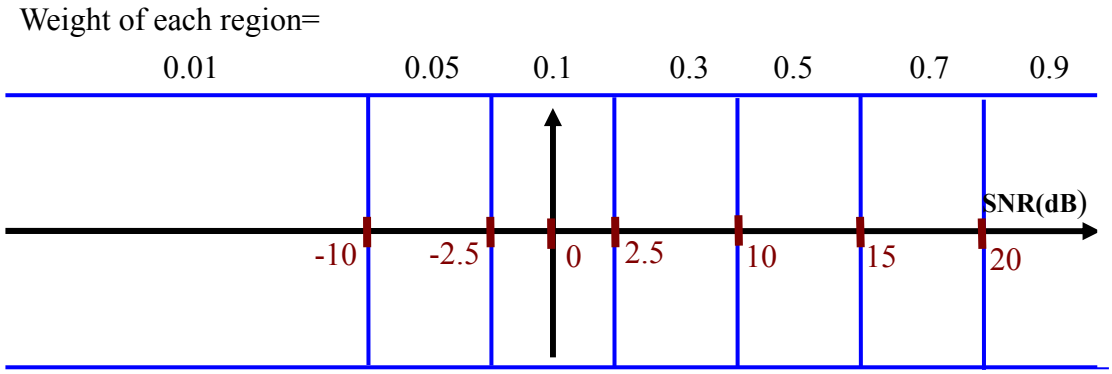

Figure 4-8 The proposed second weighting method

We can apply the WLS method in the proposed SIC-LS method discussed in Figure 4-5. Simulations show that the performance of the proposed SIC-WLS channel estimation method is satisfactory under the BPSK and QPSK modulation schemes. But, the performance is somewhat degraded under the 16QAM modulation scheme. This is because the instantaneous SNR in 64QAM is too low such that the error rate of the decision data is high. We can solve the problem by using all decisions as the pseudo pilots to do the channel estimation and the performance can be greatly enhanced. This will be discussed in our simulation chapter.

4.5 Joint time and frequency domain channel estimation with WLS

Figure 4-9 shows the block diagram of the proposed time and frequency domain channel estimation method with the SIC-WLS method. The operations conducted in Figure 4-9 is described below.

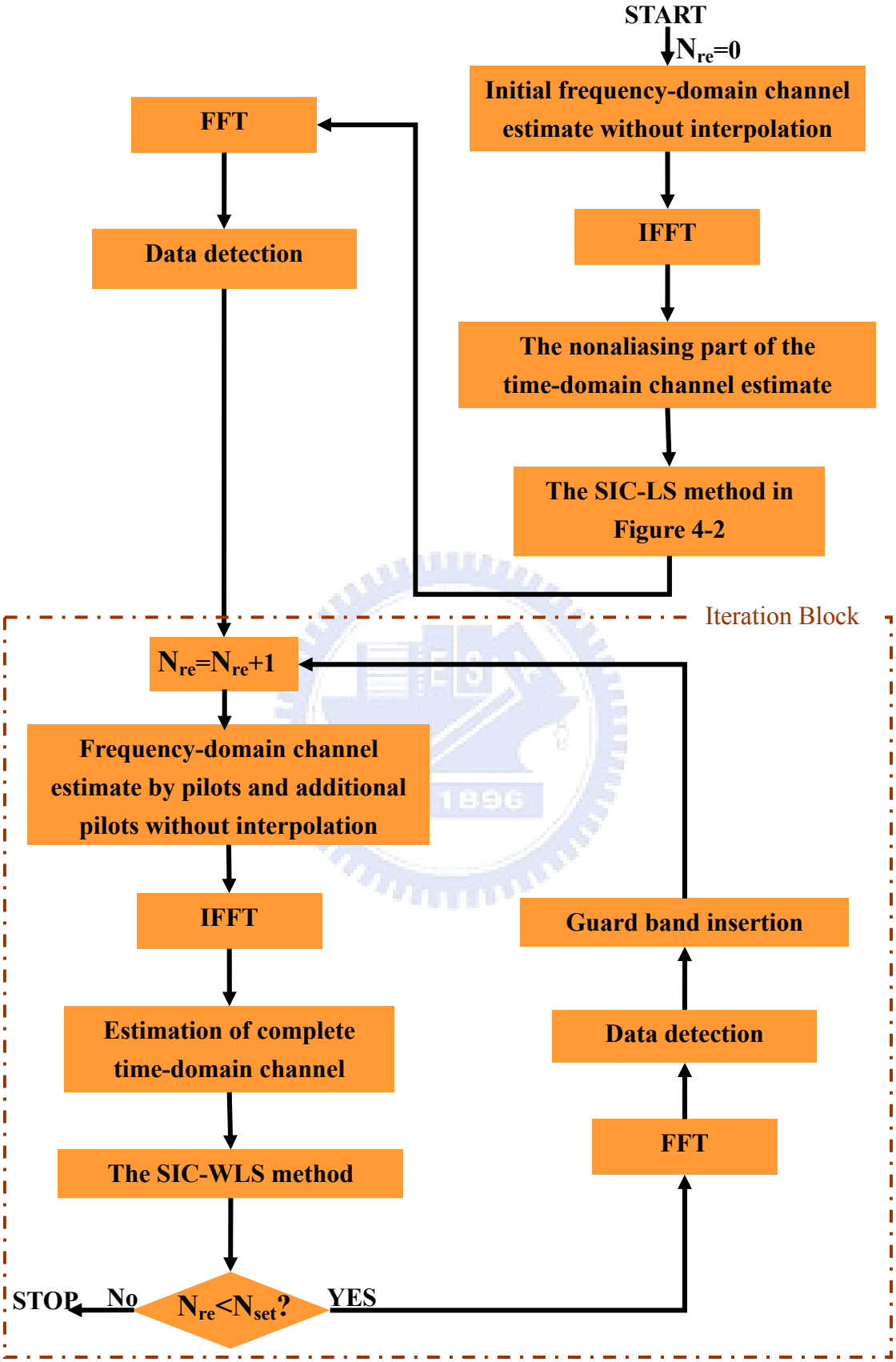

Figure 4-9 The proposed time and frequency domain channel estimation method with the SIC-WLS algorithm

STEP 1: Use the pilot subcarriers to obtain the initial frequency-domain channel estimate (without interpolation).

STEP 2: Conduct the IFFT of the frequency domain channel estimate to the time domain.

STEP 3: Find the nonaliasing portion of the initial time-domain channel estimate.

STEP 4: Iteratively find the tap with the maximum value and use the SIC-LS method in Figure 4-2 to estimate channel response of the tap until the least squared error (LSE) is smaller than the LSE threshold (the LSE threshold is larger here).

STEP 5: Conduct the FFT operation for the estimated channel to obtain the corresponding frequency-domain channel estimate.

STEP 6: Use the estimated frequency-domain channel result and received signals to estimate transmitted symbols and make data detections. Decisions at some designated subcarriers are used as pseudo pilots.

STEP 7: Insert the channel response in the guard band from the previously estimate channel response when $N_{re} \neq 0$.

STEP 8: If the number of re-estimation has not reached the preset value, go to **STEP 2**. Notice that the SIC-LS method in **STEP 4** is replaced by the SIC-WLS method discussed in Section 4.4 during channel re-estimation.

Chapter 5

Proposed Time-Variant Channel Estimation

We have discussed the channel estimation problem in linear time invariant systems in Chapter 3 and Chapter 4. It has been shown that the OFDM technique has good performance for quasi-static frequency-selective fading channels. A channel is quasi-static if it remains time-invariant during an OFDM period. For this scenario, the performance of the channel estimation methods described in Chapter 3 and Chapter 4 work well. However, in high-mobility wireless environments, the channel becomes time variant within one OFDM symbol. The orthogonality of subcarriers in one OFDM symbol is no longer held and this causes the ICI. The frequency domain channel response is no longer a diagonal matrix as that shown in (2.10). From [8], the received signal with ICI for a subcarrier can be expressed as

$$\tilde{y}_i = \tilde{h}_{ii}\tilde{x}_i + \sum_{d=1}^{N_C-1} \tilde{h}_{id}\tilde{x}_d + \tilde{w}_i, 0 \le i \le N_c - 1 \tag{5.1}$$

Rewrite (5.1) using a matrix form, we can have

$$\begin{bmatrix} \tilde{y}_0 \\ \tilde{y}_1 \\ \tilde{y}_2 \\ \vdots \\ \tilde{y}_{N_C-1} \end{bmatrix} = \begin{bmatrix} \tilde{h}_{00} & \tilde{h}_{01} & \tilde{h}_{02} & \cdots & \tilde{h}_{0(N_C-1)} \\ \tilde{h}_{10} & \tilde{h}_{11} & \tilde{h}_{12} & \cdots & \tilde{h}_{1(N_C-1)} \\ \tilde{h}_{20} & \tilde{h}_{21} & \tilde{h}_{22} & \cdots & \tilde{h}_{2(N_C-1)} \\ \vdots & \vdots & \vdots & \ddots & \vdots \\ \tilde{h}_{(N_C-1)0} & \tilde{h}_{(N_C-1)1} & \tilde{h}_{(N_C-1)2} & \cdots & \tilde{h}_{(N_C-1)(N_C-1)} \end{bmatrix} \begin{bmatrix} \tilde{x}_0 \\ \tilde{x}_1 \\ \tilde{x}_2 \\ \vdots \\ \tilde{x}_{N_C-1} \end{bmatrix} + \tilde{\mathbf{w}} \tag{5.2}$$

$$\tilde{\mathbf{y}} = \tilde{\mathbf{M}}\tilde{\mathbf{x}} + \tilde{\mathbf{w}} \tag{5.3}$$

where $\tilde{\mathbf{y}}$ is the frequency domain received signal vector, $\tilde{\mathbf{x}}$ is the frequency domain transmitted signal vector, $\tilde{\mathbf{M}}$ is the frequency domain ICI channel matrix, and $\tilde{\mathbf{w}}$ is the frequency domain AWGN noise vector. The channel estimation problem becomes more

involved. In this chapter, we will study the channel estimation problem in time-variant channels. We propose to use LS/WLS algorithm to identify the channels. Figure 5-1 shows an example of one time-variant channel tap. As we can see, the channel is variant within one OFDM symbol.

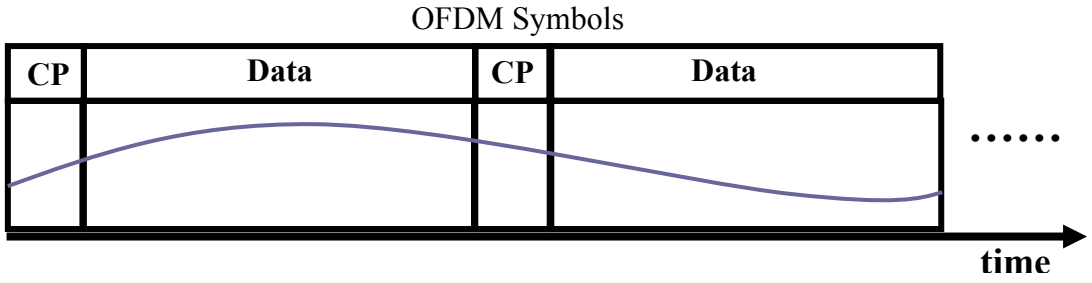

Figure 5-1 One time-varying channel tap

5.1 Linear approximation method of time-variant channel

The linear approximation method uses a straight line to fit the variation of one time-variant channel within one OFDM symbol, as shown in Figure 5-2. A straight line can be specified by two unknowns (the start point and its slope) and the number of unknowns for a complete channel is then limited. The approximation error of the the linear model has been shown to be small for the normalized Doppler up to 20% [6]. The normalized Doppler is defined as the maximum Doppler spread divided by the subcarrier spacing. Denote the maximum Doppler spread as f_D. Then, we have

$$f_D = \frac{v \times f_C}{c} \tag{5.4}$$

Where v is the mobile speed, f_C is the carrier frequency, and c is the speed of light. In the next section, we will use the LS method to identify the parameters of the linear model.

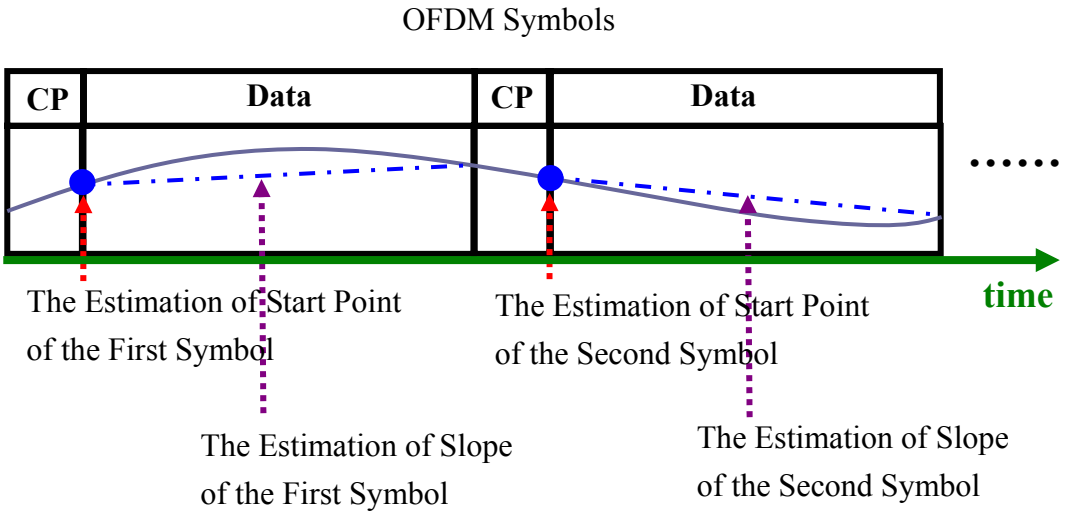

Figure 5-2 Linear approximation of a time-variant channel tap

5.2 Time domain LS time-variant channel estimator

In Section 5.1, we approximate a time-variant channel tap by a straight line; we call the channel a linear time variant (LTV) channel. An LTV channel tap can be expressed as

$$h_k(n) = h_k + n \times a_k \tag{5.5}$$

where $h_k(n)$ denote the response of the k'th tap of a channel at time instant n, h_k is the starting value, and a_k is the variation slope. Notice that we let n be zero at the start point of an OFDM symbol. Let the complete channel have N_c taps. We can then express the received an OFDM symbol as:

$$\mathbf{y} = (\mathbf{H} + \mathbf{D}_v\mathbf{A})\mathbf{x} + \mathbf{w} \tag{5.6}$$

where $\mathbf{y}$ is the time domain received signal vector, $\mathbf{x}$ is the time domain transmit signal vector, $\mathbf{w}$ is the time domain AWGN noise vector, $\mathbf{H}$ is a circulant matrix with $\mathbf{h} = [h_0, h_1, \cdots, h_{N_c-1}]^T$ as its first column, $\mathbf{A}$ is circulant matrix with $\mathbf{a} = [a_0, a_1, \cdots, a_{N_c-1}]^T$ as its first column:, and $\mathbf{D}_v$ is a diagonal matrix with

$\mathbf{v} = [0, 1, \cdots, N_c - 1]^T$ as its diagonal elements.

Transforming the time domain received signal vector into the frequency domain, we have

$$\begin{aligned}
\tilde{\mathbf{y}} &= \sqrt{N_c}\mathbf{G}\mathbf{y} \\
&= \sqrt{N_c}\mathbf{G}[(\mathbf{H} + \mathbf{D}_v\mathbf{A})\mathbf{x} + \mathbf{w}] \\
&= \sqrt{N_c}\mathbf{G}(\mathbf{H} + \mathbf{D}_v\mathbf{A})\mathbf{G}^{\mathbf{H}}\mathbf{G}\mathbf{x} + \sqrt{N_c}\mathbf{G}\mathbf{w} \\
&= (\mathbf{G}\mathbf{H}\mathbf{G}^{\mathbf{H}} + \mathbf{G}\mathbf{D}_v\mathbf{G}^{\mathbf{H}}\mathbf{G}\mathbf{A}\mathbf{G}^{\mathbf{H}})\tilde{\mathbf{x}} + \tilde{\mathbf{w}} \\
&= [\mathbf{D}_{\tilde{h}} + \mathbf{G}\mathbf{D}_v\mathbf{G}^{\mathbf{H}}\mathbf{D}_{\tilde{a}}]\tilde{\mathbf{x}} + \tilde{\mathbf{w}} \\
&= \tilde{\mathbf{M}}\tilde{\mathbf{x}} + \tilde{\mathbf{w}}
\end{aligned} \tag{5.7}$$

where $\tilde{\mathbf{y}} = \sqrt{N_c}\mathbf{G}\mathbf{y} = [\tilde{y}_0, \tilde{y}_1, \cdots, \tilde{y}_{N_c-1}]^T$ is the frequency domain received signal vector, $\tilde{\mathbf{x}} = \sqrt{N_c}\mathbf{G}\mathbf{x} = [\tilde{x}_0, \tilde{x}_1, \cdots, \tilde{x}_{N_c-1}]^T$ is the frequency domain transmitted signal vector, $\tilde{\mathbf{w}} = \sqrt{N_c}\mathbf{G}\mathbf{w} = [\tilde{w}_0, \tilde{w}_1, \cdots, \tilde{w}_{N_c-1}]^T$ is the frequency domain AWGN noise vector, $\mathbf{D}_{\tilde{h}} = \mathbf{G}\mathbf{H}\mathbf{G}^{\mathbf{H}}$ is a diagonal matrix with $\tilde{\mathbf{h}} = \sqrt{N_c}\mathbf{G}\mathbf{h}$ as its diagonal elements, $\mathbf{D}_{\tilde{a}} = \mathbf{G}\mathbf{A}\mathbf{G}^{\mathbf{H}}$ is diagonal matrix with $\tilde{\mathbf{a}} = \sqrt{N_c}\mathbf{G}\mathbf{a}$ as its diagonal elements, and $\tilde{\mathbf{M}} = \mathbf{D}_{\tilde{h}} + \mathbf{G}\mathbf{D}_v\mathbf{G}^{\mathbf{H}}\mathbf{D}_{\tilde{a}}$ is the frequency domain ICI matrix. Notice that $\mathbf{G}$ is a unitary DFT matrix with $\mathbf{G}\mathbf{G}^H = I_{Nc}$ (a $N_c \times N_c$ identity matrix).

Let

$$\mathbf{G} = \begin{bmatrix} g_{00} & g_{01} & g_{02} & \cdots & g_{0(N_c-1)} \\ g_{10} & g_{11} & g_{12} & \cdots & g_{1(N_c-1)} \\ g_{20} & g_{21} & g_{22} & \cdots & g_{2(N_c-1)} \\ \vdots & \vdots & \vdots & \ddots & \vdots \\ g_{(N_c-1)0} & g_{(N_c-1)1} & g_{(N_c-1)2} & \cdots & g_{(N_c-1)(N_c-1)} \end{bmatrix} = \begin{bmatrix} \vec{\mathbf{g}}_0 \\ \vec{\mathbf{g}}_1 \\ \vec{\mathbf{g}}_2 \\ \vdots \\ \vec{\mathbf{g}}_{N_c-1} \end{bmatrix}, \vec{\mathbf{g}}_0 = \begin{bmatrix} g_{00} \\ g_{01} \\ g_{02} \\ \vdots \\ g_{0(N_c-1)} \end{bmatrix}^T \tag{5.8}$$

From (5.7), we can have

$$\tilde{\mathbf{y}} = \sqrt{N_c}\mathbf{G}\mathbf{y} = \mathbf{G}\mathbf{H}\mathbf{G}^H\tilde{\mathbf{x}} + \mathbf{G}\mathbf{D}\mathbf{v}\mathbf{G}^H\mathbf{G}\mathbf{A}\mathbf{G}^H\tilde{\mathbf{x}} + \tilde{\mathbf{w}} \tag{5.9}$$

From the first term in the right hand side of (5.9), we can have

$$\mathbf{GHG}^H\tilde{\mathbf{x}} = \mathbf{D}_{\tilde{h}}\tilde{\mathbf{x}} = \sqrt{N_c}\begin{bmatrix} \vec{\mathbf{g}}_0\mathbf{h} & 0 & 0 & \cdots & 0 \\ 0 & \vec{\mathbf{g}}_1\mathbf{h} & 0 & \cdots & 0 \\ 0 & 0 & \vec{\mathbf{g}}_2\mathbf{h} & \cdots & 0 \\ \vdots & \vdots & \vdots & \ddots & \vdots \\ 0 & 0 & 0 & \cdots & \vec{\mathbf{g}}_{N_c-1}\mathbf{h} \end{bmatrix}\begin{bmatrix} \tilde{x}_0 \\ \tilde{x}_1 \\ \tilde{x}_2 \\ \vdots \\ \tilde{x}_{N_c-1} \end{bmatrix}$$

$$= \sqrt{N_c}\begin{bmatrix} (g_{00}h_0 + g_{01}h_1 + \cdots + g_{0(N_c-1)}h_{N_c-1})\tilde{x}_0 \\ (g_{10}h_0 + g_{11}h_1 + \cdots + g_{1(N_c-1)}h_{N_c-1})\tilde{x}_1 \\ (g_{20}h_0 + g_{21}h_1 + \cdots + g_{2(N_c-1)}h_{N_c-1})\tilde{x}_2 \\ \vdots \\ (g_{(N_c-1)0}h_0 + g_{(N_c-1)1}h_1 + \cdots + g_{(N_c-1)(N_c-1)}h_{N_c-1})\tilde{x}_{N_c-1} \end{bmatrix}$$

$$= \sqrt{N_c}\begin{bmatrix} \tilde{x}_0\vec{\mathbf{g}}_0 \\ \tilde{x}_1\vec{\mathbf{g}}_0 \\ \tilde{x}_2\vec{\mathbf{g}}_2 \\ \vdots \\ \tilde{x}_{N_c-1}\vec{\mathbf{g}}_{N_c-1} \end{bmatrix}\begin{bmatrix} h_0 \\ h_1 \\ h_2 \\ \vdots \\ h_{N_c-1} \end{bmatrix} \tag{5.10}$$

The second term in the right hand side of (5.9) is $\mathbf{GD}_v\mathbf{G}^H\mathbf{GAG}^H\tilde{\mathbf{x}}$. For the first half of $\mathbf{GD}_v\mathbf{G}^H\mathbf{GAG}^H\tilde{\mathbf{x}}$, we have

$$\mathbf{GD}_v\mathbf{G}^H = \mathbf{G}\begin{bmatrix} 0 & 0 & 0 & \cdots & 0 \\ 0 & 1 & 0 & \cdots & 0 \\ 0 & 0 & 2 & \cdots & 0 \\ \vdots & \vdots & \vdots & \ddots & 0 \\ 0 & 0 & 0 & \cdots & N_c-1 \end{bmatrix}\mathbf{G}^H \tag{5.11}$$

Let

$$\mathbf{GD}_v\mathbf{G}^H = \begin{bmatrix} w_{00} & w_{01} & w_{02} & \cdots & w_{0(N_c-1)} \\ w_{10} & w_{11} & w_{12} & \cdots & w_{1(N_c-1)} \\ w_{20} & w_{21} & w_{22} & \cdots & w_{2(N_c-1)} \\ \vdots & \vdots & \vdots & \ddots & \vdots \\ w_{(N_c-1)0} & w_{(N_c-1)1} & w_{(N_c-1)2} & \cdots & w_{(N_c-1)(N_c-1)} \end{bmatrix} = \begin{bmatrix} \vec{\mathbf{w}}_0 \\ \vec{\mathbf{w}}_1 \\ \vec{\mathbf{w}}_2 \\ \vdots \\ \vec{\mathbf{w}}_{N_c-1} \end{bmatrix} \tag{5.12}$$

For the second half of $\mathbf{GD}_v\mathbf{G}^H\mathbf{GAG}^H\tilde{\mathbf{x}}$, we have

$$\mathbf{GAG}^H\tilde{\mathbf{x}} = \mathbf{D}_{\tilde{a}}\tilde{\mathbf{x}} = \sqrt{N_c}\begin{bmatrix} \vec{\mathbf{g}}_0\mathbf{A} & 0 & 0 & \cdots & 0 \\ 0 & \vec{\mathbf{g}}_1\mathbf{A} & 0 & \cdots & 0 \\ 0 & 0 & \vec{\mathbf{g}}_2\mathbf{A} & \cdots & 0 \\ \vdots & \vdots & \vdots & \ddots & \vdots \\ 0 & 0 & 0 & \cdots & \vec{\mathbf{g}}_{N_c-1}\mathbf{A} \end{bmatrix}\begin{bmatrix} \tilde{x}_0 \\ \tilde{x}_1 \\ \tilde{x}_2 \\ \vdots \\ \tilde{x}_{N_c-1} \end{bmatrix}$$

(5.13)

And,

$$\mathbf{GD}_v\mathbf{G}^H\mathbf{GAG}^H\tilde{\mathbf{x}} =$$

$$\begin{bmatrix} w_{00} & w_{01} & w_{02} & \cdots & w_{0(N_c-1)} \\ w_{10} & w_{11} & w_{12} & \cdots & w_{1(N_c-1)} \\ w_{20} & w_{21} & w_{22} & \cdots & w_{2(N_c-1)} \\ \vdots & \vdots & \vdots & \ddots & \vdots \\ w_{(N_c-1)0} & w_{(N_c-1)1} & w_{(N_c-1)2} & \cdots & w_{(N_c-1)(N_c-1)} \end{bmatrix}\sqrt{N_c}\begin{bmatrix} \vec{\mathbf{g}}_0\mathbf{A} & 0 & 0 & \cdots & 0 \\ 0 & \vec{\mathbf{g}}_1\mathbf{A} & 0 & \cdots & 0 \\ 0 & 0 & \vec{\mathbf{g}}_2\mathbf{A} & \cdots & 0 \\ \vdots & \vdots & \vdots & \ddots & \vdots \\ 0 & 0 & 0 & \cdots & \vec{\mathbf{g}}_{N_c-1}\mathbf{A} \end{bmatrix}\begin{bmatrix} \tilde{x}_0 \\ \tilde{x}_1 \\ \tilde{x}_2 \\ \vdots \\ \tilde{x}_{N_c-1} \end{bmatrix}$$

$$= \sqrt{N_c}\begin{bmatrix} w_{00}\vec{\mathbf{g}}_0\mathbf{A} & w_{01}\vec{\mathbf{g}}_1\mathbf{A} & w_{02}\vec{\mathbf{g}}_2\mathbf{A} & \cdots & w_{0(N_c-1)}\vec{\mathbf{g}}_{N_c-1}\mathbf{A} \\ w_{10}\vec{\mathbf{g}}_0\mathbf{A} & w_{11}\vec{\mathbf{g}}_1\mathbf{A} & w_{11}\vec{\mathbf{g}}_2\mathbf{A} & \cdots & w_{1(N_c-1)}\vec{\mathbf{g}}_{N_c-1}\mathbf{A} \\ w_{20}\vec{\mathbf{g}}_0\mathbf{A} & w_{21}\vec{\mathbf{g}}_1\mathbf{A} & w_{22}\vec{\mathbf{g}}_2\mathbf{A} & \cdots & w_{2(N_c-1)}\vec{\mathbf{g}}_{N_c-1}\mathbf{A} \\ \vdots & \vdots & \vdots & \ddots & \vdots \\ w_{(N_c-1)0}\vec{\mathbf{g}}_0\mathbf{A} & w_{(N_c-1)1}\vec{\mathbf{g}}_1\mathbf{A} & w_{(N_c-1)2}\vec{\mathbf{g}}_2\mathbf{A} & \cdots & w_{(N_c-1)(N_c-1)}\vec{\mathbf{g}}_{N_c-1}\mathbf{A} \end{bmatrix}\begin{bmatrix} \tilde{x}_0 \\ \tilde{x}_1 \\ \tilde{x}_2 \\ \vdots \\ \tilde{x}_{N_c-1} \end{bmatrix}$$

$$= \sqrt{N_c}\begin{bmatrix} w_{00}\vec{\mathbf{g}}_0\mathbf{A}\tilde{x}_0 + w_{01}\vec{\mathbf{g}}_1\mathbf{A}\tilde{x}_1 + \cdots + w_{0(N_c-1)}\vec{\mathbf{g}}_{N_c-1}\mathbf{A}\tilde{x}_{N_c-1} \\ w_{10}\vec{\mathbf{g}}_0\mathbf{A}\tilde{x}_0 + w_{11}\vec{\mathbf{g}}_1\mathbf{A}\tilde{x}_1 + \cdots + w_{1(Nc-1)}\vec{\mathbf{g}}_{N_c-1}\mathbf{A}\tilde{x}_{N_c-1} \\ w_{20}\vec{\mathbf{g}}_0\mathbf{A}\tilde{x}_0 + w_{21}\vec{\mathbf{g}}_1\mathbf{A}\tilde{x}_1 + \cdots + w_{2(Nc-1)}\vec{\mathbf{g}}_{N_c-1}\mathbf{A}\tilde{x}_{N_c-1} \\ \vdots \\ w_{(N_c-1)0}\vec{\mathbf{g}}_0\mathbf{A}\tilde{x}_0 + w_{(N_c-1)1}\vec{\mathbf{g}}_1\mathbf{A}\tilde{x}_1 + \cdots + w_{(N_c-1)(N_c-1)}\vec{\mathbf{g}}_{N_c-1}\mathbf{A}\tilde{x}_{N_c-1} \end{bmatrix}$$

$$= \sqrt{N_c}\begin{bmatrix} \vec{\mathbf{w}}_0 \\ \vec{\mathbf{w}}_1 \\ \vec{\mathbf{w}}_2 \\ \vdots \\ \vec{\mathbf{w}}_{N_c-1} \end{bmatrix}\begin{bmatrix} \tilde{x}_0 & 0 & 0 & \cdots & 0 \\ 0 & \tilde{x}_1 & 0 & \cdots & 0 \\ 0 & 0 & \tilde{x}_2 & \cdots & 0 \\ \vdots & \vdots & \vdots & \ddots & \vdots \\ 0 & 0 & 0 & \cdots & \tilde{x}_{N_c-1} \end{bmatrix}\begin{bmatrix} \vec{\mathbf{g}}_0\mathbf{A} \\ \vec{\mathbf{g}}_1\mathbf{A} \\ \vec{\mathbf{g}}_2\mathbf{A} \\ \vdots \\ \vec{\mathbf{g}}_{N_c-1}\mathbf{A} \end{bmatrix}$$

$$= \sqrt{N_c} \begin{bmatrix} \tilde{\mathbf{w}}_0 \\ \tilde{\mathbf{w}}_1 \\ \tilde{\mathbf{w}}_2 \\ \vdots \\ \tilde{\mathbf{w}}_{N_c-1} \end{bmatrix} \begin{bmatrix} \tilde{x}_0 & 0 & 0 & \cdots & 0 \\ 0 & \tilde{x}_1 & 0 & \cdots & 0 \\ 0 & 0 & \tilde{x}_2 & \cdots & 0 \\ \vdots & \vdots & \vdots & \ddots & \vdots \\ 0 & 0 & 0 & \cdots & \tilde{x}_{N_c-1} \end{bmatrix} \mathbf{G} \begin{bmatrix} a_0 \\ a_1 \\ a_2 \\ \vdots \\ a_{N_c-1} \end{bmatrix} \tag{5.14}$$

Combining the result of (5.10) and (5.14) and ignoring the noise term, we can rewrite (5.9) into the matrix form as:

$$\tilde{\mathbf{y}} = \mathbf{GHG}^{\mathbf{H}} \tilde{\mathbf{x}} + \mathbf{GDvG}^{\mathbf{H}} \mathbf{GAG}^{\mathbf{H}} \tilde{\mathbf{x}} \Rightarrow$$

$$\begin{bmatrix} \tilde{y}_0 \\ \tilde{y}_1 \\ \tilde{y}_2 \\ \vdots \\ \tilde{y}_{N_c-1} \end{bmatrix} = \sqrt{N_c} \left\{ \begin{bmatrix} \tilde{x}_0 \tilde{\mathbf{g}}_0 \\ \tilde{x}_1 \tilde{\mathbf{g}}_1 \\ \tilde{x}_2 \tilde{\mathbf{g}}_2 \\ \vdots \\ \tilde{x}_{N_c-1} \tilde{\mathbf{g}}_{N_c-1} \end{bmatrix} \begin{bmatrix} h_0 \\ h_1 \\ h_2 \\ \vdots \\ h_{N_c-1} \end{bmatrix} + \begin{bmatrix} \tilde{\mathbf{w}}_0 \\ \tilde{\mathbf{w}}_1 \\ \tilde{\mathbf{w}}_2 \\ \vdots \\ \tilde{\mathbf{w}}_{N_c-1} \end{bmatrix} \begin{bmatrix} \tilde{x}_0 & 0 & 0 & \cdots & 0 \\ 0 & \tilde{x}_1 & 0 & \cdots & 0 \\ 0 & 0 & \tilde{x}_2 & \cdots & 0 \\ \vdots & \vdots & \vdots & \ddots & \vdots \\ 0 & 0 & 0 & \cdots & \tilde{x}_{N_c-1} \end{bmatrix} \mathbf{G} \begin{bmatrix} a_0 \\ a_1 \\ a_2 \\ \vdots \\ a_{N_c-1} \end{bmatrix} \right\} \tag{5.15}$$

Let

$$\begin{bmatrix} \tilde{\mathbf{w}}_0 \\ \tilde{\mathbf{w}}_1 \\ \tilde{\mathbf{w}}_2 \\ \vdots \\ \tilde{\mathbf{w}}_{N_c-1} \end{bmatrix} \begin{bmatrix} \tilde{x}_0 & 0 & 0 & \cdots & 0 \\ 0 & \tilde{x}_1 & 0 & \cdots & 0 \\ 0 & 0 & \tilde{x}_2 & \cdots & 0 \\ \vdots & \vdots & \vdots & \ddots & \vdots \\ 0 & 0 & 0 & \cdots & \tilde{x}_{N_c-1} \end{bmatrix} \mathbf{G} =$$

$$\begin{bmatrix} v_{00} & v_{01} & v_{02} & \cdots & v_{0(N_c-1)} \\ v_{10} & v_{11} & v_{12} & \cdots & v_{1(N_c-1)} \\ v_{20} & v_{21} & v_{22} & \cdots & v_{2(N_c-1)} \\ \vdots & \vdots & \vdots & \ddots & \vdots \\ v_{(N_c-1)0} & v_{(N_c-1)1} & v_{(N_c-1)2} & \cdots & v_{(N_c-1)(N_c-1)} \end{bmatrix} = \begin{bmatrix} \tilde{\mathbf{v}}_0 \\ \tilde{\mathbf{v}}_1 \\ \tilde{\mathbf{v}}_2 \\ \vdots \\ \tilde{\mathbf{v}}_{N_c-1} \end{bmatrix} \tag{5.16}$$

We can finally rewrite (5.15) as

$$\begin{bmatrix} \tilde{y}_0 \\ \tilde{y}_1 \\ \tilde{y}_2 \\ \vdots \\ \tilde{y}_{N_c-1} \end{bmatrix} = \sqrt{N_c} \begin{bmatrix} \tilde{x}_0 \vec{\mathbf{g}}_0 & \vec{\mathbf{v}}_0 \\ \tilde{x}_1 \vec{\mathbf{g}}_1 & \vec{\mathbf{v}}_1 \\ \tilde{x}_2 \vec{\mathbf{g}}_2 & \vec{\mathbf{v}}_2 \\ \vdots & \vdots \\ \tilde{x}_{N_c-1} \vec{\mathbf{g}}_{N_c-1} & \vec{\mathbf{v}}_{N_c-1} \end{bmatrix} \begin{bmatrix} h_0 \\ h_1 \\ h_2 \\ \vdots \\ h_{N_c-1} \\ a_0 \\ a_1 \\ a_2 \\ \vdots \\ a_{N_c-1} \end{bmatrix} \tag{5.17}$$

And then

$$\tilde{\mathbf{y}} = \begin{bmatrix} \mathbf{B} & \mathbf{V} \end{bmatrix} \times \mathbf{h}_a \tag{5.18}$$

where $\tilde{\mathbf{y}} = [\tilde{y}_0, \tilde{y}_1, \ldots \tilde{y}_{Nc-1}]^T$ is the frequency domain received vector, $\mathbf{B} = \sqrt{N_c} \left\{ \left[\tilde{x}_0 \vec{\mathbf{g}}_0, \tilde{x}_1 \vec{\mathbf{g}}_1, \ldots \tilde{x}_{Nc-1} \vec{\mathbf{g}}_{N_c-1} \right]^T \right\}$, $\mathbf{V} = \sqrt{N_c} \left\{ \left[\vec{\mathbf{v}}_0, \vec{\mathbf{v}}_1, \ldots \vec{\mathbf{v}}_{N_c-1} \right]^T \right\}$, and $\mathbf{h}_a$ is the parameters we want to estimate. Now, we can use (5.17) to conduct the LS estimation. Since only the data on pilot subcarriers are available, we then select them from the rows of $\mathbf{Y}$ and $\begin{bmatrix} \mathbf{B} & \mathbf{V} \end{bmatrix}$ when using the LS algorithm. Here, we assume that the number of significant taps is much smaller than N_c, and the delay of each significant tap is known. In other words, many elements in $\mathbf{h}_a$ will be zero. Only do the columns of $\mathbf{B}$, $\mathbf{V}$ corresponding to the significant taps need to be considered. Figure 5-3 depicts the entries we need to consider when conducting the LS algorithm for (5.17).

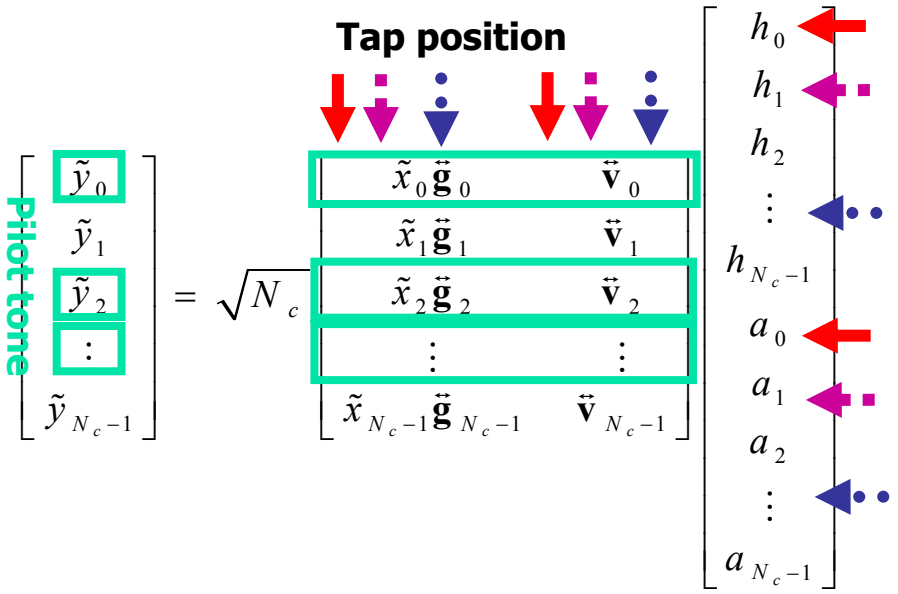

Figure 5-3 Entries need to be considered in (5.17)

After removing irrelevant elements in (5.18), we can have

$$\tilde{\mathbf{y}}_p = \left[\mathbf{B}_{pk}\ \mathbf{V}_{pk}\right] \times \mathbf{h}_{a_k} = \mathbf{Q} \times \mathbf{h}_{a_k} \tag{5.19}$$

where $\tilde{\mathbf{y}}_p = \left[Y_{m_0}, Y_{m_1}, \ldots Y_{m_{M-1}}\right]^T$ is the frequency domain received signal vector on pilot subcarriers, $\mathbf{B}_{pk}$ is a sub-matrix of $\mathbf{B}$ whose rows are determined by the positions of pilot subcarriers, and columns by the positions of significant taps, and $\mathbf{V}_{pk}$ is a sub-matrix of $\mathbf{V}$ whose rows and columns are determined as those of $\mathbf{B}_p$ and $\mathbf{h}_{a_k} = \left[\left[h_{k_0}, h_{k_1}, \ldots h_{k_{K-1}}\right], \left[a_{k_0}, a_{k_1}, \ldots a_{k_{K-1}}\right]\right]^T$ contains the parameters we want to estimate and then, we have

$$\mathbf{Q} = \left[\mathbf{B}_{pk}\mathbf{V}_{pk}\right] = \begin{bmatrix} B_{m_0,k_0} & B_{m_0,k_1} & \cdots & B_{m_0,k_{K-1}} & v_{m_0,k_0} & v_{m_0,k_1} & \cdots & v_{m_0,k_{K-1}} \\ B_{m_1,k_0} & B_{m_1,k_1} & \cdots & B_{m_1,k_{K-1}} & v_{m_1,k_0} & v_{m_1,k_1} & \cdots & v_{m_1,k_{K-1}} \\ \vdots & \vdots & \ddots & \vdots & \vdots & \vdots & \ddots & \vdots \\ B_{m_{M-1},k_0} & B_{m_{M-1},k_1} & \cdots & B_{m_{M-1},k_{K-1}} & v_{m_{M-1},k_0} & v_{m_{M-1},k_1} & \cdots & v_{m_{M-1},k_{K-1}} \end{bmatrix}$$, where

$M_i, 0 \le i \le M-1$ is pilot locations, M is the number of pilots, $k_i, 0 \le i \le K-1$ is channel taps' positions and K is the number of channel taps.

The LS solution is can then be obtained by

$$\mathbf{h}_{a_k} = \left(\mathbf{Q}^H \mathbf{Q}\right)^{-1} \mathbf{Q}^H \tilde{\mathbf{y}}_p \tag{5.20}$$

Compared to the LS channel estimate for the time-invariant channel, the number of parameters in (5.20) is doubled. This is because for each tap we need to estimate two parameters, the value of the starting value and the variation slope. As a result, the accuracy of the estimation result is affected. To improve the performance, we can use decisions as pseudo pilots as discussed in Section 4.2 and Section 4.3. As the number of pilots increases, the performance of the LS estimate can be improved. As we did in Chapter 4, the channel estimation with decisions can be made iteratively and the estimation performance can be further improved. Figure 5-4 shows the LS estimation for the time-variant channel with decisions.

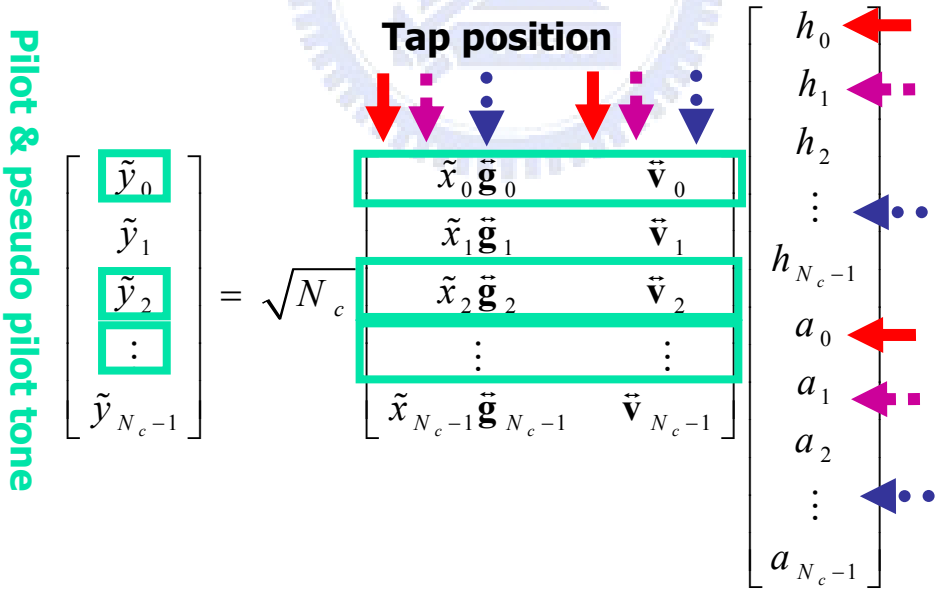

Figure 5-4 The LS time-variant channel estimation with decisions

Rewriting Equation (5.19), we can obtain

$$\tilde{\mathbf{y}}_{p'} = \left[\mathbf{B}_{p'k}\ \mathbf{V}_{p'k}\right] \times \mathbf{h}_{a_k}{}' = \mathbf{Q}' \times \mathbf{h}_{a_k}{}' \tag{5.21}$$

where $\mathbf{Q}' = \left[\mathbf{B}_{p'k}\ \mathbf{V}_{p'k}\right]$ and the rows of $\mathbf{B}_{p'k}$ and $\mathbf{V}_{p'k}$ are the rows of $\mathbf{B}$ and $\mathbf{V}$ on the positions of pilots and decisions. And, the LS solution now becomes

$$\mathbf{h}_{a_k}{}' = \left(\mathbf{Q}'^{H}\mathbf{Q}'\right)^{-1}\mathbf{Q}'^{H}\tilde{\mathbf{y}}_{p'} \tag{5.22}$$

Since not all decisions are correct, the performance of the LS channel estimator may not always satisfactory. So, we can use the WLS algorithm as discussed in Section 4.4 to solve the problem.

5.3 Time domain time-variant channel estimation with WLS

We have discussed the WLS algorithm in Section 4.4. The weighting matrix is denoted by a diagonal matrix $\mathbf{D} = diag(d_0, d_1, \cdots, d_{J-1})$, $\mathbf{j} = j_o, j_1, \cdots, j_{J-1}$ are the positions of pilots and pseudo pilots. Figure 5-5 shows how the weights are added in (5.20).

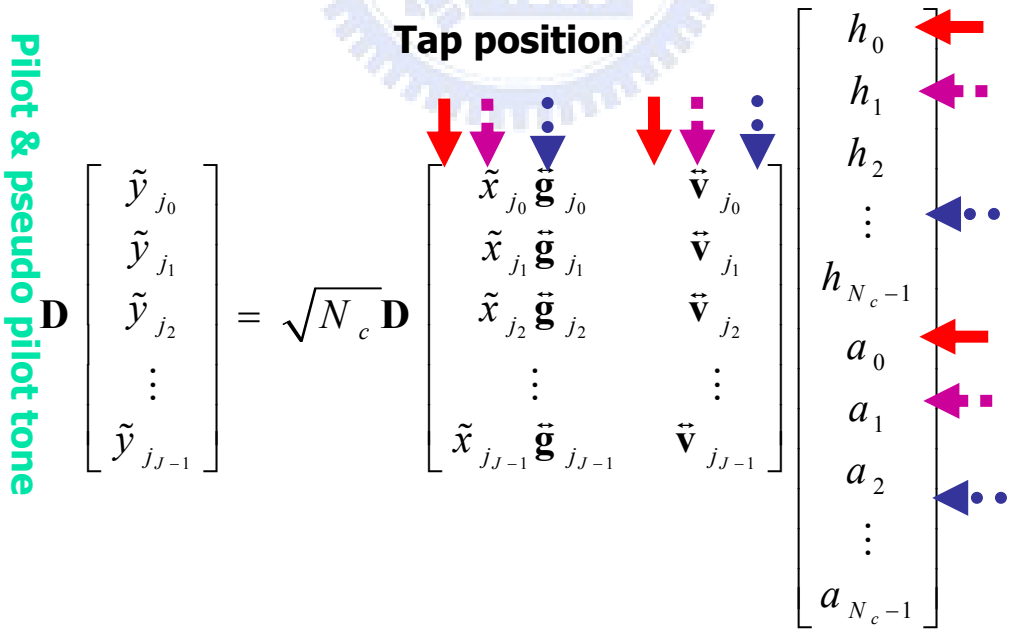

Figure 5-5 Weighting method in WLS algorithm

Thus, (5.21) now becomes

$$\mathbf{D}\tilde{\mathbf{y}}_{p'} = \mathbf{D}\left[\mathbf{B}_{p'k} \;\; \mathbf{V}_{p'k}\right] \times \mathbf{h}_{a_k,wls} = \mathbf{Q}'' \times \mathbf{h}_{a_k,wls} \tag{5.23}$$

where $\mathbf{Q}'' = \mathbf{D}\left[\mathbf{B}_{p'k} \;\; \mathbf{V}_{p'k}\right]$ and the solution of the WLS channel estimate is then

$$\mathbf{h}_{a_k,wls} = \left(\mathbf{Q}''^{H}\mathbf{Q}''\right)^{-1}\mathbf{Q}''^{H}\mathbf{D}\tilde{\mathbf{y}}_{p'} \tag{5.24}$$

Here, we use a simple weight scheme: the weight of a pilot is set to be 1 and the weights for decisions are smaller than one and all the same. The decision weight for different modulation schemes and different ICI levels may be different and it will be determined in the simulation chapter. The comparison of the LS and WLS channel estimator will also be shown in the simulation chapter.

5.4 Time-variant channel estimation by time domain WLS channel estimator

Figure 5-6 shows the block diagram of the complete scheme for the time-variant channel estimation. As discussed in Section 4.1, we only identify the channel taps in the non-aliasing region. The detail operation is summarized in the following procedure.

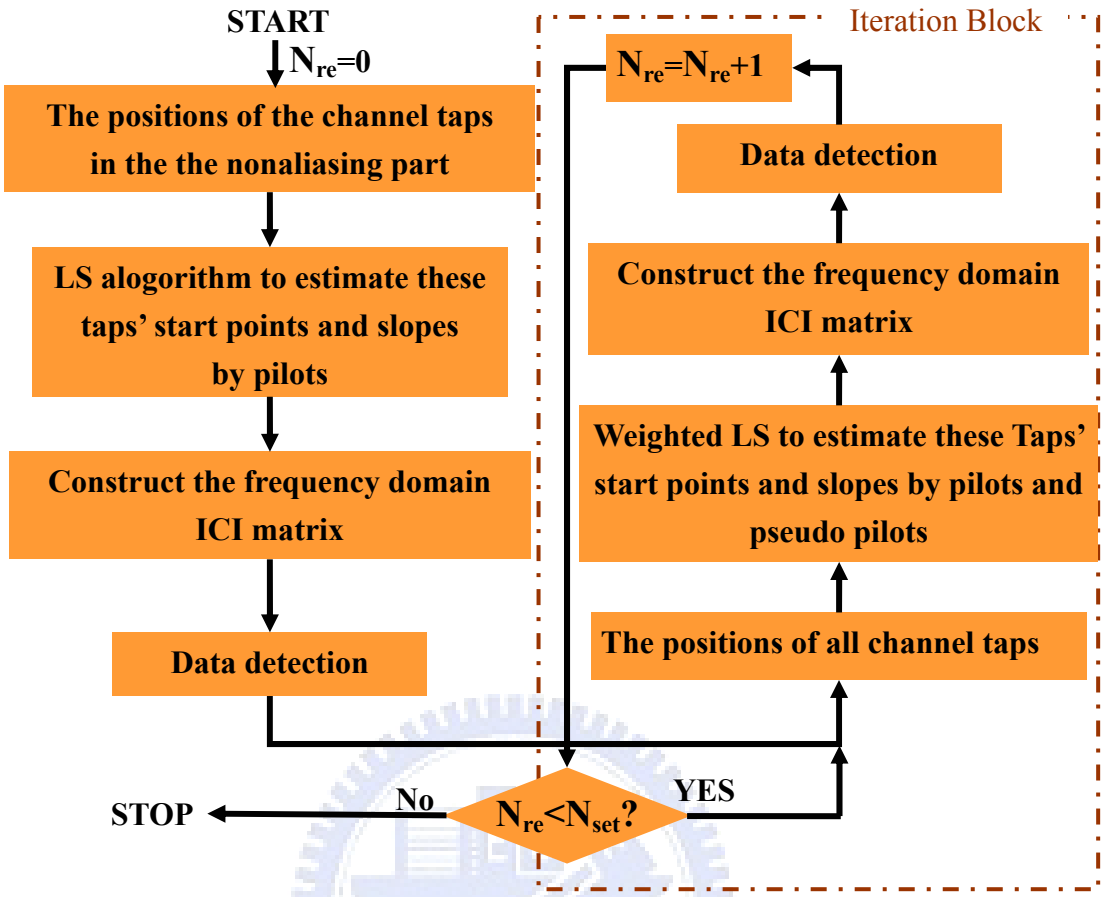

Figure 5-6 Time Domain time-variant WLS channel estimation

STEP 1: We assume that the channel taps' positions in the nonaliasing area can be identify.

STEP 2: Use the LS algorithm discussed in Section 5.2 to estimate the parameters of the time-variant channel.

STEP 3: Construct the ICI matrix $\tilde{\mathbf{M}}$ from Equation (5.7).

STEP 4: Use the zero forcing equalizer to obtain estimate transmit symbols ($\tilde{\mathbf{y}} = \tilde{\mathbf{M}}\tilde{\mathbf{x}} + \tilde{\mathbf{w}}$, $\hat{\tilde{\mathbf{x}}} = \tilde{\mathbf{M}}^{-1}\tilde{\mathbf{y}}$) and make decisions as discussed in Section 4.1.3. Using decisions as pseudo pilots; here, we let the pilot density be 1/3 as that we did in Section 4.2.

STEP 5: Assume that al1 the channel taps' positions are known (discussed in Section 4.3).

STEP 6: Use WLS algorithm discussed in Section 5.3 to re-estimate all the parameters of the channel taps.

STEP 7: Construct the ICI matrix $\tilde{\mathbf{M}}$ from (5.7).

STEP 8: Use the zero forcing equalizer to re-estimate transmit symbols ($\hat{\tilde{\mathbf{x}}} = \tilde{\mathbf{M}}^{-1}\tilde{\mathbf{y}}$).

STEP 9: Go to **STEP 4** if the number of re-estimation, N_{re} is less than a preset number N_{set}.

Chapter 6

Simulation Results

In this Chapter, we conduct simulation to evaluate the performance of the proposed joint time and frequency domain channel estimator in both the time-invariant and time-variant channels. In our channel model, there are 6 channel taps (paths) and the average power of these 6 taps will be determined according to the signal-to-noise ratio (SNR) used. The bit-error-rate (BER) is used as the performance index. We consider two OFDM systems; one is the standard DVB-T system and the other is an OFDM system we define. For the former system, we use two types of channels with different delay spreads. The maximum delay (MD) for the first one is smaller than 64Ts and that for the second one is between 171Ts and 256Ts. The channel estimate for the first-type channel in the DVB-T system will not be aliased while that for the second-type channel will be aliased. We refer the first-type channel as Channel A and the second-type of channel as Channel B. The MD of the channel used for our defined system is between 43Ts and 64Ts and the corresponding channel estimate will be aliased. We refer this type of channel as Channel C. The FFT size is set as 2048 in the DVB-T system and the FFT size is set as 512 in our defined system. Figure 6-1 shows one example of the channel. Figure 6-2 shows the variation of the 6 taps in the fading environment.

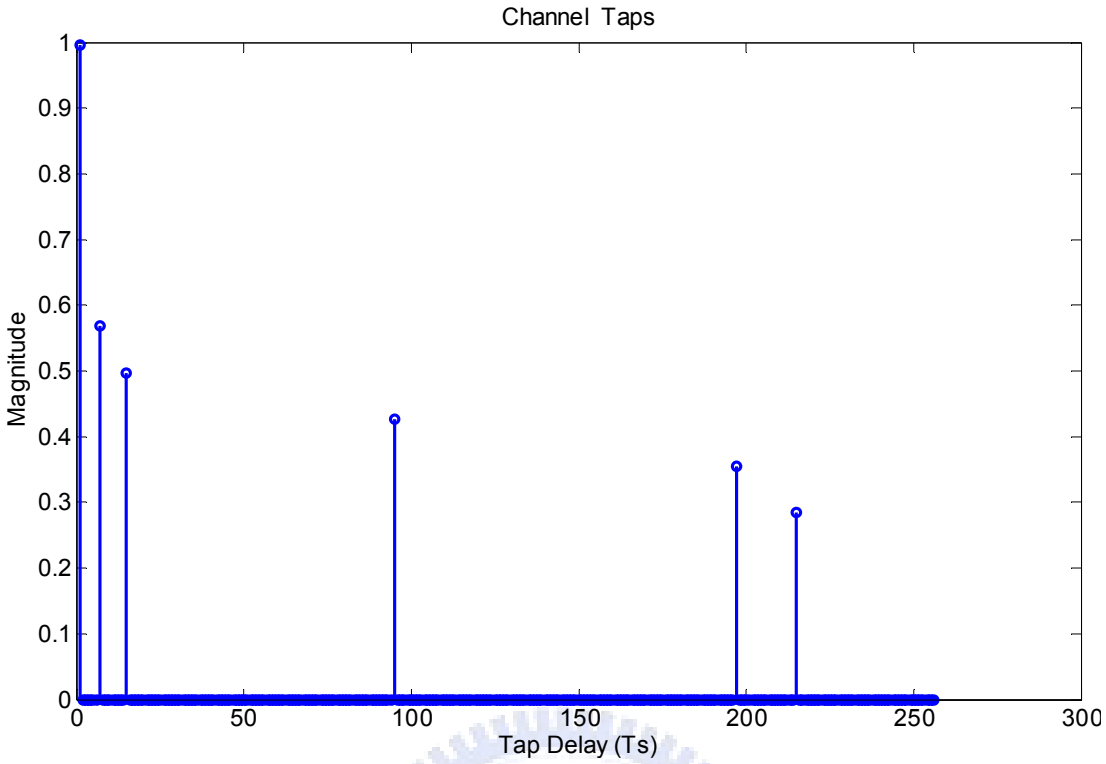

Figure 6-1 An example of 6-tap channel

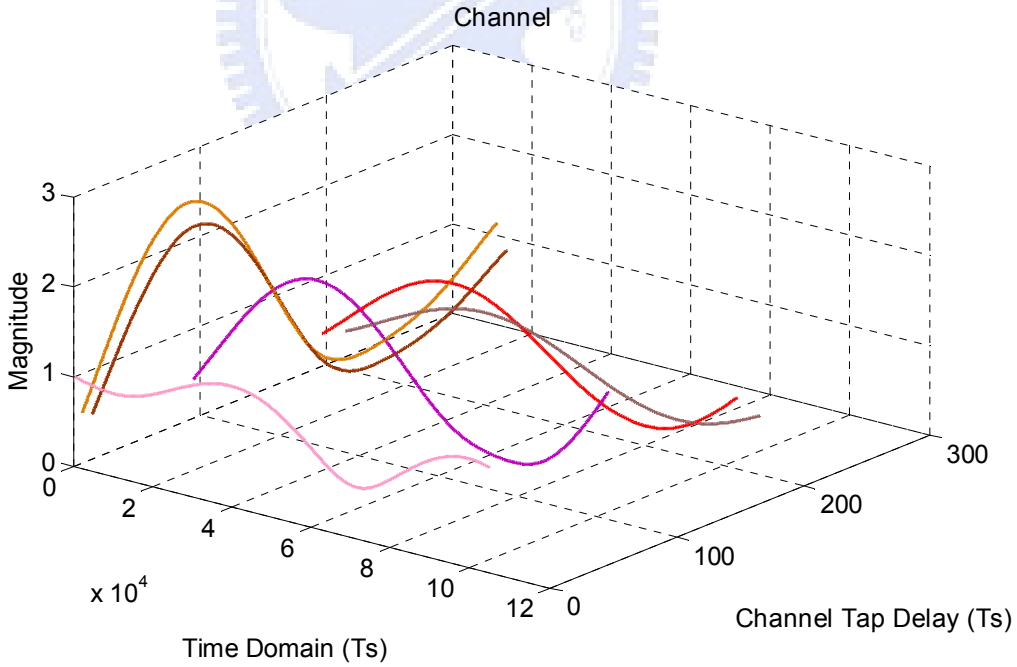

Figure 6-2 Variation of channel taps in fading environment

6.1 Results of channel estimation in Chapter 3

Table 6-1 shows the parameters of the 6 channel taps used in simulations. The system we consider here is the 2K-mode DVB-T system and the size of the CP is 256 (1/8 of 2048). Modulation schemes such as QPSK, 16QAM and 64QAM are used. The delays of the channel taps are randomly changed for every 7 OFDM symbols. For a block of consecutive 7 OFDM symbols, they remain the same.

Tap Number	Average Power (Lin)	Average Power (dB)
1	0.9951	-0.0215
2	0.5727	0.2.421
3	0.4992	-3.0172
4	0.4273	-3.6927
5	0.3558	-4.4880
6	0.2845	-5.4595

Table 6-1 Parameters of multipath fading channel

6.1.1 Results of different interpolation methods

Figure 6-3 shows the performance comparison for different interpolation methods with Channel A. The pilot density here is 1/3 and only the channel response in the frequency domain is estimation. The modulation used is QPSK. Figure 6-4 shows the performance comparison for Channel B. Notice that the positions of the channel taps in a block of 7 OFDM symbols are the same such that the two-dimensional interpolation method can be effectively applied. In the figures, “1D linear” indicates the one-dimensional linear interpolation method, “1D cubic” the one-dimensional cubic interpolation method, “2D linear & linear” the two-dimensional linear interpolation method (linear interpolation both in the temporal and frequency domains), “2D linear & cubic” the two-dimensional

interpolation method with the linearly interpolation in the temporal domain and cubic interpolation in the frequency domain, “2D cubic & cubic” the two-dimensional cubic interpolation method (cubic interpolation both in the temporal and frequency domains).

We can see from Figure 6-3 and Figure 6-4 that two-dimensional interpolation methods are better than one-dimensional interpolation methods. And the cubic interpolation is better than linear interpolation. Also, the performance of “2D linear & cubic” is similar to “2D cubic & cubic”. This is because the channel taps’ positions in a block of 7 OFDM symbols are the same and the variation of channel among the symbols is small. And since the complexity of operation of linear interpolation is lower, we can use “2D linear & cubic” as the interpolation scheme in the joint time and frequency domain channel estimation methods described in Chapter 3.

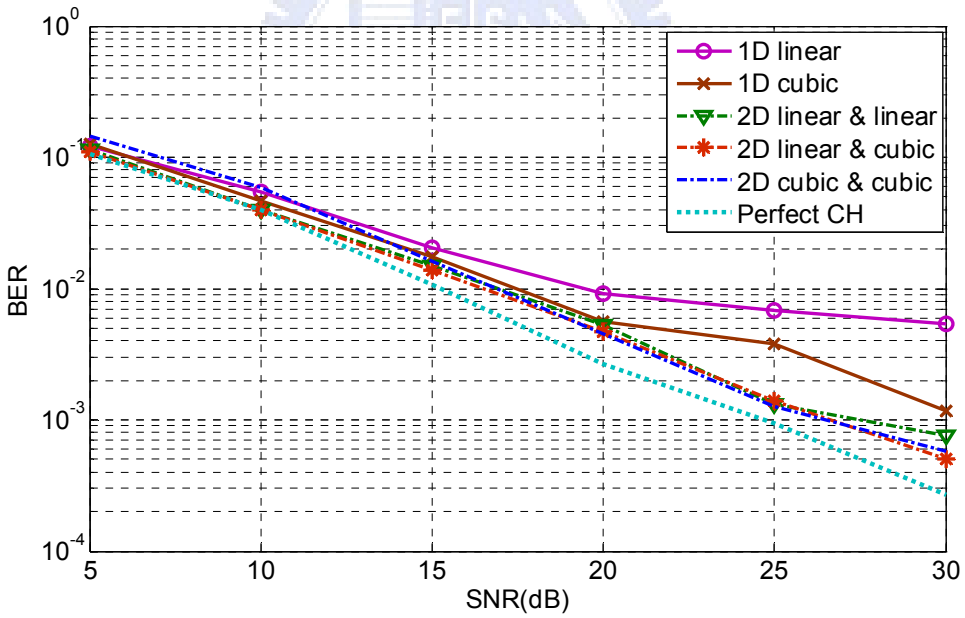

Figure 6-3 Comparison of different interpolation methods (Chanel A)

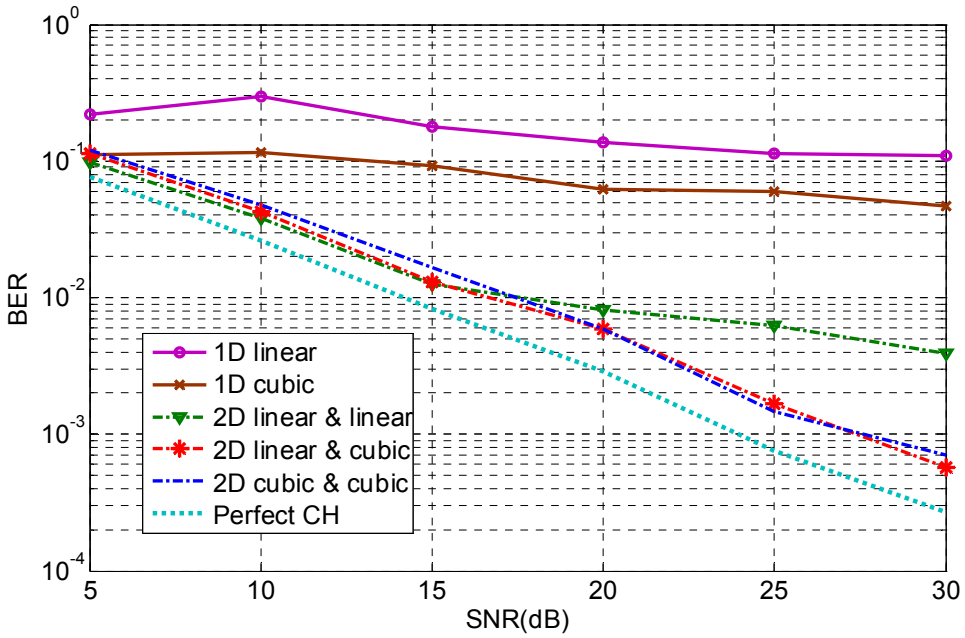

Figure 6-4 Comparison of different interpolation methods (Channel B)

6.1.2 Results of joint time and frequency domain channel estimation

Figure 6-5 and Figure 6-6 show the performance comparison for the algorithm depicted in Figure 3-9 and Figure 3-10. The modulation scheme is also QPSK. For benchmarking, the performance of the ideal channel is also shown in the Figures.

We can see from Figure 6-5 and Figure 6-6 that the performances of the joint time/frequency domain channel estimation method is good under QPSK, and the performance is improved along with the number of iteration. We also can see that the performance with 6 and 10 iteration is almost the same. This shows that 6 iterations will be sufficient. Figure 6-7 and 6-8 show the performance comparison for QPSK, 16QAM, and 64QAM. These figures show that the performance of the channel estimation is also good with 16QAM and 64QAM.

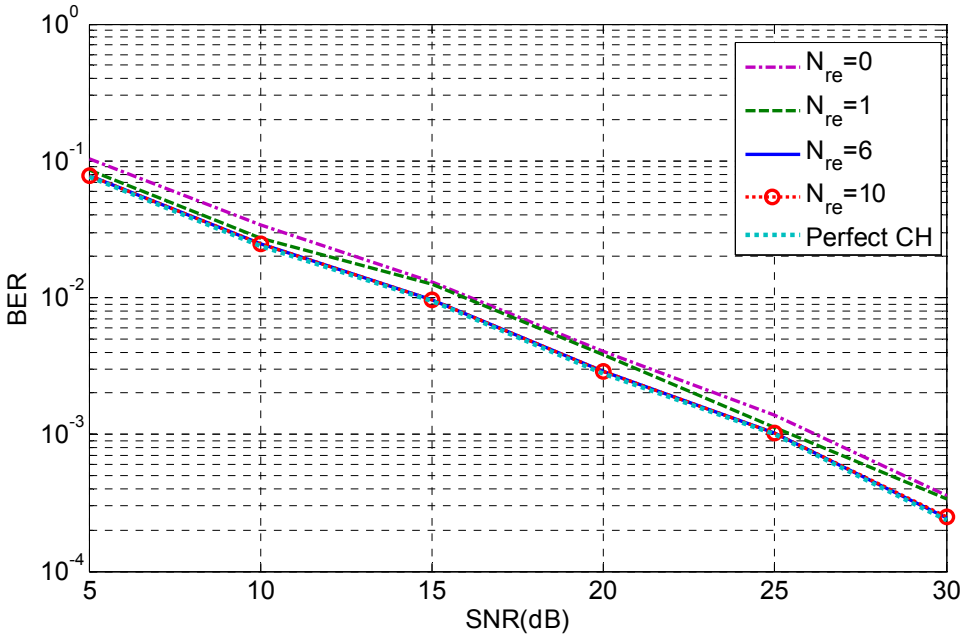

Figure 6-5 Performance of the joint time/frequency channel estimate (QPSK, Channel A)

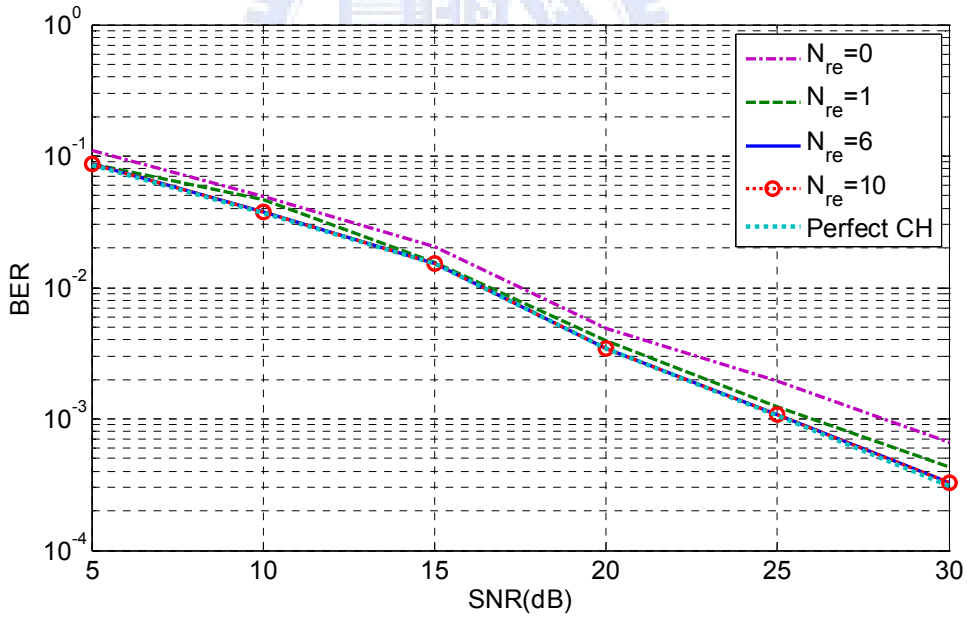

Figure 6-6 Performance of the joint time/frequency channel estimate (QPSK, Channel B)

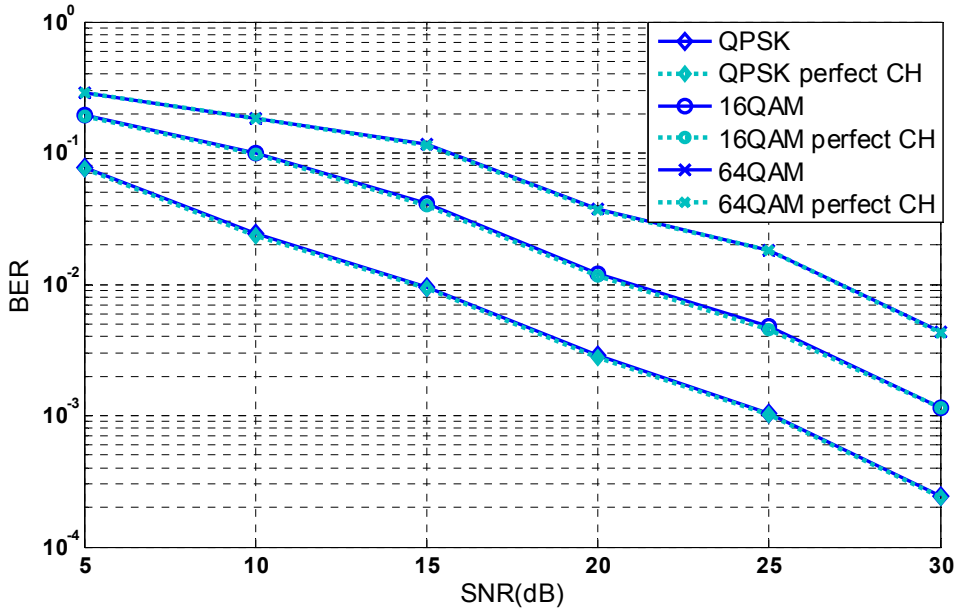

Figure 6-7 Performance of the joint time/frequency channel estimate for QPSK, 16QAM, 64QAM (Channel A)

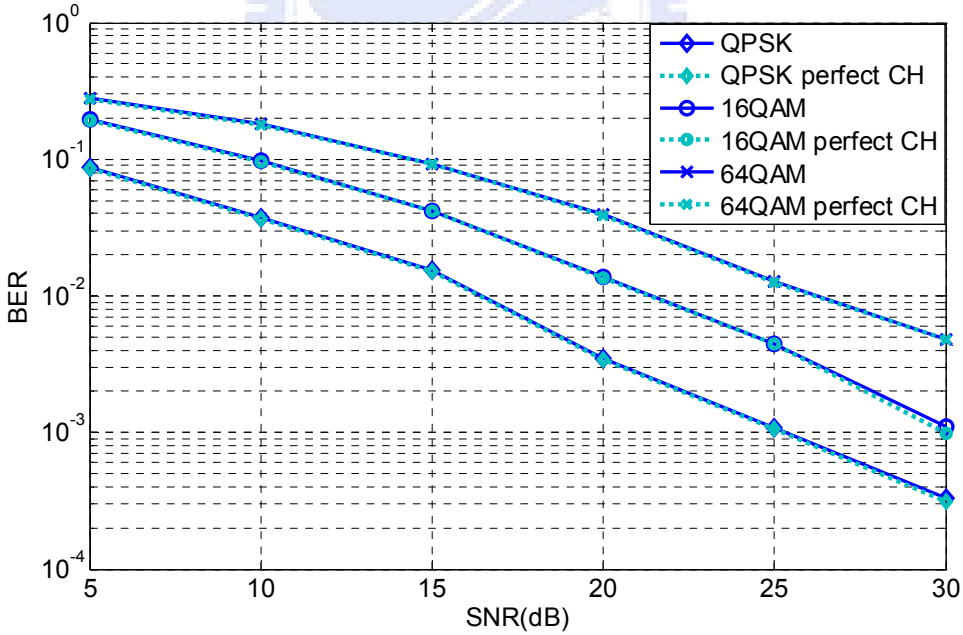

Figure 6-8 Performance of the joint time/frequency channel estimate for QPSK, 16QAM, 64QAM (Channel B)

6.2 Results of channel estimation in Chapter 4

The channel model is the same as the one shown in Table 6-1. The only difference is that the tap positions are changed for each OFDM symbol, and the delays of the channel taps in the aliasing area are set random (one or two taps). The simulation setup is also the same as that in Section 6.1. The channel estimation method is that depicted in Figure 4-5.

6.2.1 Comparison for the choice of pseudo pilots

We have discussed the choice of pseudo pilots in Section 4.3. Figure 6-9 shows the BER performance for the different choices for pseudo pilots. As defined, pseudo pilots are obtained from decisions and they can be erroneous. Figure 6-10 shows the SER of the pseudo pilots used. Figure 6-11 and 6-12 are similar to those in Figure 6-9 and 6-10 except for that Channel B is used. Here, guard band insertion is not conducted.

We can see from Figure 6-9 and Figure 6-11 that the best choice for the addition pilots is to use all detected data as the pseudo pilots. If one out three detected data is used as pseudo pilots, its performance is worse than the previous case. However, in order to compare with the performance of the conventional joint time/frequency domain channel estimator in Chapter 3, we will use the scheme with one out of three detected data as the pseudo pilots. In the simulations below, we will use the setting for simulations.

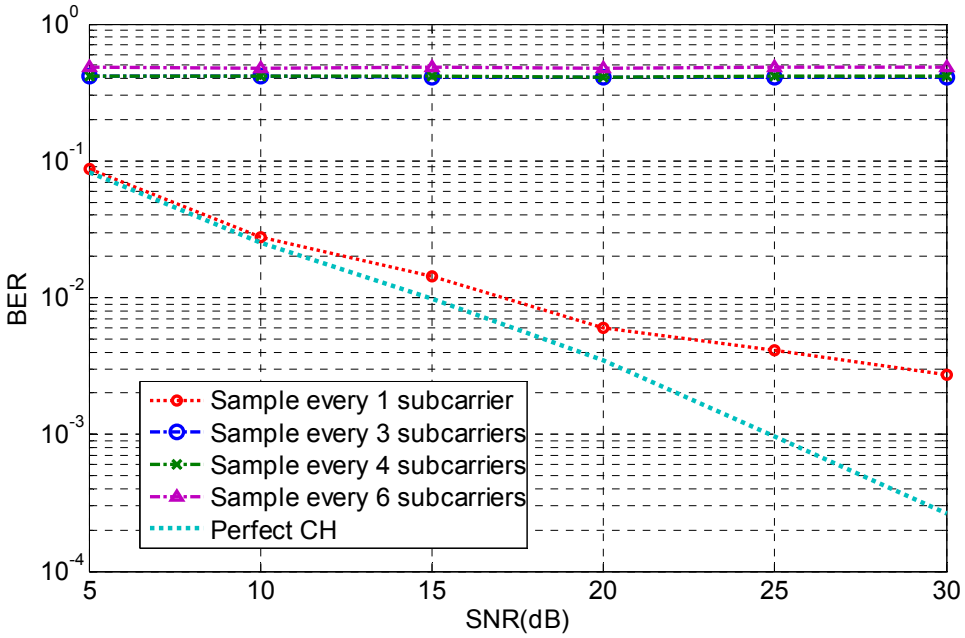

Figure 6-9 BER comparison of different pseudo pilot selection schemes (without guard band insertion, Channel A)

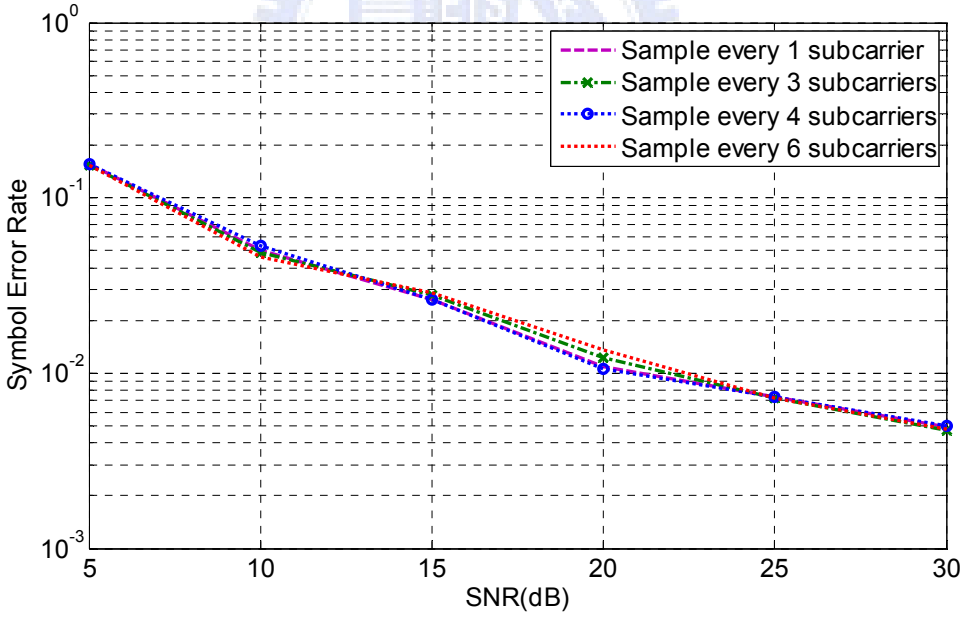

Figure 6-10 SER of pseudo pilots for different pseudo pilot selection schemes (without guard band insertion, Channel A)

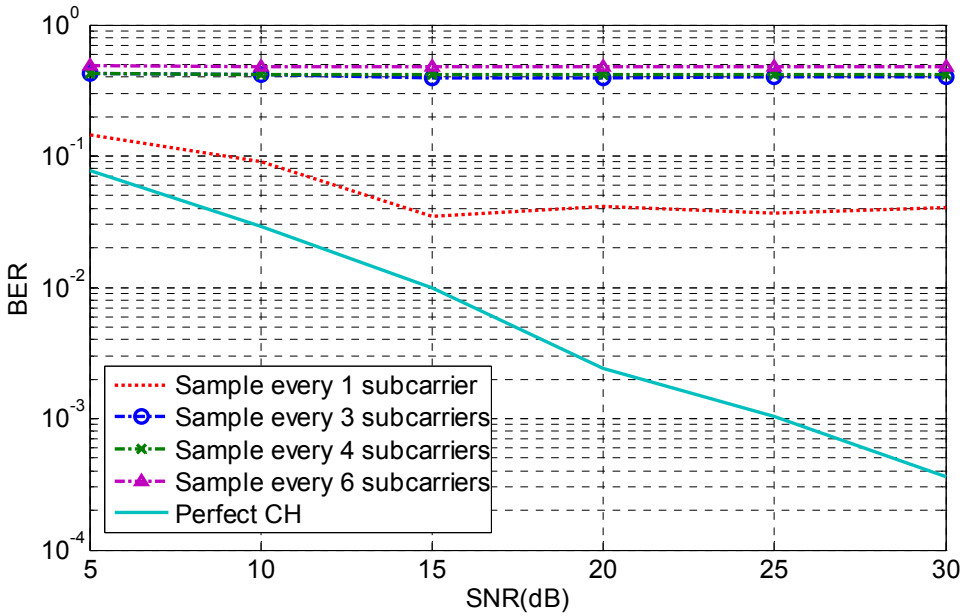

Figure 6-11 BER comparison of different pseudo pilot selection schemes (without guard band insertion, Channel B)

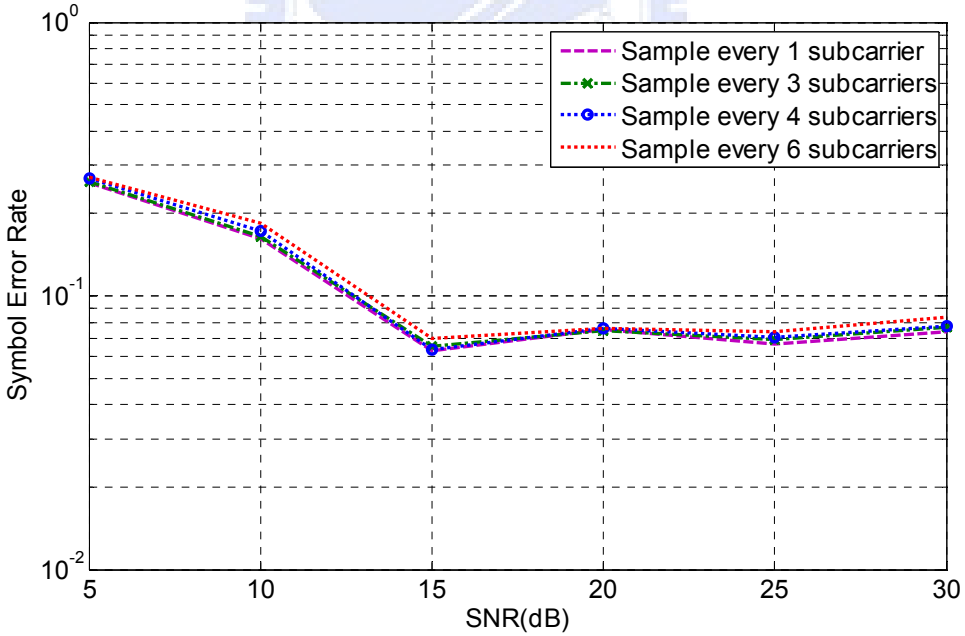

Figure 6-12 SER of pseudo pilots for different pseudo pilot selection schemes (without guard band insertion, Channel B)

Figure 6-13 compares the performance for the channel estimator with or without the

guard band insertion. We can see that under the same number of iterations, the performance with the guard band insertion is much better than that without. Notice that we conduct the guard band insertion only when the channel response is completely estimated.

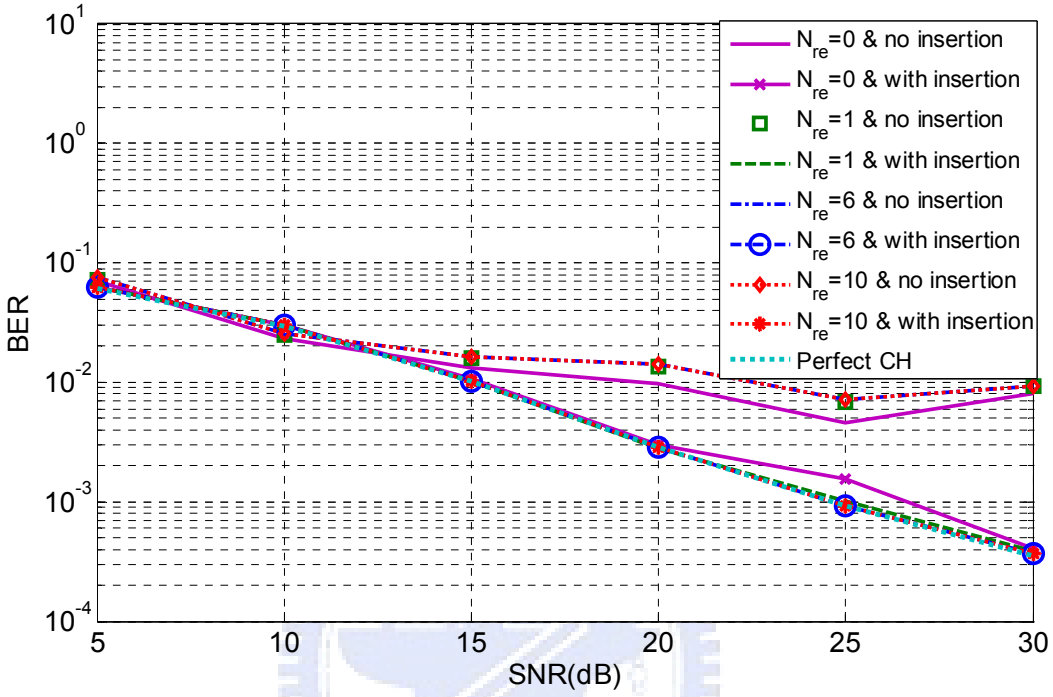

Figure 6-13 Performance comparison for the channel estimator with/without guard band insertion (Channel A)

6.2.2 The Results of iterative channel estimation with pilots and pseudo pilots

Figure 6-14 and Figure 6-15 show the performance of the proposed estimator for different number of iterations. The modulation scheme is QPSK. Here, guard band insertion is conducted and the data in the original pilots are used in the SIC-LS algorithm. In other words, the pseudo pilots are only used to help locate channel taps. As we can see, the performance is satisfactory when the number of iteration is 6. Also, its performance is almost as good as that when the number of iteration is 10.

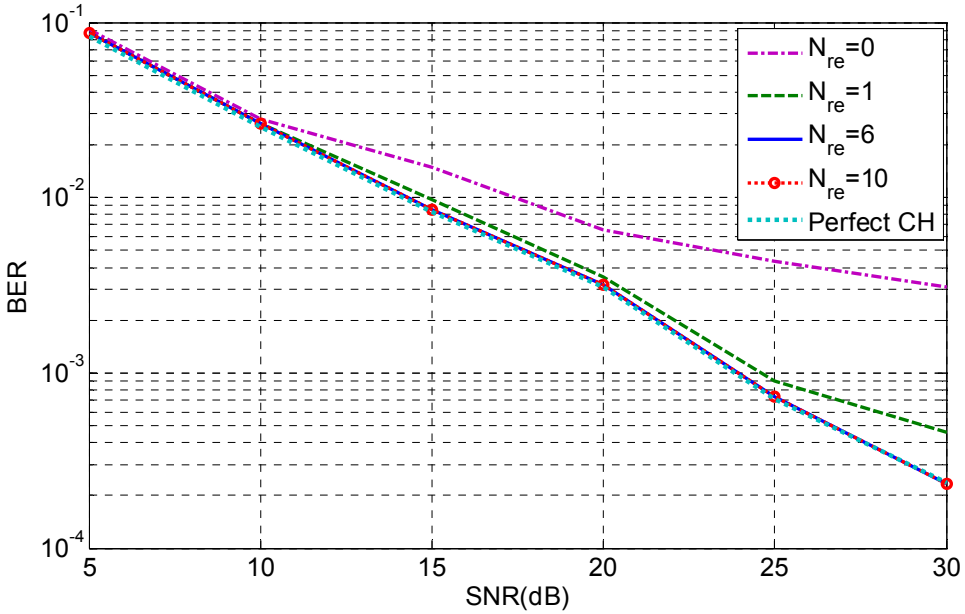

Figure 6-14 Performance comparison for the channel estimator with different numbers of iteration (SIC-LS uses pilots, Channel A)

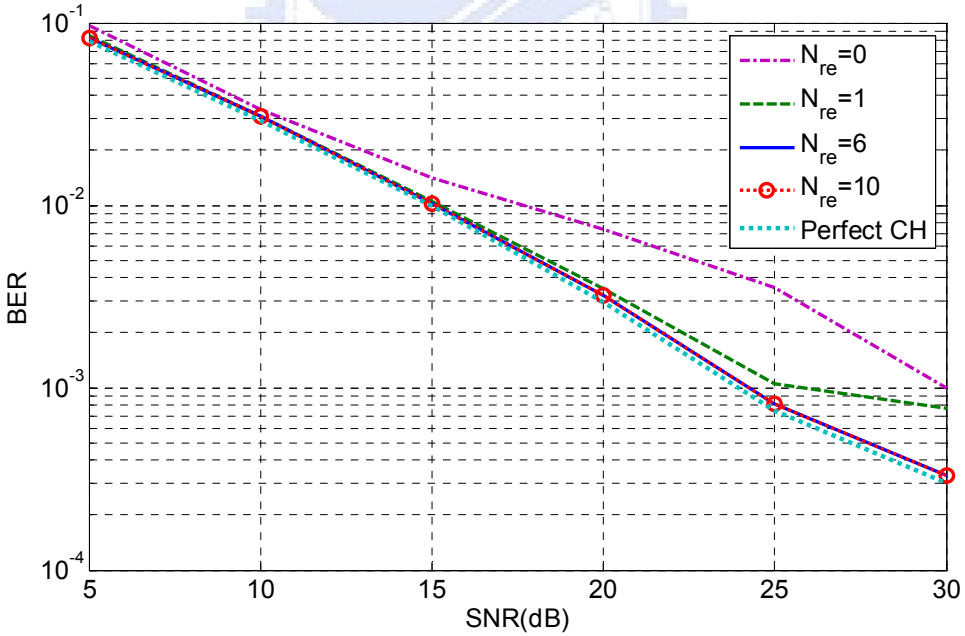

Figure 6-15 Performance comparison for the channel estimator with different numbers of iteration (SIC-LS uses pilots, Channel B)

Figure 6-16 and Figure 6-17 show the performance of the proposed channel estimation

method with QPSK, 16QAM, 64QAM modulation. The number of iteration is set as 6. As we can see, for each case the performance is almost as good as the perfect channel.

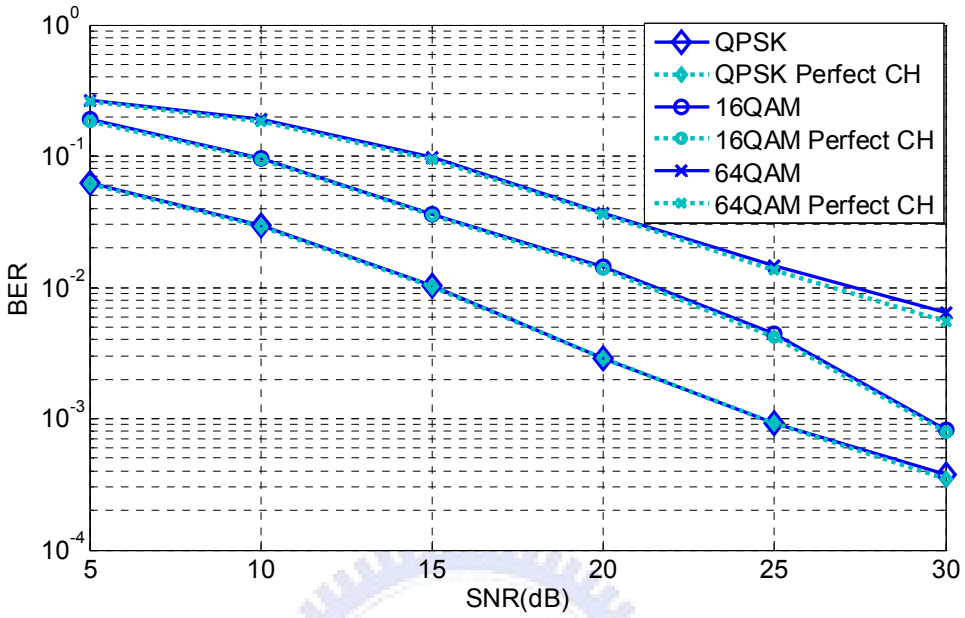

Figure 6-16 Performance comparison for the channel estimator with QPSK, 16QAM, and 64QAM (SIC-LS uses pilots, Channel A)

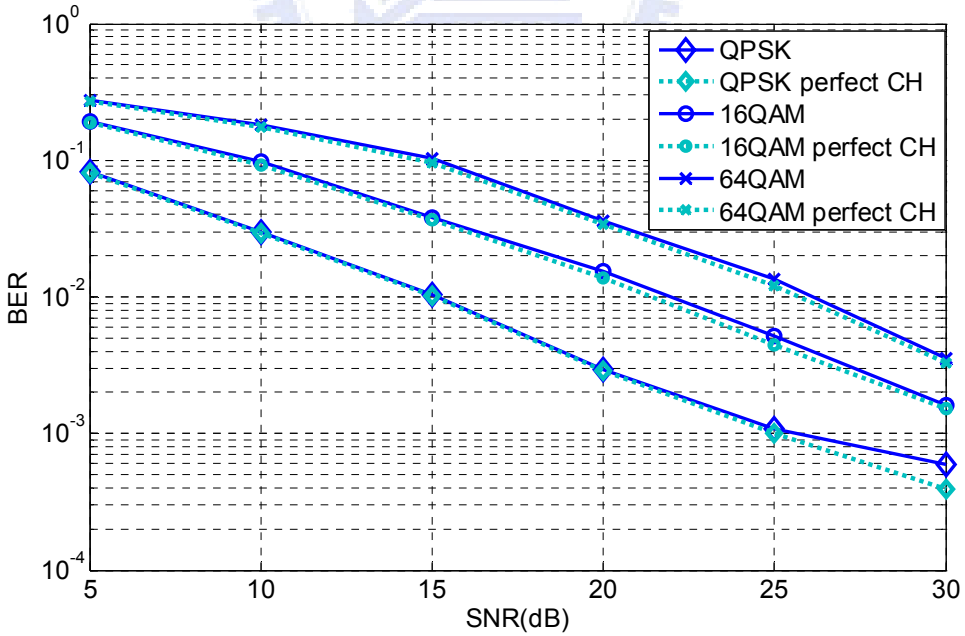

Figure 6-17 Performance comparison for the channel estimator with QPSK, 16QAM, and 64QAM (SIC-LS uses pilots, Channel B)

Figure 6-18 and Figure 6-19 show the performance of the proposed estimator when

both pilots and pseudo pilots are used in the SIC-LS algorithm. The performances with one, 6 and 10 iterations are almost the same and it is also the same with that of the perfect channel. We also see that the performance is similar to that in Figure 6-14 and Figure 6-15.

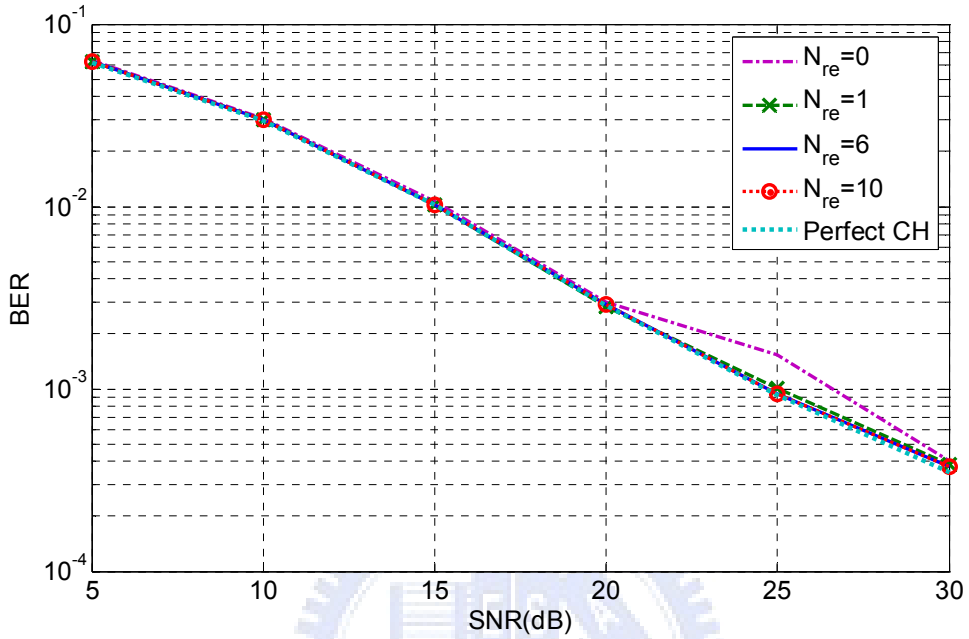

Figure 6-18 Performance comparison for the channel estimator with different numbers of iteration (SIC-LS uses original and pseudo pilots, Channel A)

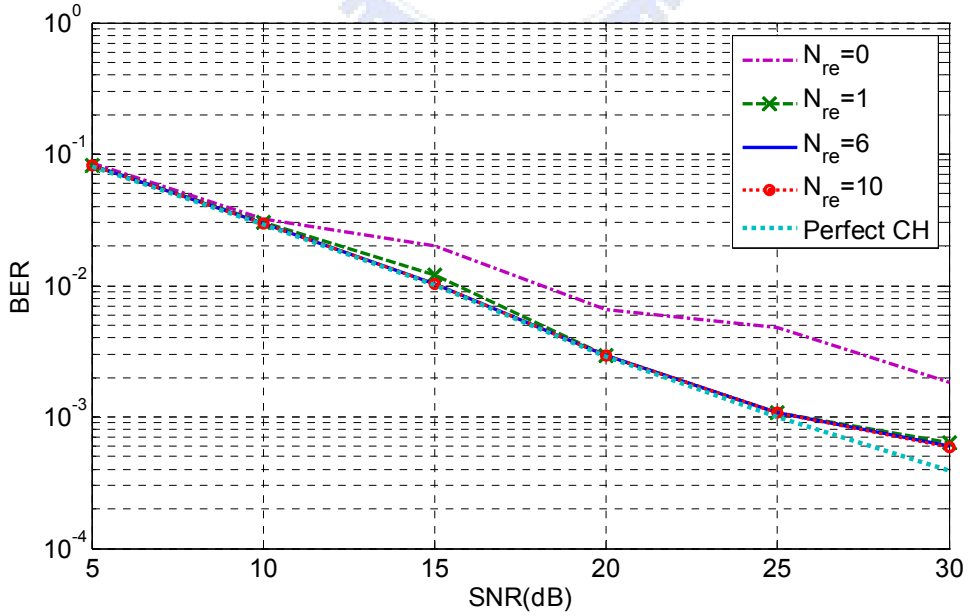

Figure 6-19 Performance comparison for the channel estimator with different numbers of iteration (SIC-LS uses original and pseudo pilots, Channel B)

Figure 6-20 and Figure 6-21 show the performance of the proposed estimator when all the detected data are taken as pseudo pilots. Compared to Figure 6-18 and Figure 6-19 (only one out of three is used as a pseudo pilot), the performance here is better. In Figure 6-20, the performance is still satisfactory even when there is no iteration. In Figure 6-21, only one iteration is sufficient to obtain good performance.

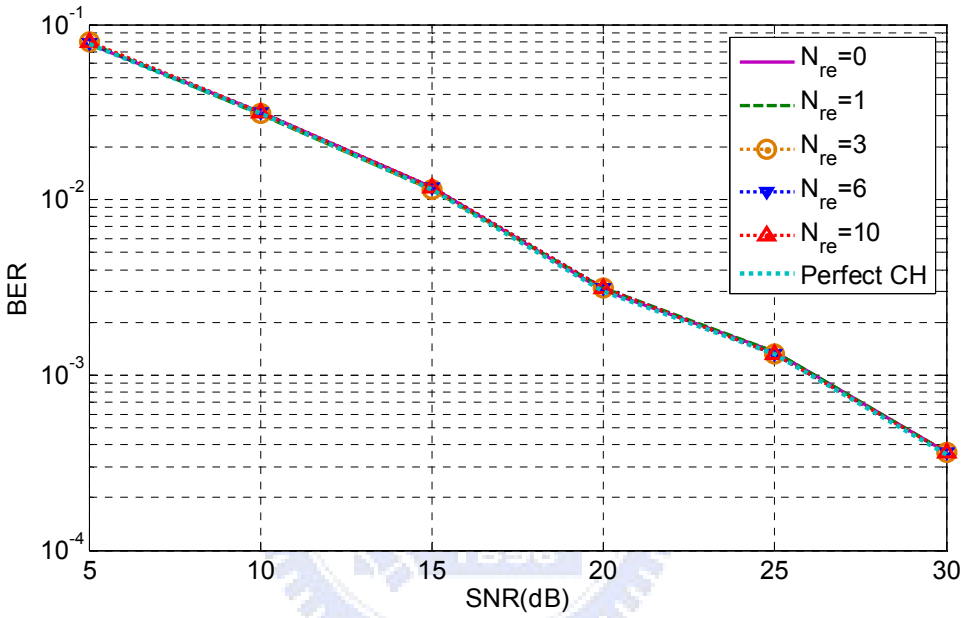

Figure 6-20 Performance comparison for the channel estimator with different numbers of iteration (SIC-LS uses original pilots and all decisions, Channel A)

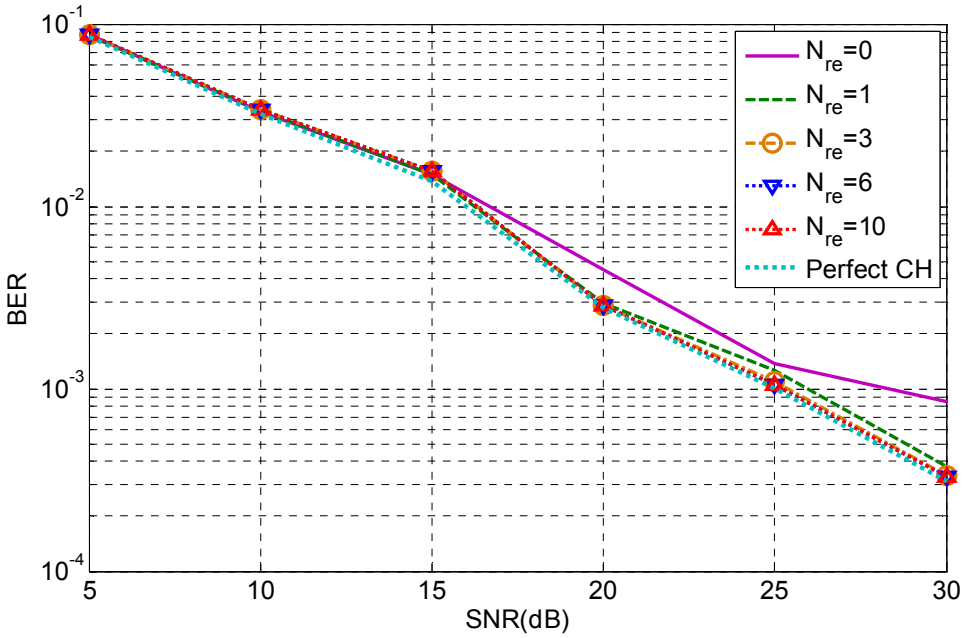

Figure 6-21 Performance comparison for the channel estimator with different numbers of iteration (SIC-LS uses original pilots and all decisions, Channel B)

6.3 Results of WLS algorithm

In this section, we report simulation results for the system we have defined. As mentioned, the number of subcarriers and the FFT size is 512 and the pilot density is 1/12. The CP size here is 64 (1/8 of 512) and the guard band size is also 64. The number of pilots here is 39. Modulation schemes QPSK, 16QAM and 64QAM are used in our simulations. The delays of the channel taps are also set random for different OFDM symbols.

Figure 6-22 shows the performance of the proposed channel estimation (without weighting). The modulation scheme is QPSK. Here one out of three decisions is used as a pseudo pilot, and the SIC-LS method uses pilots only. As we can see, the performance is far from satisfactory even the number of iteration is large. This is because the number of pilots is not large enough such that the SIC-LS method cannot function properly.

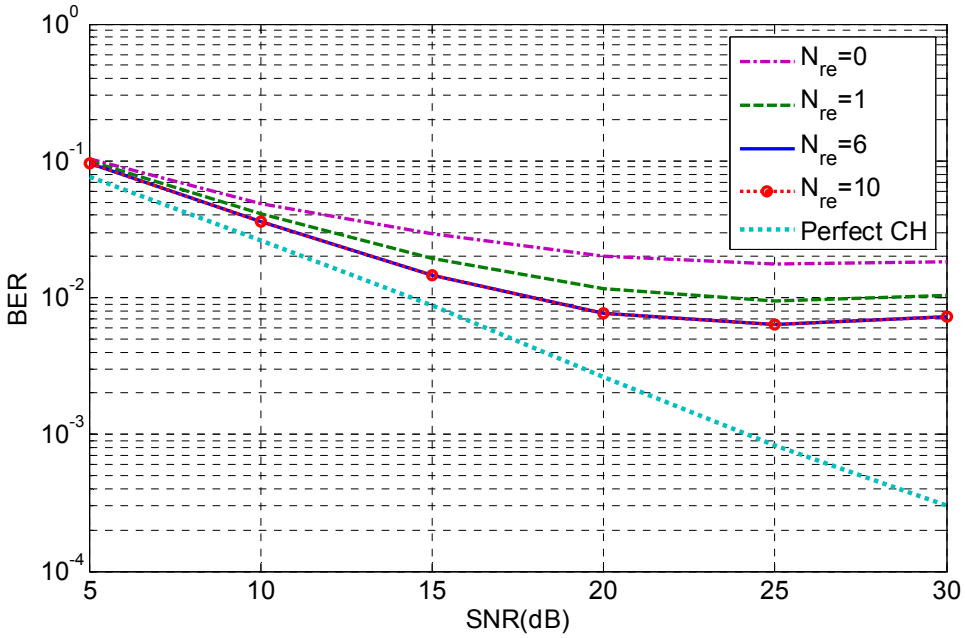

Figure 6-22 Comparison of the proposed channel estimator (no weighting, SIC-LS uses pilots, Channel C)

Figure 6-23 shows the performance of the proposed channel estimation (without weighting) for the QPSK, 16QAM, 64QAM modulation. Different from that in Figure 6-22, the SIC-LS method now uses the original and pseudo pilots. It is apparent that the performance has been improved. However, for 16QAM and 64QAM, the performance in high SNR areas seems less satisfactory. Unlike the DVB-T system, the number of pseudo pilots is not large. As a result, erroneous decisions will affect the estimation performance more seriously.

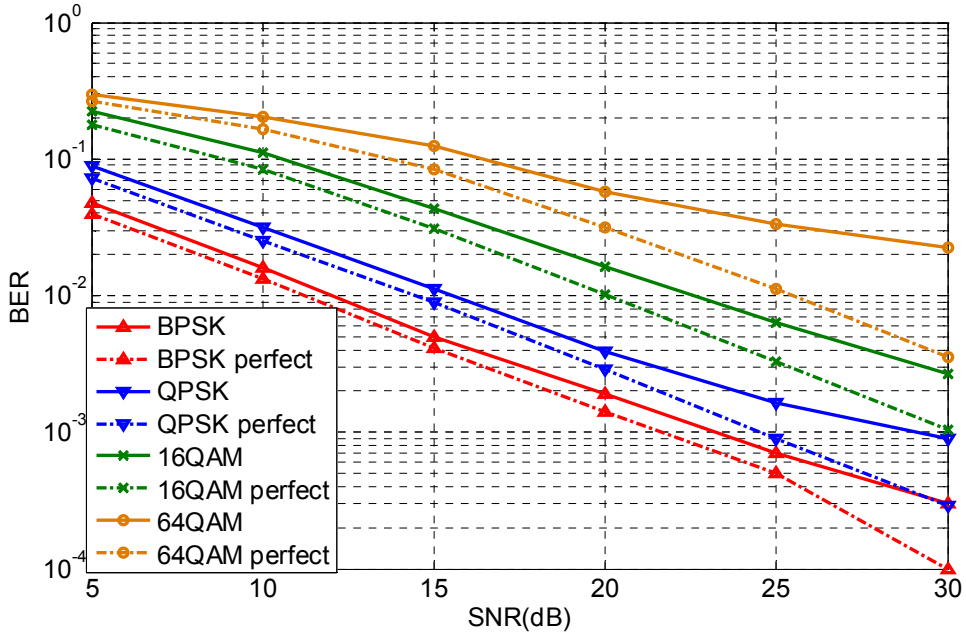

Figure 6-23 Performance of the proposed channel estimator (no weighting, QPSK, 16QAM, and 64QAM, Channel C)

6.3.1 Results of the weighted LS algorithm by pilots and pseudo pilots

Figure 6-24 shows the performance of the proposed channel estimation method with the WLS algorithm. The channel estimation method is that depicted in Figure 4-9. Here, the number of iteration is set as 6, one out of 3 decisions is used as a pseudo pilot, and the modulation scheme is BPSK. Here, we apply the first weighting scheme as described in Section 4.4. The weight of each decision regions is shown in Table 6-2 and the weights of pilots are all 1. In the table, x represents the estimated transmitted signal. We have tried some combinations with different regions and different weights. The weight values in Table 6-2 are obtained by trial-and-error. As we can see, the performance in Figure 6-24 is somewhat degraded in high SNR region.

Region	$x < -2$ $2 < x$	$-2 \le x < -1.5$ $1.5 < x \le 2$	$-1.5 \le x \le -0.5$ $0.5 \le x \le 1.5$
Weight	0.2	0.5	0.7

Table 6-2 The weights of the first weighting method

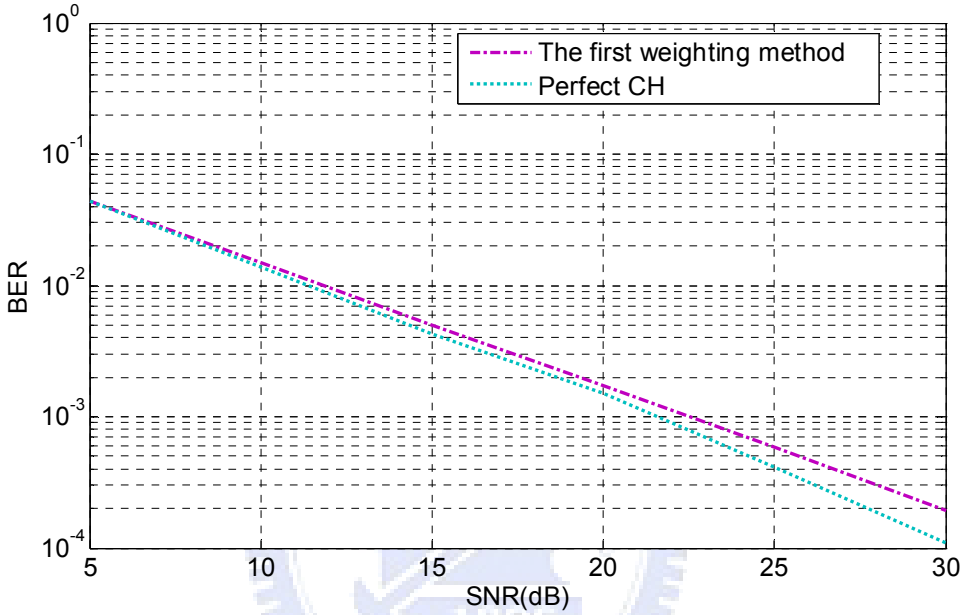

Figure 6-24 Performance of proposed channel estimation method with WLS (the first weighting method, Channel C)

Figure 6-25 shows the performance of the proposed channel estimation method with the WLS algorithm. Here, the second weighting method is applied. The weight is determined by the SNR of each subcarrier as discussed in Section 4.4. Table 6-3 shows the weights. In the table, x represents the SNR(dB) of each subcarrier and the weight for a pilot is 1. The weight values in Table 6-3 are also obtained with trial-and-error. As we can see, the performance is improved with the second weighting scheme.

Region	$x \le -5$	$-5 < x \le 0$	$0 < x \le 5$	$5 < x < 10$	$10 \le x$
Weight	0.05	0.1	0.5	0.7	1

Table 6-3 The weights of the second weighting method

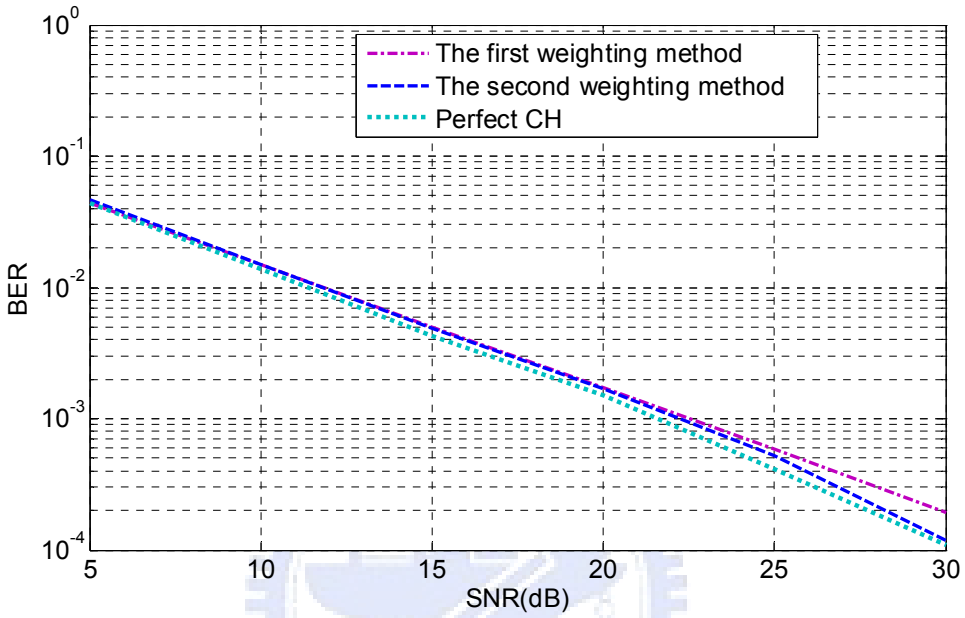

Figure 6-25 Performance of proposed channel estimation method with WLS (the second weighting method, Channel C)

We now conduct simulations to evaluate the performance of the proposed estimator with the WLS algorithm for QPSK, 16QAM, 64QAM. The weights for the WLS algorithm are shown in Table 6-4, Table 6-5 and Table 6-6. Similar to the previous cases, the weights of pilots are all 1.

Region	$x \le 0$	$0 < x \le 5$	$5 < x \le 8$	$8 < x < 10$	$10 \le x$
Weight	0.1	0.35	0.7	0.8	1

Table 6-4 Weights used for QPSK

Region	$x \le 0$	$0 < x \le 10$	$10 < x \le 15$	$15 < x < 20$	$20 \le x$
Weight	0.05	0.3	0.85	0.9	1

Table 6-5 Weights used for 16QAM

Region	$x \le 0$	$0 < x \le 10$	$10 < x \le 15$	$15 < x \le 20$	$20 < x \le 25$	$25 < x < 30$	$30 \le x$
Weight	0.05	0.3	0.4	0.45	0.55	0.6	0.8

Table 6-6 Weights used for 64QAM

Figure 6-26 shows the performance comparison. From the figure, we see that the performance of the proposed WLS channel estimator for BPSK and QPSK is very close to the optimum, that for 16QAM is improved (compared with the one without weighting), and that for 64QAM is not improved (compared with the one without weighting).

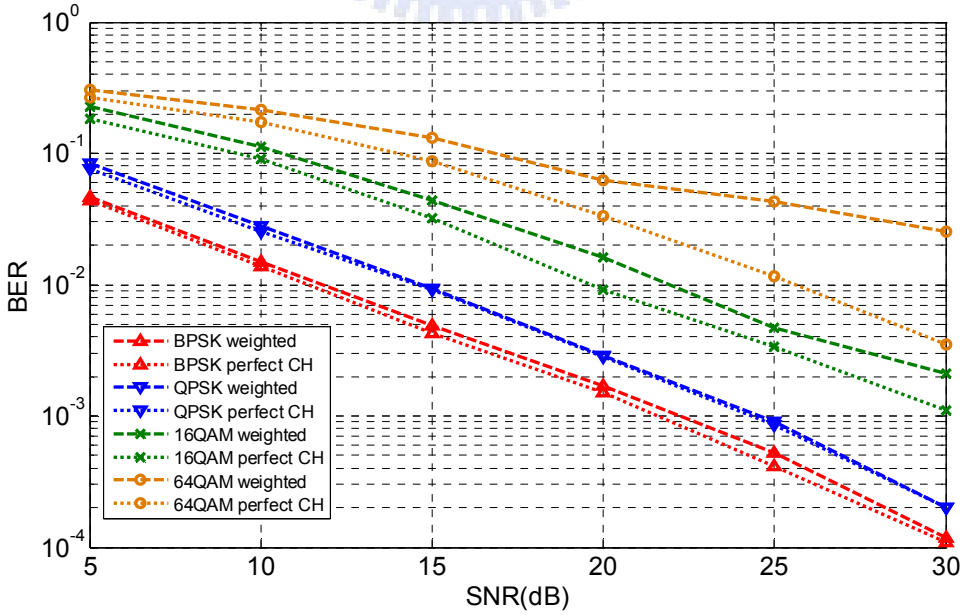

Figure 6-26 Performance of proposed channel estimation method with WLS for BPSK, QPSK,

16QAM, 64QAM (Channel C)

Figure 6-27 shows the performance comparison for the proposed channel estimators with LS and WLS methods for BPSK, QPSK, 16QAM, and 64QAM.

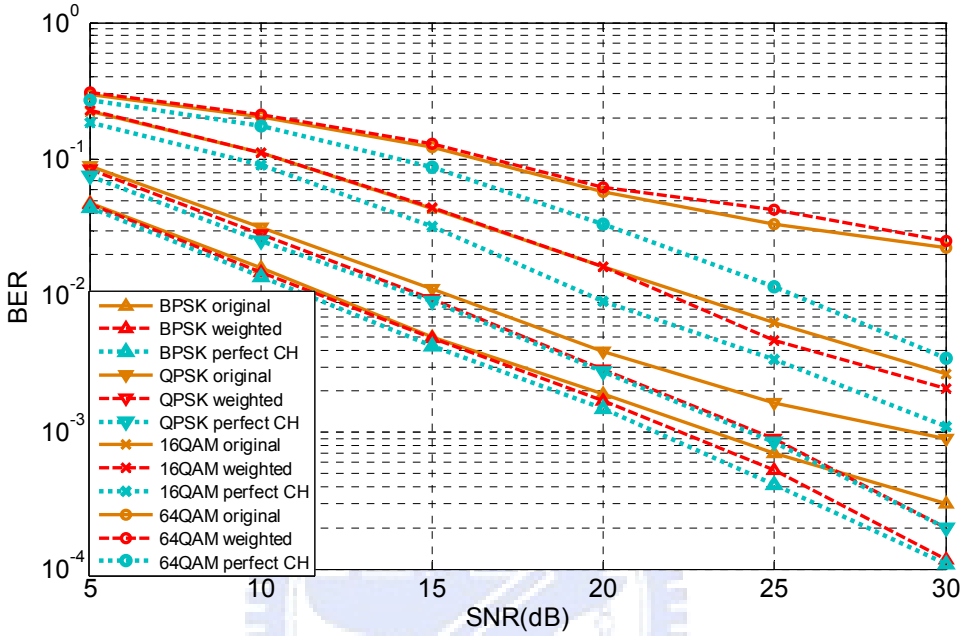

Figure 6-27 Performance comparison for proposed channel estimators with LS and WLS methods (BPSK, QPSK, 16QAM, 64QAM, Channel C)

In order to further improve the performance of the proposed channel estimator with the WLS method, we use all the decisions as the pseudo pilots. Figure 6-28 and Figure 6-29 show the performance of the proposed channel estimator with the WLS method for 16QAM and 64QAM. The weights used in the simulation f or16QAM and 64QAM are the same as those in Table 6-5 and 6-6. We can see that the performance is almost as good as the optimum.

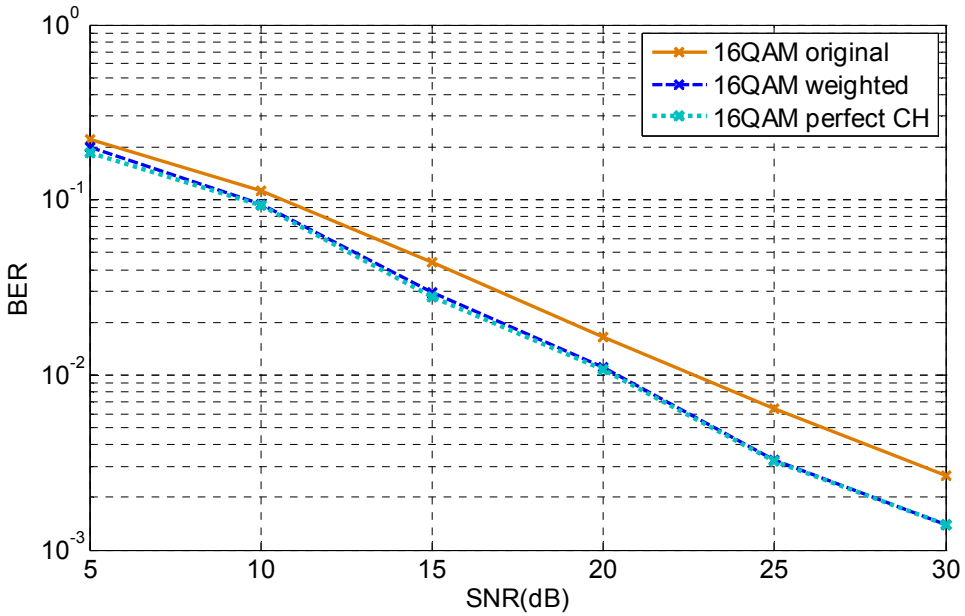

Figure 6-28 Performance of proposed channel estimators with WLS method for 16QAM (all decisions are used, Channel C)

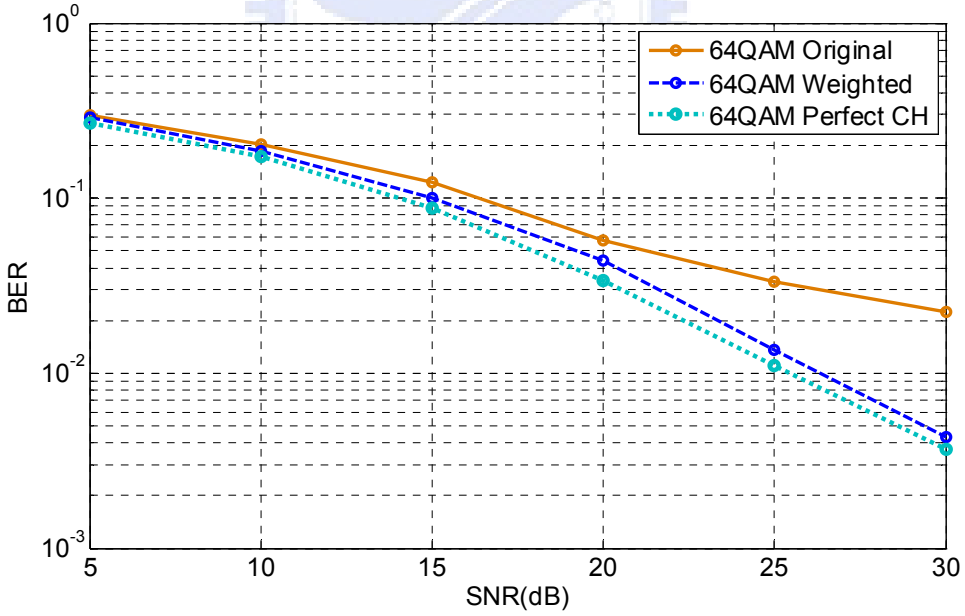

Figure 6-29 Performance of proposed channel estimators with WLS method for 64QAM (all decisions are used, Channel C)

6.3.2 The Weighted LS channel estimation with different aliasing power

In this Section, we would like to test how strong the aliasing power we can tolerate for the proposed channel estimator with the WLS method in the DVB-T system. The parameters of the DVB-T system are the same as those in Section 6.2. For the WLS method, all decisions are used as pilots. The power profiles of the first 4 taps are the same as those in Table 6-1. We let the last two taps be located in the aliasing area. Table 6-7, Table 6-8, Table 6-9 are the channel power profiles used for QPSK, 16QAM, and 64QAM. For the QPSK scheme, the total power is 4.1955 (2.4882+1.7073) and the maximum power we can use for the last two taps is 1.7073 (40.7% of the total power). For the 16QAM scheme, the total power is 3.8399 (2.4882+1.3517) and the maximum power we can use for the last two taps is 1.3517 (35.2% of the total power). Finally, for the 64QAM scheme, the total power is 3.413 (2.4882+0.9248) and the maximum power we can use for the last two taps is 0.9248 (27.1% of the total power). Figure 6-30, Figure 6-31 and Figure 6-32 show the simulation results.

Aliasing or not	Tap Number	Average Power (Lin)	Total Power(Lin)
Nonaliasing	1	0.9951	2.4882 (0.593 of the total power)
	2	0.5727	
	3	0.4992	
	4	0.4273	
Aliasing	5	0.8539	1.7073 (0.407 of the total power)
	6	0.8534	

Table 6-7 The channel taps power for QPSK scheme

Aliasing or not	Tap Number	Average Power (Lin)	Total Power(Lin)
Nonaliasing	1	0.9951	2.4882 (0.648 of the total power)
	2	0.5727	
	3	0.4992	
	4	0.4273	
Aliasing	5	0.7116	1.3517 (0.352 of the total power)
	6	0.6401	

Table 6-8 The channel taps power for 16QAM scheme

Aliasing or not	Tap Number	Average Power (Lin)	Total Power(Lin)
Nonaliasing	1	0.9951	2.4882 (0.729 of the total power)
	2	0.5727	
	3	0.4992	
	4	0.4273	
Aliasing	5	0.4981	0.9248 (0.271 of the total power)
	6	0.4267	

Table 6-9 The channel taps power for 64QAM scheme

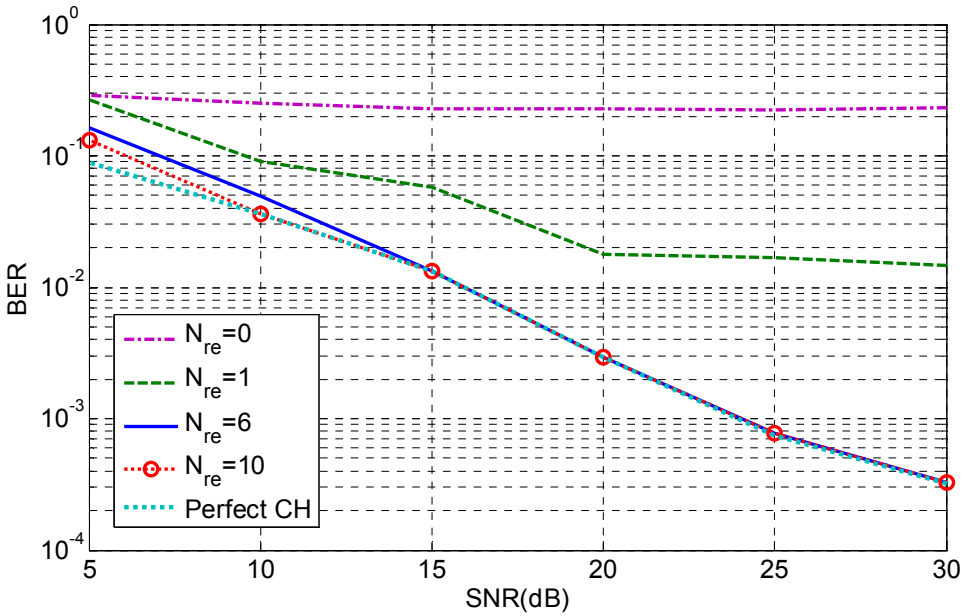

Figure 6-30 Performance of proposed channel estimators with WLS method for QPSK (all decisions are used, DVB-T, Channel B)

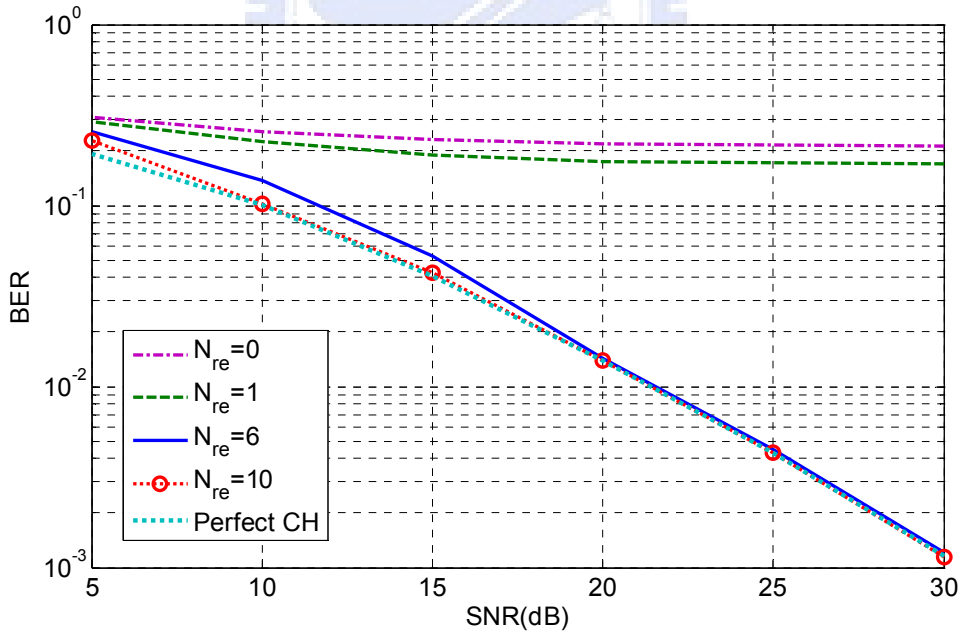

Figure 6-31 Performance of proposed channel estimators with WLS method for 16QAM (all decisions are used, DVB-T, Channel B)

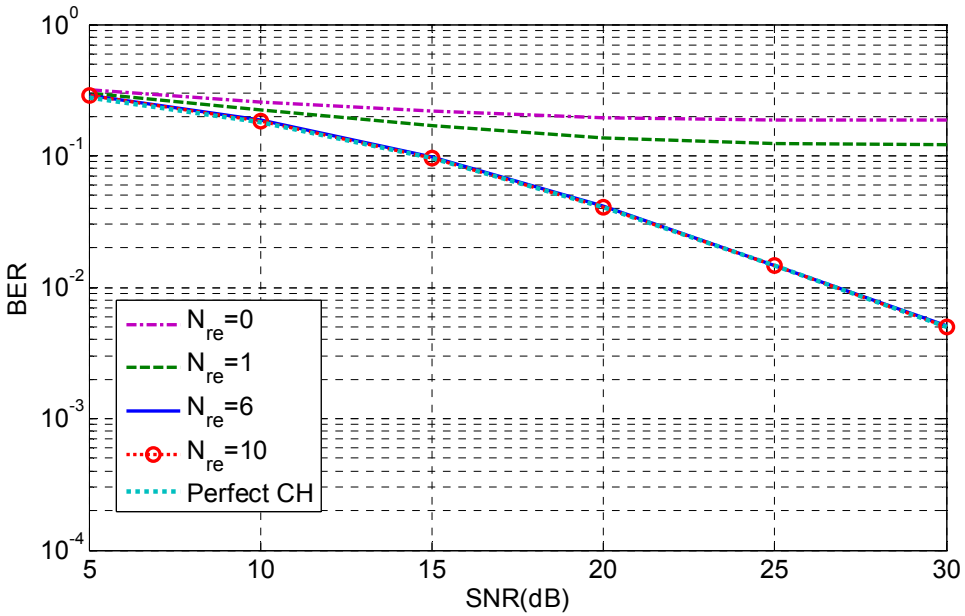

Figure 6-32 Performance of proposed channel estimators with WLS method for 64QAM (all decisions are used, DVB-T, Channel B)

6.4 Results of proposed time-variant channel estimation in Chapter 5

In this section, we evaluate the performances of the proposed time-variant channel estimation method. The simulations are conducted for the 2K-mode DVB-T system with the CP size of 256 (1/8 of 2048). Also, modulation schemes QPSK, 16QAM and 64QAM are used. The delays of the channel taps are still randomly set (with one tap or two taps in the aliasing area), and the tap positions are changed for different OFDM symbols. In this section, we will consider two cases; one is for the normalized Doppler frequency of 0.0244, and the other is for the normalized Doppler frequency of 0.1016. For all simulations, we assume that the tap positions are known. Also, one out of three decisions is used as a pseudo pilot.

6.4.1 Results of proposed time-variant channel estimation with normalized Doppler frequency of 0.0244

The channel power profile is shown in Table 6-10. The time-variant channel is generated with Jake's model and the normalized Doppler frequency is set to 0.0244.

Tap Number	Average Power (Lin)	Average Power (dB)
1	0.953	-0.2091
2	1.086	0.3583
3	0.9873	-0.0555
4	0.6999	-1.5496
5	0.5139	-2.8912
6	0.3728	-4.2852

Table 6-10 Channel tap power profile

Figure 6-33 and 6-34 show the performance of the proposed time-variant channel estimation method for QPSK. Here, the SIC-LS method uses the data in pilots only. We can

see that the performance is slightly worse than the optimum.

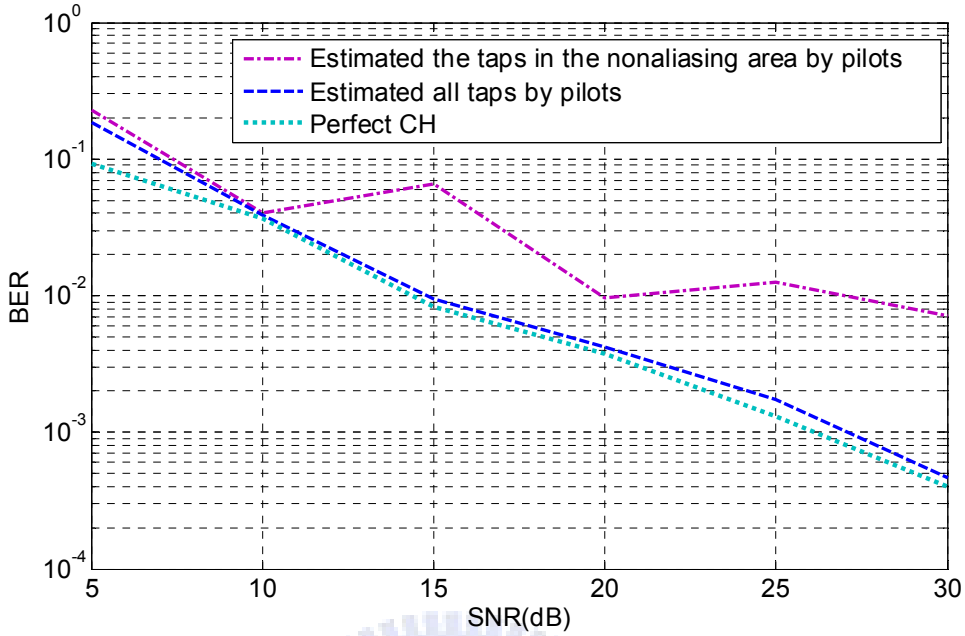

Figure 6-33 Performance of proposed time-variant channel estimator for QPSK (SIC-LS uses pilots, Channel A)

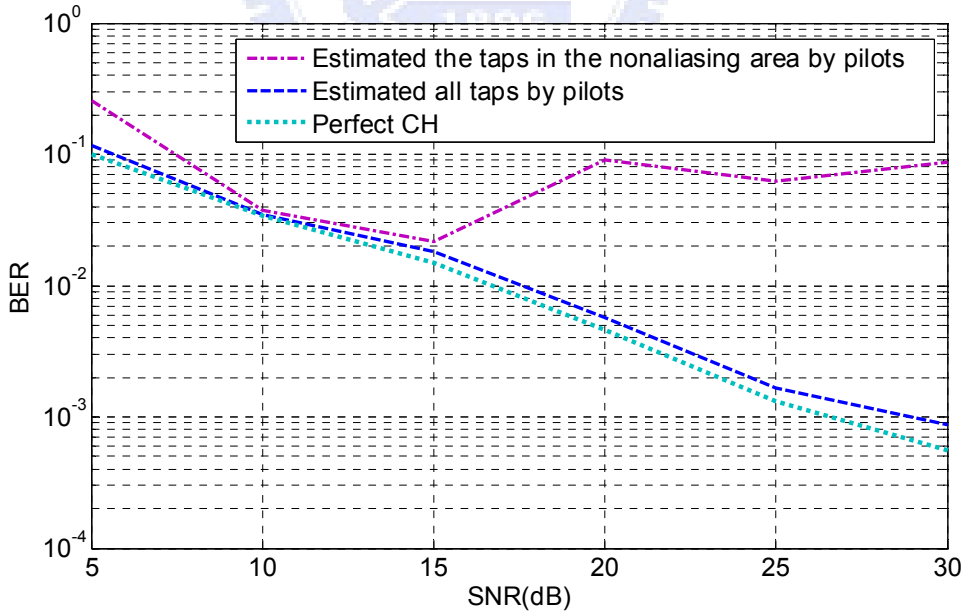

Figure 6-34 Performance of proposed time-variant channel estimator for QPSK (SIC-LS uses pilots, Channel B)

Figure 6-35 and Figure 6-36 show the performance of the proposed time-variant channel estimation method for QPSK. Here, the SIC-LS algorithm uses original and pseudo pilots. Figure 6-35 and 6-36 show the simulation results. We can see that the performance is improved a little bit. Note that the proposed estimator here requires three iterations to converge (for Channel B). This is because decision errors can occur so the performance is not good in the first and second iteration.

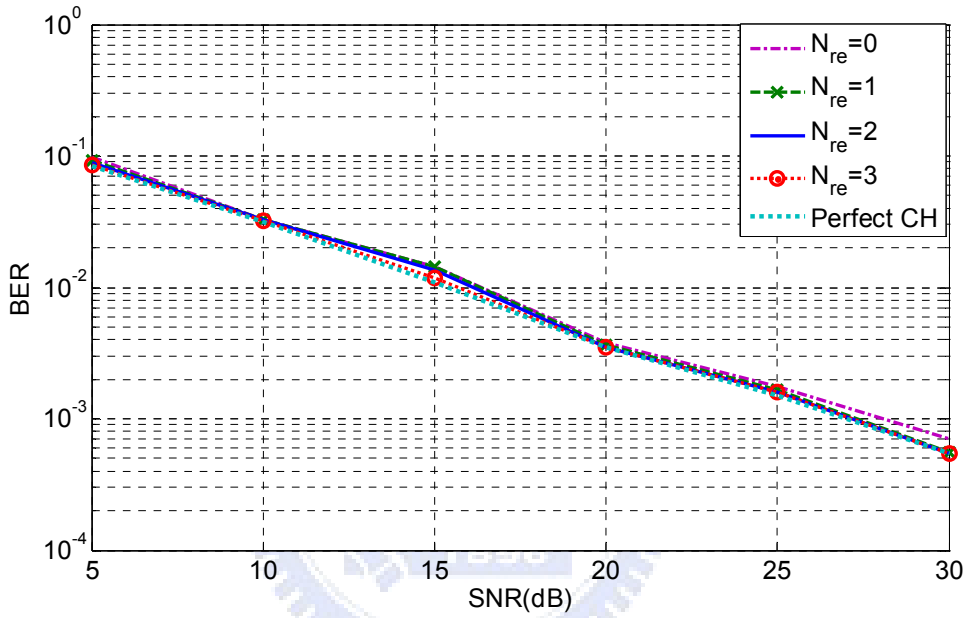

Figure 6-35 Performance of proposed time-variant channel estimator for QPSK (SIC-LS uses original and pseudo pilots, Channel A)

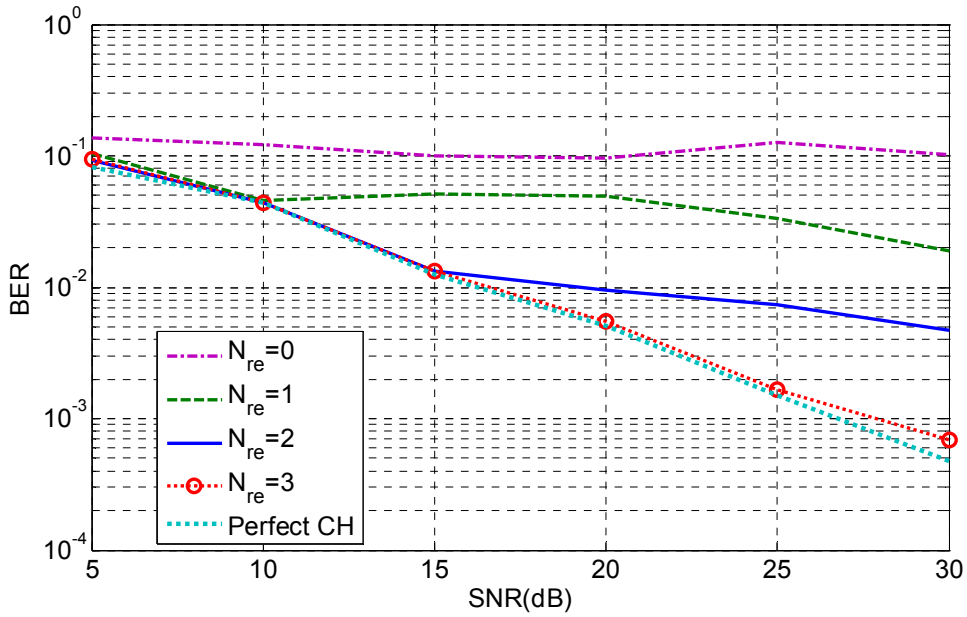

Figure 6-36 Performance of proposed time-variant channel estimator for QPSK (SIC-LS uses original and pseudo pilots, Channel B)

Figure 6-37 to Figure 6-42 show the performance of the proposed time-variant channel estimator with the WLS algorithm for QPSK, 16QAM and 64QAM. The SIC-WLS uses original and pseudo pilots. The weights of pilots are all set to be 1 and the weights of pseudo pilots are all set to be 0.8. We can see that in all cases (except for 64QAM in Channel B) the performance of the estimator is as good as the optimum.

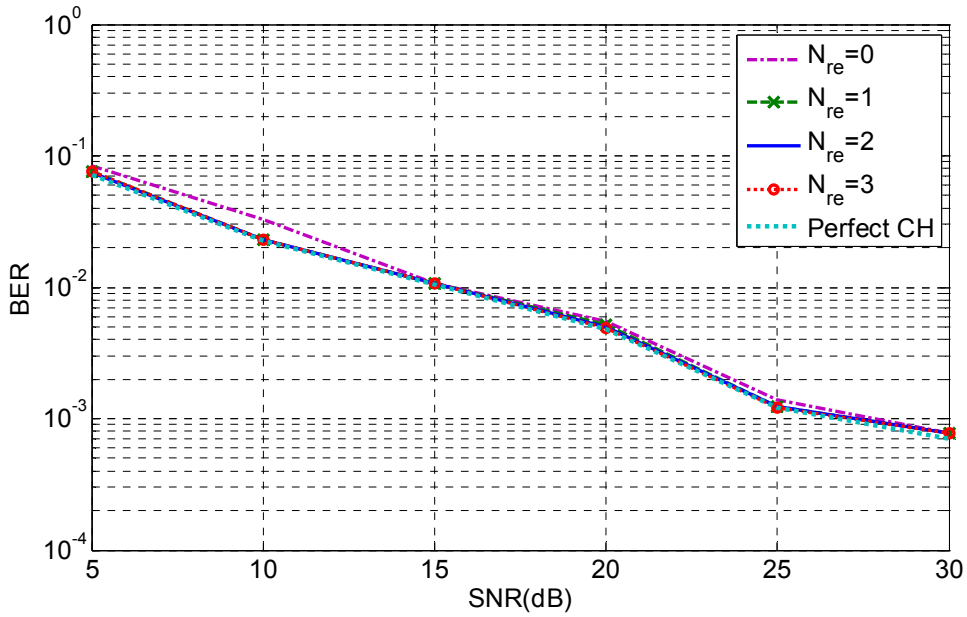

Figure 6-37 Performance of proposed time-variant channel estimator with WLS for QPSK (SIC-WLS uses original and pseudo pilots, Channel A)

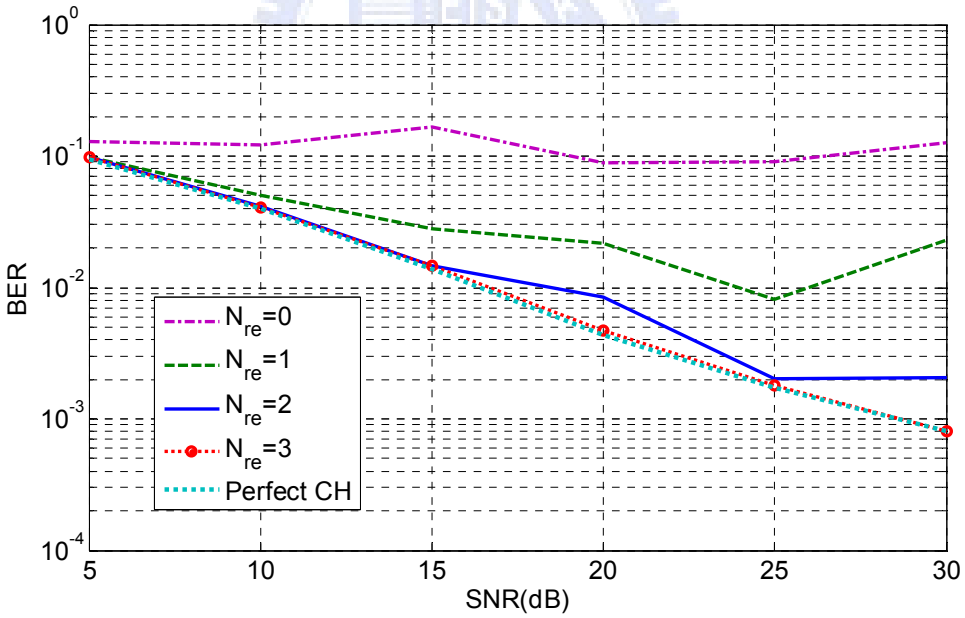

Figure 6-38 Performance of proposed time-variant channel estimator with WLS for QPSK (SIC-WLS uses original and pseudo pilots, Channel B)

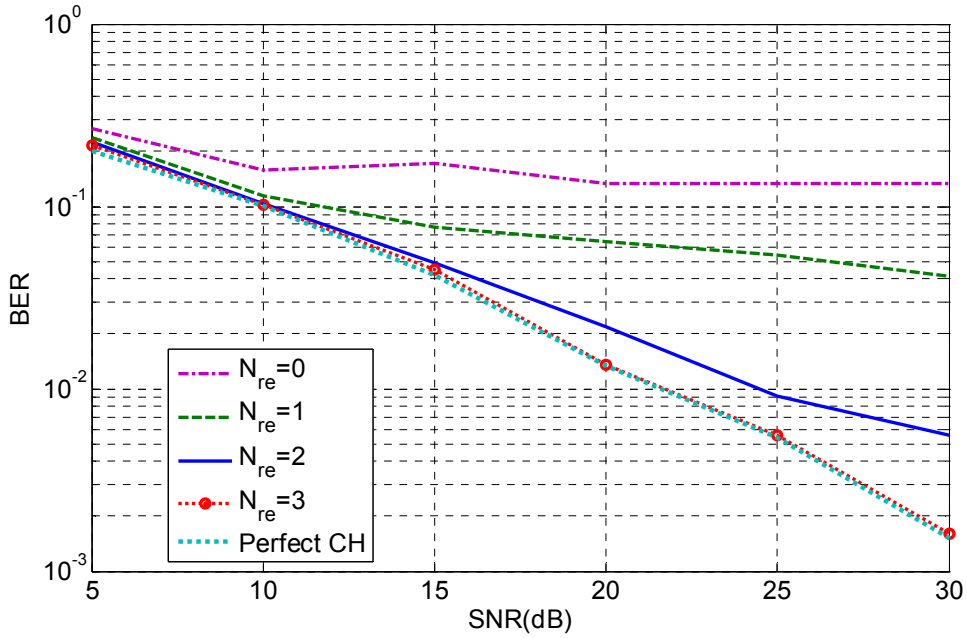

Figure 6-39 Performance of proposed time-variant channel estimator with WLS for 16QAM (SIC-WLS uses original and pseudo pilots, Channel A)

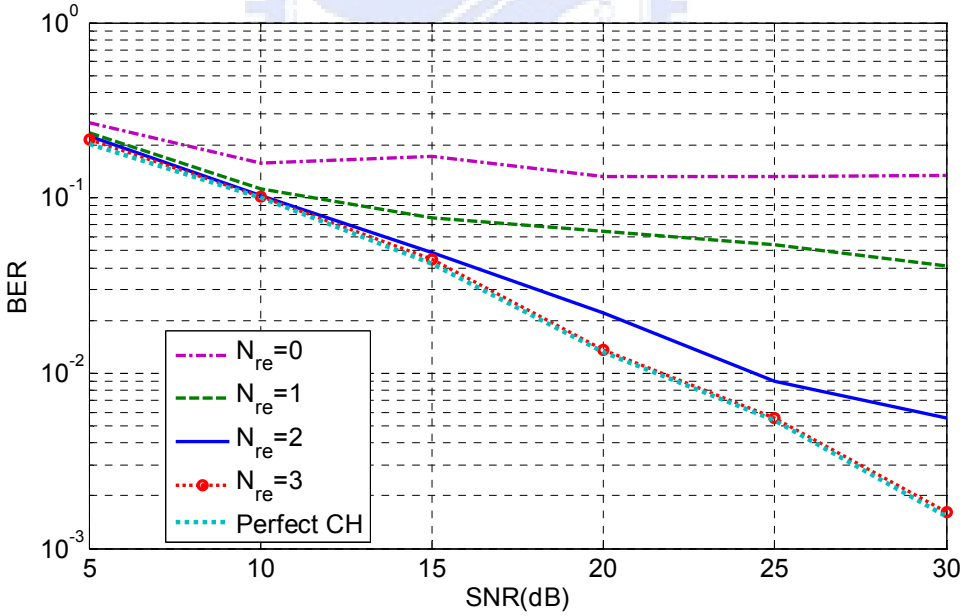

Figure 6-40 Performance of proposed time-variant channel estimator with WLS for 16QAM (SIC-WLS uses original and pseudo pilots, Channel B)

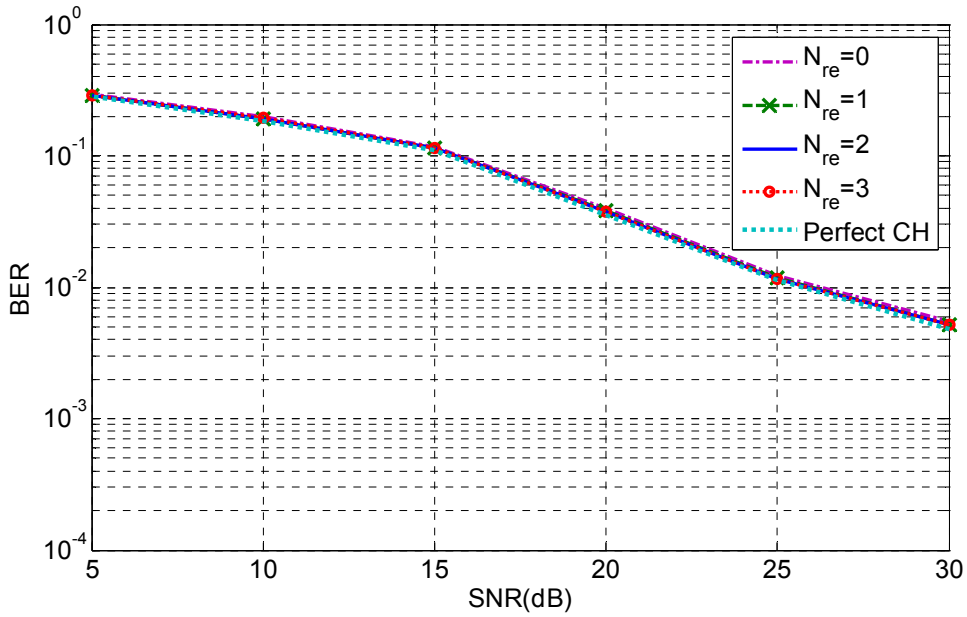

Figure 6-41 Performance of proposed time-variant channel estimator with WLS for 64QAM (SIC-WLS uses original and pseudo pilots, Channel A)

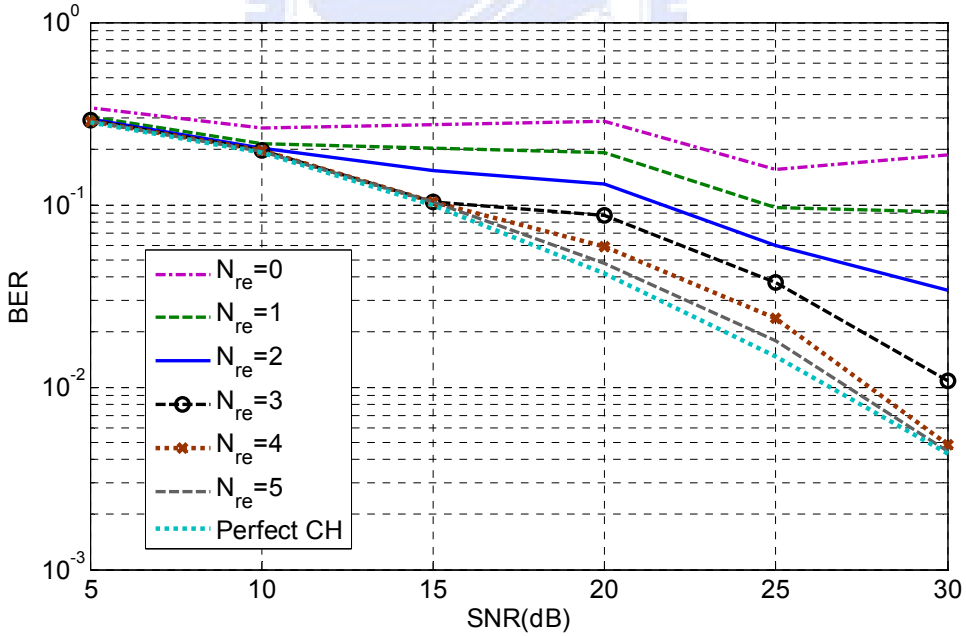

Figure 6-42 Performance of proposed time-variant channel estimator with WLS for 64QAM (SIC-WLS uses original and pseudo pilots, Channel B)

6.4.2 Results of proposed time-variant channel estimation with normalized Doppler frequency 0.1016

The normalized Doppler frequency is 0.1016 and the channel power profile is shown in Table 6-11. We apply the proposed estimator with the WLS algorithm, and the SIC-WLS method uses original and pseudo pilots. We change the weights of the pseudo pilots since the ICI effect is more severe here. The weights of pseudo pilots are all equal to 0.65 and the weights of pilots are still 1. Figure 6-43 to Figure 6-48 show the performance of proposed estimator with the WLS method for QPSK, 16QAM and 64QAM. We can see that the performance for all cases can be made satisfactory with the iteration number less than 5. Besides, for Channel A, only 3 iterations is required (except the 64QAM scheme).

Tap Number	Average Power (Lin)	Average Power (dB)
1	4.3594	6.3943
2	1.1591	0.6412
3	0.6446	-1.9071
4	0.4854	-3.1390
5	0.3997	-3.9827
6	0.3416	-4.6648

Table 6-11 Channel power profile

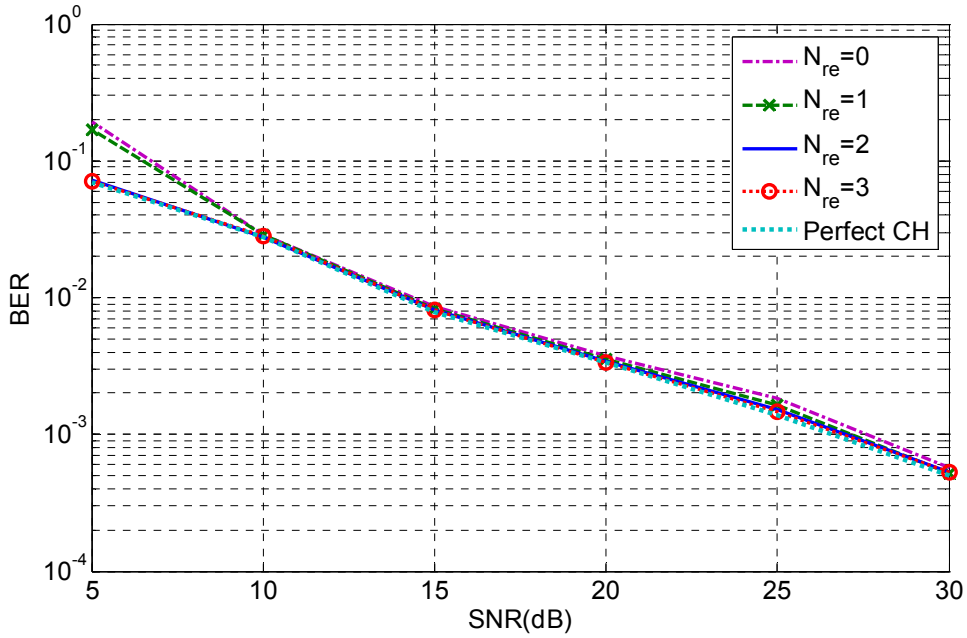

Figure 6-43 Performance of proposed time-variant channel estimator with WLS for QPSK

(SIC-WLS uses original and pseudo pilots, Channel A)

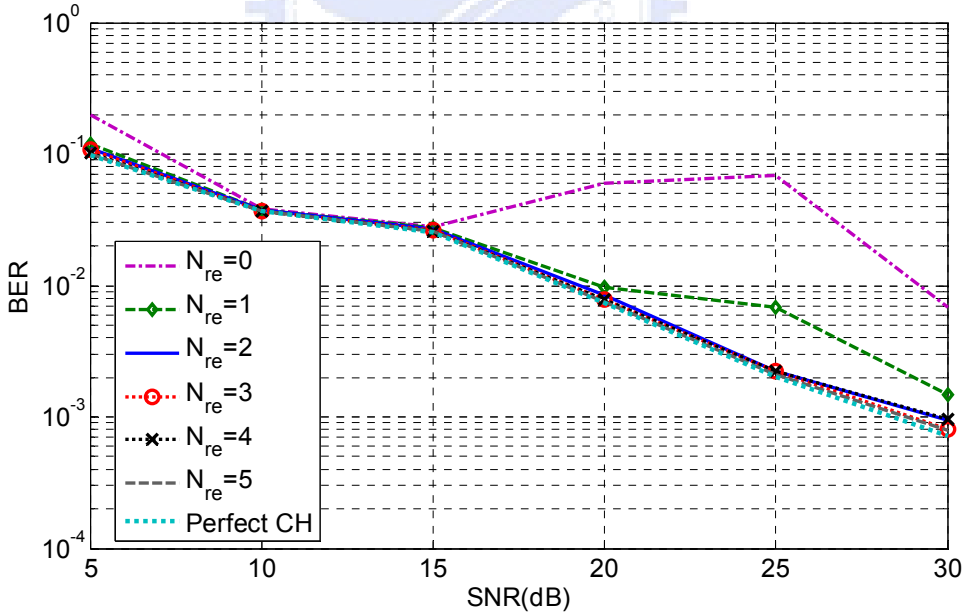

Figure 6-44 Performance of proposed time-variant channel estimator with WLS for QPSK

(SIC-WLS uses original and pseudo pilots, Channel B)

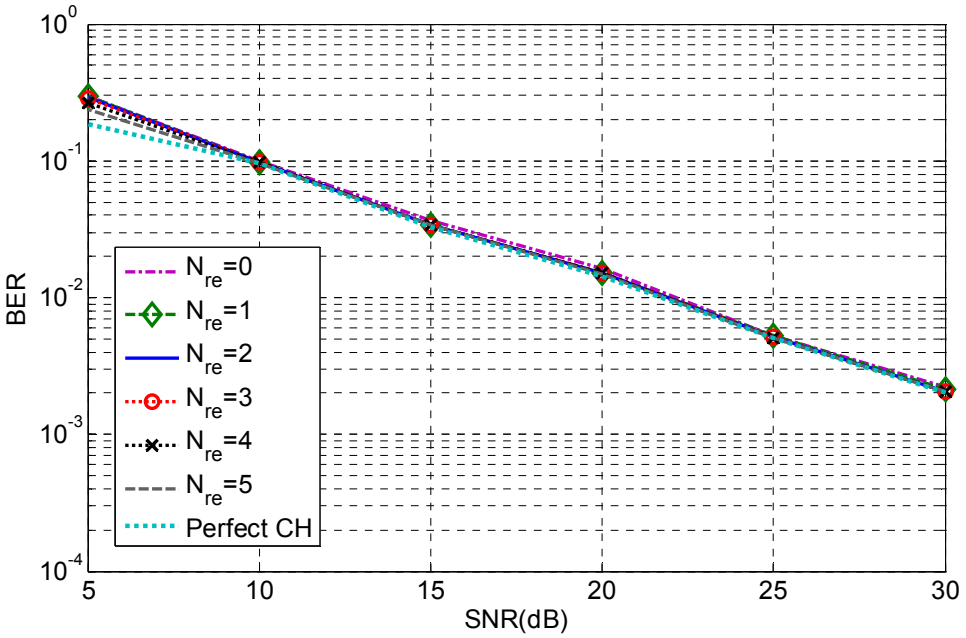

Figure 6-45 Performance of proposed time-variant channel estimator with WLS for 16QAM

(SIC-WLS uses original and pseudo pilots, Channel A)

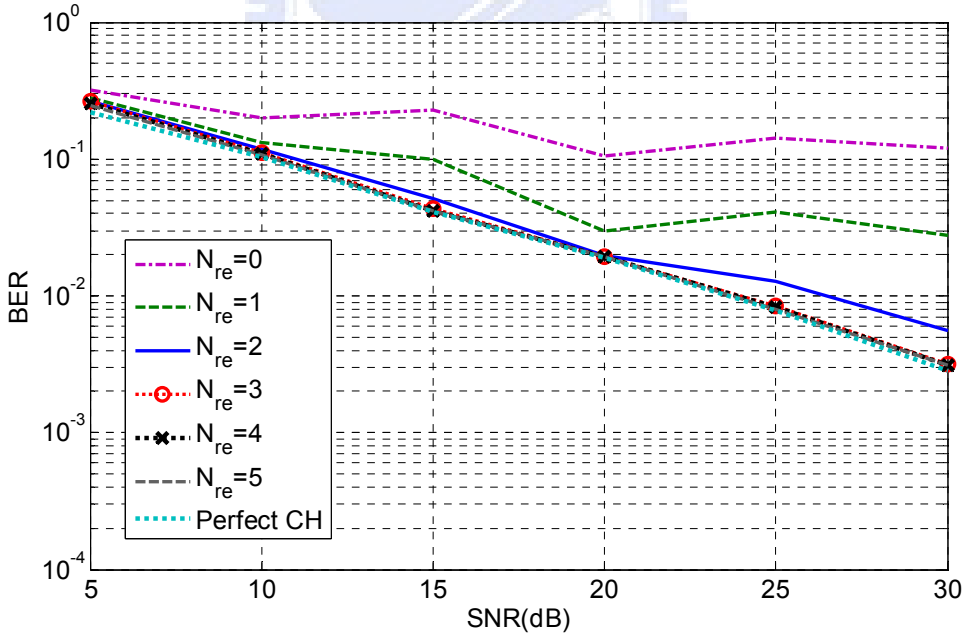

Figure 6-46 Performance of proposed time-variant channel estimator with WLS for 16QAM

(SIC-WLS uses original and pseudo pilots, Channel B)

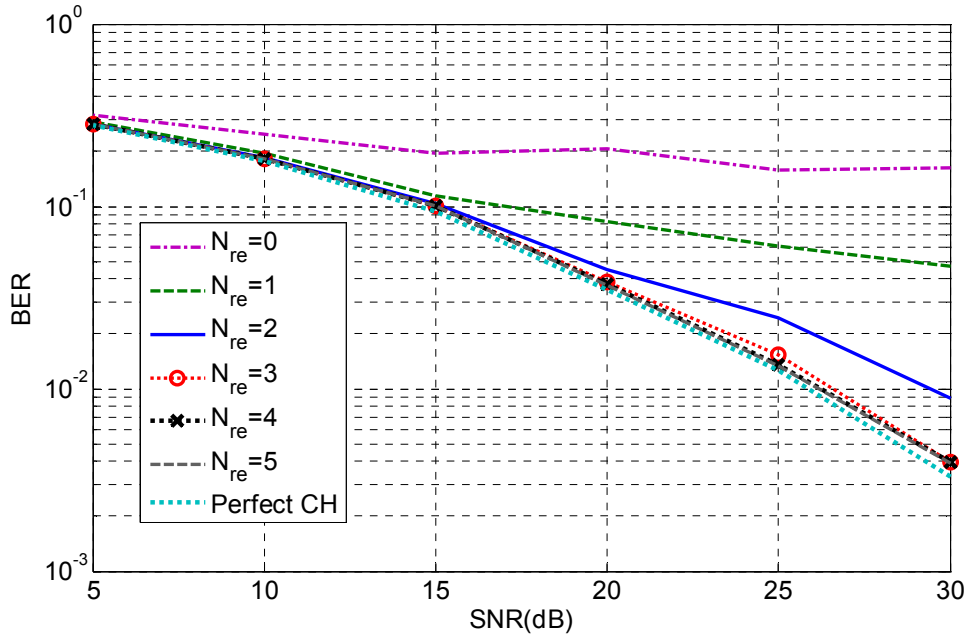

Figure 6-47 Performance of proposed time-variant channel estimator with WLS for 64QAM (SIC-WLS uses original and pseudo pilots, Channel A)

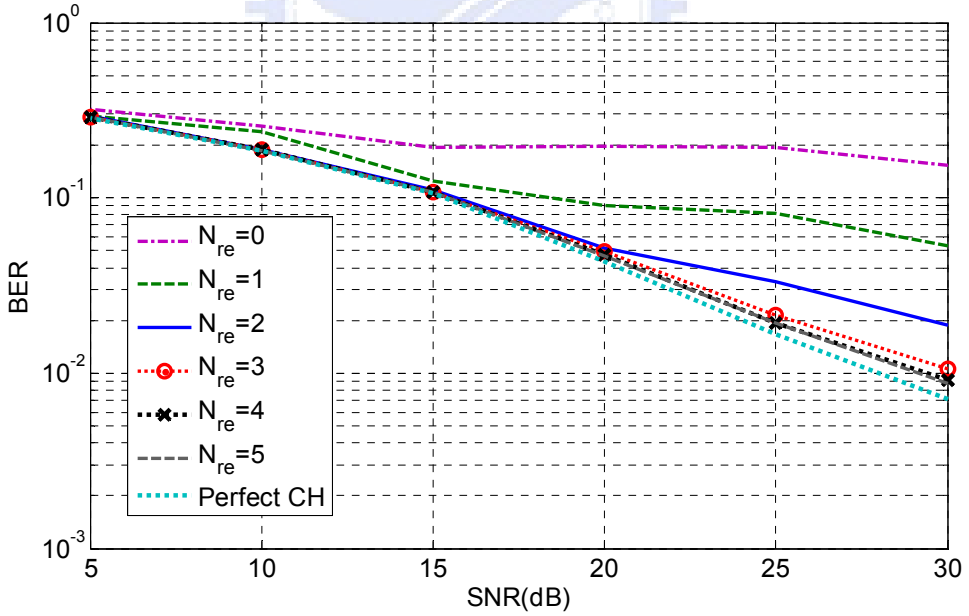

Figure 6-48 Performance of proposed time-variant channel estimator with WLS for 64QAM (SIC-WLS uses original and pseudo pilots, Channel B)

Chapter 7

Conclusions and Future Works

In this thesis, we propose new channel estimators for time invariant/variant channels, and apply the methods to DVB-T systems. The distinct feature of the proposed algorithms is that only one OFDM symbol is required even when the pilot density is low. Basically, our methods belong to the joint time and frequency domain channel estimation with decision feedback. The main idea is to use decision data as pseudo pilots for time and frequency domain channel estimation. The performance of the proposed algorithms is shown to be superior. When the number of pilots is not sufficient, we can use the WLS instead of the LS algorithm in the proposed method. The good performance of the proposed methods can still maintain.

Then, we extend the proposed channel estimators developed for the time-invariant channels to the channel estimation of time variant channels. Since the number of the parameters is doubled, more pilots are required in the scenario. Simulations show that the performance of the proposed estimators is satisfactory even when the mobile speed is high.

As shown, the proposed estimators for time variant channels require the inversion of a matrix. Also, the ICI cancellation method requires the inversion of a huge matrix. Thus, the computational complexity will be high. How to obtain a low-complexity channel estimation and ICI cancellation algorithm can serve as a topic for future work. In this thesis, we only consider single-input-single-output (SISO) systems. The multiple-input-multiple-output (MIMO)-OFDM systems becomes popular in recent years, we can also extend the proposed algorithm to the channel estimation problem in MIMO-OFDM system. This also serves as a topic for further research.

Reference

[1] A. R. S. Bahai and B. R. Saltzberg, “Multi-carrier Digital Communications Theory and Applications of OFDM,” New York: Kluwer Academic, 1999.

[2] Keng-Hsien Lin, “Design of a Baseband Receiver for DVB-T Standard,” MS Thesis, NTU, 2005.

[3] Shiang-Lun Kao, “Joint Time and Frequency Domain Channel Estimation for High-Mobility OFDM Systems,” MS Thesis, NCTU, 2007.

[4] Yun-Jen Lai, “Joint time-and-frequency-domain channel estimation and ICI cancellation in DVB-T systems,” MS Thesis, NCTU, 2008.

[5] Steven M. KAY, “Fundamentals of Statistical Signal Processing : Estimation Theory, ” Prentice Hall, 1993

[6] Y.-S. Choi, P. J. Voltz, and F. A. Cassara, “On channel estimation and detection for multicarrier signals in fast and selective rayleigh fading channels,” *IEEE Trans. Commun.*, vol. 49, pp. 1375–1387, Aug. 2001.

[7] Chao-Yuan Hsu, and Wen-Rong Wu, “A Low-complexity ICI Mitigation Method for High-speed Mobile OFDM Systems,” *IEEE International Symposium on Circuits and Systems*, Island of Kos, Greece, May 2006.

[8] Y. Mostofi and D. C. Cox, “ICI Mitigation for Pilot-Aided OFDM Mobile Systems,” *IEEE Transactions on Wireless Communications*, vol. 4, no. 2, pp. 765-774, Mar. 2005.

[9] Charles K. Sestok, and Predrag Radosavljevic, “Frequency-Domain ICI Estimation, Shortening, and Cancellation in OFDM Receivers,” *IEEE International Symposium on Broadband Multimedia Systems and Broadcasting*, April 2006.

[10] Y. –H. Yeh, and S. -G. Chen, “Reduction of Doppler-induced ICI interference

prediction," *IEEE PIMRC 2004*, *15th IEEE international Symposium*, vol. 1, pp. 653-657, Sept. 2004.

[11] W. –S. Hou and B. -S. Chen, "ICI cancellation for OFDM Communication Systems in Time-Varing Multipath Fading Channels," *IEEE Trans. Commun.*, vol. 4, no. 5, pp. 2100-2110, Sep. 2005.

[12] W. G. Jeon, K. H. Chang, and Y. S. Cho, "An equalization technique for orthogonal frequency-division multiplexing systems in time-variant multipath channels," *IEEE Trans. Commun.*, vol. 47, pp. 27–32, Jan. 1999.

[13] Hongmei Wang, Xiang Chen, Shidong Zhou, Yan Yao, "A Low-Complexity ICI Cancellation Scheme in Frequency Domain for OFDM in Time-varying Multipath Channels," *16th IEEE international Symposium on Personal*, *Indoor and Mobile Radio Communications*, 2005.

[14] Chin-Jung Tsai, "Design of Channel Estimation and Data Detection for OFDM Systems in Time-varying and Multipath Fading Channels," MS Thesis, NCTU, 2006.

[15] Weinstein, S.B., Ebert, P.M. , "Data Transmission by Frequency-Division Multiplexing Using the Discrete Fourier Transform," *IEEE Transactions on Communication Technology*, vol. 19, no. 5, pp. 628-634, October 1971.